NASA CONTRACTOR REPORT

NASA CR-1091

NASA CR-1091

RESEARCH AND DEVELOPMENT OF A VORTEX VALVE FOR FLOW MODULATION OF A 16-PERCENT ALUMINIZED 5500° F PROPELLANT GAS

by T. W. Keranen and A. Blatter

Prepared by
BENDIX RESEARCH LABORATORIES
Southfield, Mich.
for Langley Research Center

NATIONAL AERONAUTICS AND SPACE ADMINISTRATION • WASHINGTON, D. C. • JUNE 1968

NASA CR-1091

RESEARCH AND DEVELOPMENT OF A VORTEX VALVE FOR FLOW MODULATION OF A 16-PERCENT ALUMINIZED 5500° F PROPELLANT GAS

By T. W. Keranen and A. Blatter

Issued by Originator as Report No. 4227

Prepared under Contract No. NAS 1-5199 by
BENDIX RESEARCH LABORATORIES
Southfield, Mich.

for Langley Research Center

NATIONAL AERONAUTICS AND SPACE ADMINISTRATION

For sale by the Clearinghouse for Federal Scientific and Technical Information
Springfield, Virginia 22151 – CFSTI price $3.00

ABSTRACT

The flow of hot (5500°F) gas from a solid propellant gas generator has been successfully throttled by a fluidic, no-moving-part, vortex valve. The vortex valve has been demonstrated in a system simulating a hot gas secondary injection thrust vector control (SITVC) system. The hot gas vortex valves were controlled by a pilot stage utilizing a flapper-nozzle and vortex amplifier valve arrangement which modulated the flow of a 2000°F pilot stage solid propellant gas generator. Materials found suitable for the 5500°F hot gas application consist of silver-infiltrated tungsten, carbon or silica phenolic and solid carbon.

The development effort consisted of six hot gas firings which demonstrated satisfactory material selection, hot gas flow modulation, and steady-state and dynamic performance of a simulated SITVC system.

TABLE OF CONTENTS

LIST OF ILLUSTRATIONS

LIST OF TABLES

RESEARCH AND DEVELOPMENT OF A VORTEX VALVE FOR FLOW MODULATION OF A 16-PERCENT ALUMINIZED 5500°F PROPELLANT GAS

By T. W. Keranen and A. Blatter

Bendix Research Laboratories

SUMMARY

This program (Phase I) has successfully demonstrated a vortex valve controlled simulated secondary injection thrust vector control system by modulating the flow of highly (16%) aluminized, 5500°F, solid propellant gas. The vortex valves developed during this program have the capability to turn off the flow of 1 lb/sec of 5500°F gas at 750 psia, and are able to control this gas for more than 50 seconds.

Six 5500°F hot gas tests were accomplished during this phase. The first hot gas test was for a materials and design evaluation, and no attempt was made to throttle flow with the vortex valve. This test revealed the necessity of keeping the aluminized solid propellant gas hot enough to prevent the solidification of aluminium oxide inside the vortex valve and associated manifolding.

The second and third tests were single vortex valve hot gas performance tests which utilized one main stage vortex valve and a manually controlled 2000°F pilot stage. These tests established valve structural design technology and preliminary vortex valve performance. The vortex valve performance was less than expected because some valve deterioration was caused by the 5500°F gas.

The fourth, fifth and sixth tests were complete vortex valve-controlled SITVC system hot gas bench tests. The system tested consisted of a torque motor and flapper-nozzle valve which controlled a vortex amplifier valve pilot stage; two vortex valves operated in push-pull for the main stage; a 2000°F solid propellant gas generator (SPGG) as the gas source for the pilot stage; and a 5500°F SPGG main stage gas source. These three hot gas system tests demonstrated the ability of the vortex valve to control a SITVC system by successfully containing and modulating 5500°F hot gas. The vortex valve demonstrated modulation capability for a duration in excess of 50 seconds.

The Phase II effort of this program is currently in progress and will result in a seventh hot gas system test. The system to be tested will utilize the No. 6 Hot Gas Test hardware, but it will be installed on a solid propellant rocket engine. The 30 lb/sec rocket engine will be fired in the horizontal position. One of the vortex valves will inject into the rocket engine nozzle in the vertical plane, and the

other vortex valve will inject in the horizontal plane. The test is scheduled for October 1967 at Allegany Ballistics Laboratory, Cumberland, Maryland.

The technology resulting from this program provides a sound basis for the design and feasibility testing of a vortex valve controlled direct chamber bleed SITVC system. This development effort would result in a vortex valve control system installed in the combustion chamber of a submerged nozzle rocket engine to produce a lightweight, inherently simple and highly reliable SITVC system.

INTRODUCTION

A rocket vehicle can be steered by deflecting the engine thrust. Ordinarily, directional control of the thrust vector is achieved by mounting the thrust engine on gimbals or by adding auxiliary movable engines. An alternate method of providing thrust vector control is by the technique known as Secondary Injection Thrust Vector Control (SITVC). The engine is stationary and fluid jets deflect the rocket thrust gases to steer the vehicle. The fluid is injected into the thrust nozzle downstream of the engine (hence, the name "secondary injection"). Response is fast because the jets can be modulated rapidly in contrast to the mechanical method in which large engine masses are moved by servo actuators. The SITVC technique eliminates the need for complex seals and joints inherent in mechanical nozzle deflection systems.

Almost any fluid might be used for secondary injection, but it is most efficient to inject a high-temperature gas. The gas can be supplied from an independent source, or it might be bled from the engine itself. In the case of a solid propellant engine, the valves that control the secondary injection must withstand temperatures of 5000°F or more. In this severe environment, a fluidic device with no moving parts, such as a vortex valve, offers the possibility of greater reliability than a mechanical moving-part valve.

Solid propellant gases contain material that can readily plug clearances and small passages; the vortex valve, with its large passages and no-moving-parts design, is less susceptible to plugging than conventional valve techniques. In the case of highly aluminized 5500°F solid propellant gas, there is a tendency for aluminum oxide to "plate out" on flow channel surfaces. The development of vortex valves to control this gas must include heat transfer techniques to avoid solidifying the aluminum oxide.

The program results described in this report are for the development of a vortex valve to modulate the flow of 5500°F highly aluminized (16%) gas. To achieve this goal, it was necessary to develop a valve structure capable of containing such flow without failure and without undue heat loss from the gas. These objectives have been accomplished. A possible application of the technology resulting from this program is the design and operation of a vortex valve controlled SITVC system similar to the submerged nozzle rocket engine installation depicted in Figure 1. Therefore, in this program, the 5500°F vortex valve was tested as part of a complete simulated single-axis secondary injection thrust vector control system.

Vortex Valve Concept

The vortex valve is a fluidic element that utilizes certain basic fluid phenomena to perform a valving or controlling function without the

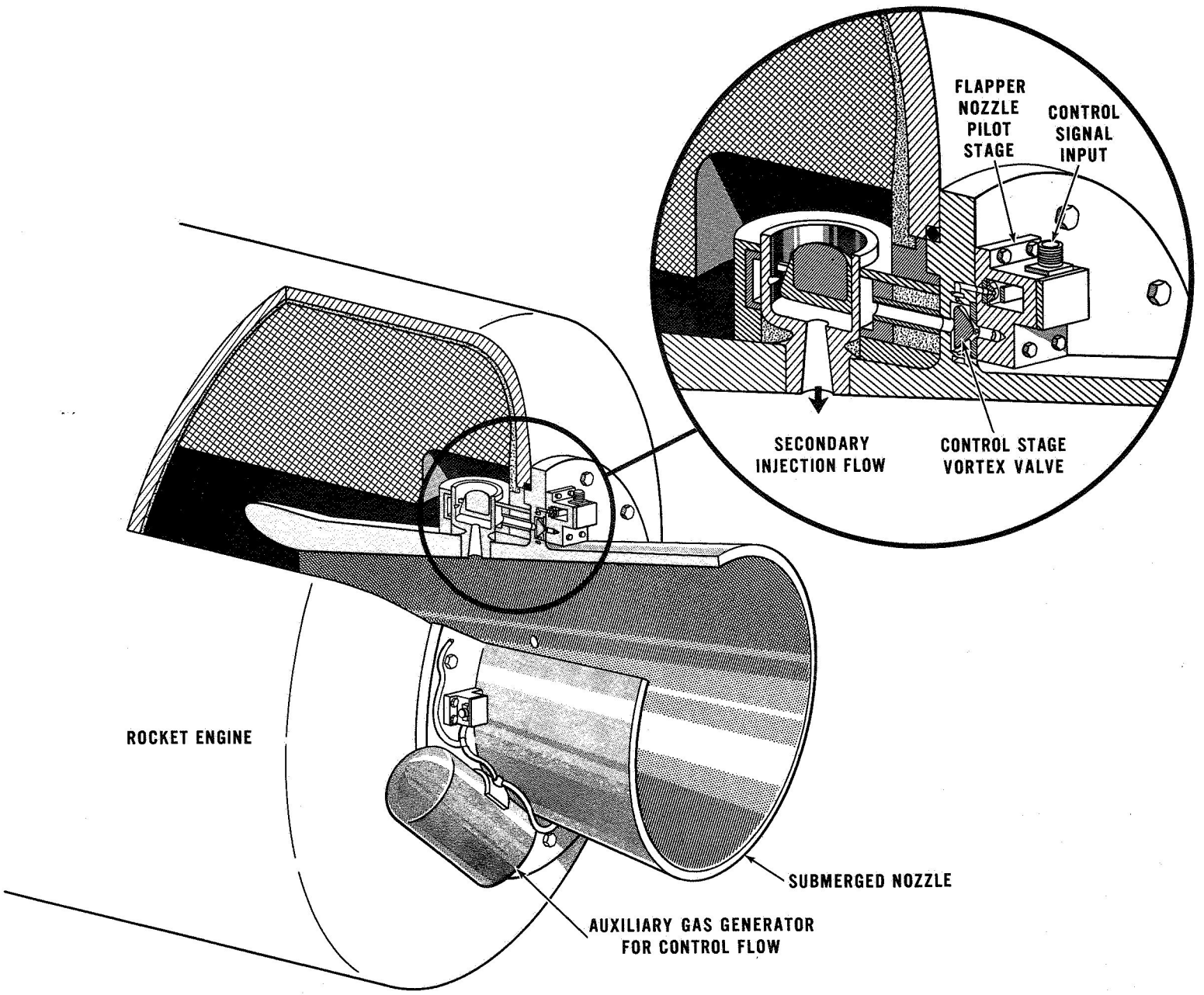

Figure 1 - Vortex Valve Secondary Injection Thrust Vector Control System — Buried Nozzle Installation

use of mechanical moving parts. The vortex valve is a unique fluidic element in that it is capable of throttling flow, whereas other fluidic devices are only flow diverters.

The basic vortex valve and its operation are illustrated in Figure 2. The vortex valve functions by the interaction between properly introduced control and supply flows. The valve supply flow is introduced radially into a cylindrical vortex chamber. In the absence of control flow, the supply flow proceeds radially toward the center outlet hole. The limiting restriction that establishes maximum valve flow is the outlet orifice at the center of the chamber. The modulation of supply flow is accomplished by the addition of a tangential control flow into the valve. The control flow imparts a rotational flow component to the supply flow as it passes the control injector. Thus, the supply flow entering the vortex chamber has a tangential velocity component in addition to the radial component. As the flow swirls toward the center of the valve, conservation of its angular momentum causes the tangential velocity to increase. This substantial increase in tangential velocity of the fluid causes a centrifugal pressure buildup across the vortex flow field in a radial direction. This pressure gradient opposes the incoming supply flow and provides the means for modulating the supply flow. The strength of the vortex flow field, which is a function of control flow, produces a valving characteristic; i.e., an increase in control flow causes a reduction in total valve flow. Typical vortex valve performance is shown in Figure 3.

For efficient mixing of control and supply flows, the supply flow enters the chamber through an annular inlet formed by a "button" that is slightly smaller than the chamber diameter.

The vortex valve is relatively insensitive to minor internal geometry variations such as small changes in chamber diameter, button diameter, etc. The vortex valve is sensitive to the tangency between the control hole and vortex chamber and to the product of the control hole area and the orifice coefficient. The performance for any given vortex valve under constant test conditions should be as reproducible as the performance repeatability of a simple orifice.

The vortex valve is ideally suited for high-temperature work for two reasons: First, the vortex valve contains no moving parts and, therefore, has no dynamic seals and no possibility of the binding or seizing which is characteristic of close-clearance moving parts. Secondly, the vortex valve components are all symmetrical in construction; therefore, there is negligible unsymmetrical component distortion or reduction in flow areas, caused by thermal expansion, to affect valve performance.

Program Plan

The overall goal of the program was to demonstrate the performance of the vortex valve in a simulated secondary injection thrust vector

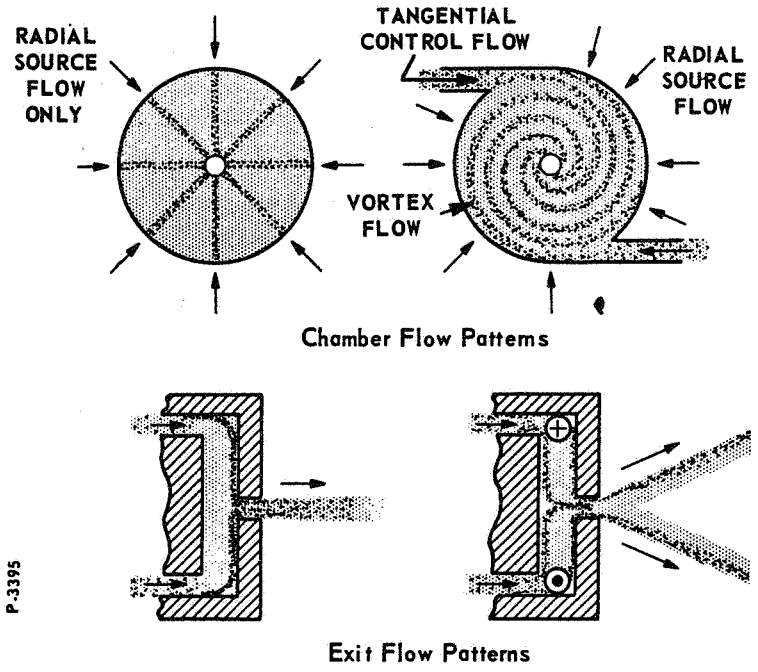

Figure 2 - Vortex Valve Configuration and Operation

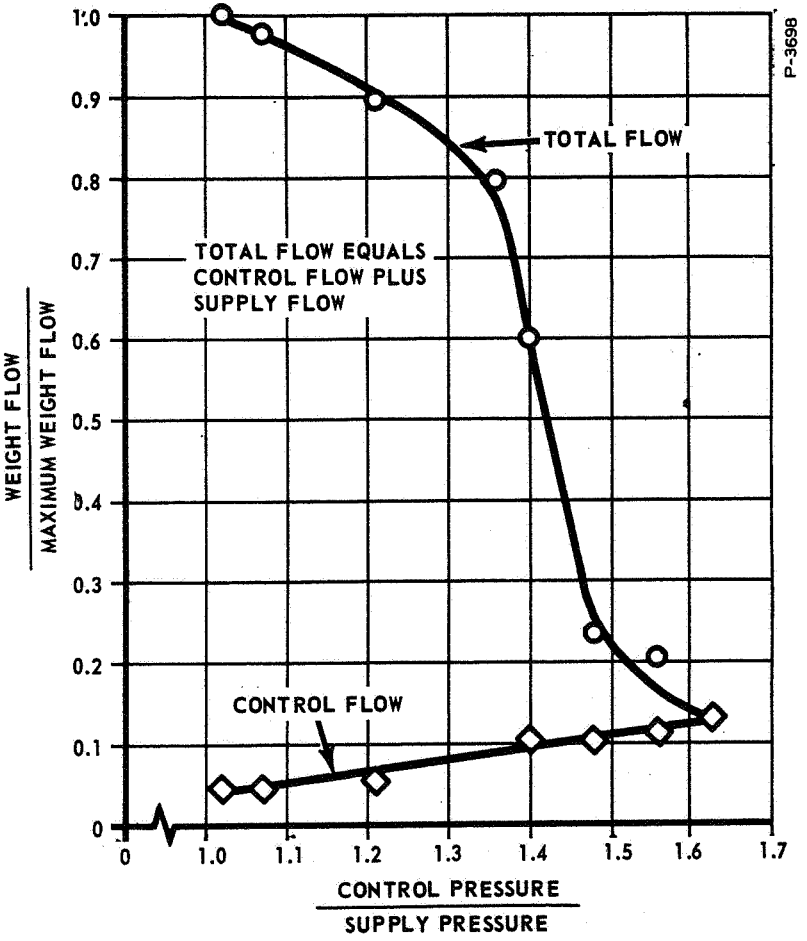

Figure 3 - Typical Vortex Valve Flow Turndown Performance

control system. To accomplish this, it was necessary to select vortex valve construction materials which would survive exposure to 5500°F solid propellant gas. Thus, the program plan consisted of the following steps.

(1) Perform a material survey and select the vortex valve construction materials. Perform a thermal analysis to establish the basis for a vortex valve and manifolding design.

(2) Conduct a materials evaluation test with an inoperative vortex valve.

(3) Design a vortex valve utilizing the material information previously obtained and conduct two single vortex valve hot gas tests to establish the vortex valve performance.

(4) Design a simple vortex valve and manifold system to simulate a SITVC system, and a warm gas pilot stage to control the vortex valves. Conduct two firings to establish the system steady-state and dynamic performance.

(5) Design a vortex valve and manifold system suitable for installation on a ground test rocket engine. Assemble and test the system to establish the overall system performance and operation.

(6) A parallel, Phase II effort will utilize the same system hardware to perform a secondary injection thrust vector control test on the NASA-supplied EM-72 rocket engine. The engine will be modified to produce a flow rate of 30 lb/sec for this test, and TVC data will be obtained.

SYSTEM DESCRIPTION AND PERFORMANCE

The system developed in this program is a simulated, single axis, vortex valve controlled secondary injection thrust vector control (SITVC) system for utilization with solid propellant rockets. The system is shown schematically in Figure 4.

The system contains a main stage which modulates the flow of 5500°F gas and a pilot stage which controls the main stage. The main stage consists of two push-pull operated vortex valves which are supplied from a 5500°F solid propellant gas generator (SPGG). The main stage vortex valves, as shown in Figure 5, represent secondary injection valves that could be installed on a rocket engine.

The push-pull mode of main stage operation was utilized to impart a constant load to the 5500°F SPGG during system operation so that the SPGG would have a constant output. The main stage push-pull operation is such that when one vortex valve output flow is decreased the other vortex valve output flow is increased a similar amount. The net result of this push-pull operation is that the total output flow from the two vortex valves is approximately constant.

The main stage system receives control inputs from the pilot stage. The pilot stage consists of two push-pull operated vortex valves which are controlled by a torque-motor flapper-nozzle valve. The pilot stage is supplied with gas from a 2000°F SPGG. The vortex amplifier valves are separated from the 2000°F SPGG by three subsonic orifices which provide the required pressure differentials between the vortex valve supply and control. The pilot stage operation is initiated by an electrical signal to the torque motor which produces a displacement of the flapper. The flapper displacement causes a reduction in flow through one of the nozzles and an increase in the nozzle upstream pressure. This increased pressure results in increased control flow to one of the vortex amplifier valves and a reduced output flow from that side of the pilot stage. This pilot stage vortex amplifier valve output flow is the control flow to the main stage vortex valve on that side. Reduction of this control flow permits an increase in the flow out of that main stage valve. Conversely, the other half of the system experiences a reduction in main stage valve flow. A detailed system analysis is provided in Appendix A.

The simulated, single-axis SITVC system used in this program was designed as a heavyweight bench test model. An actual flyable vortex valve controlled SITVC system installed on a solid propellant rocket engine would be similar to the system shown in Figure 1. This type of system would not require an auxiliary 5500°F SPGG because the main stage vortex valves would be supplied directly from the rocket engine. Also, in this system the main stage vortex valves would be independently controlled (not push-pull) and would normally be in the full turndown

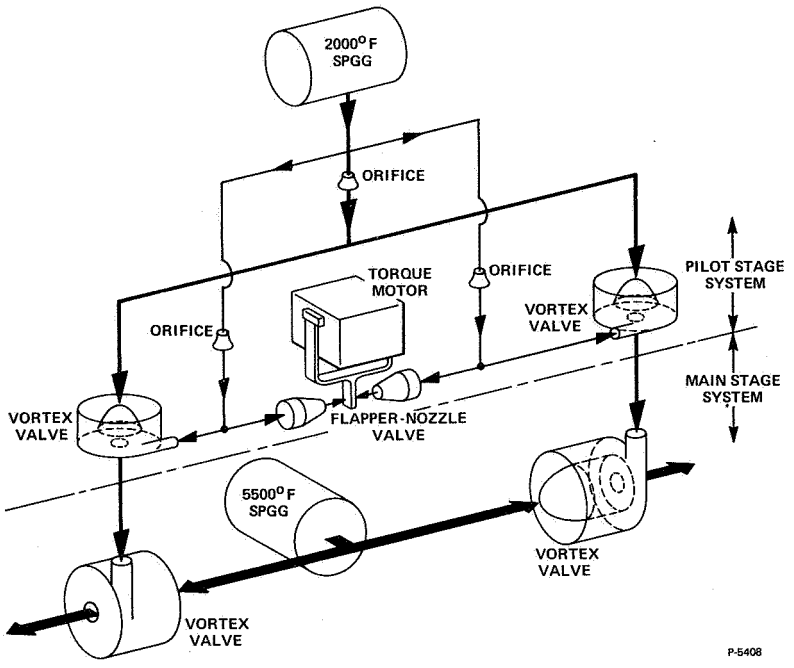

Figure 4 - Schematic of the Simulated Single-Axis Secondary Injection Thrust Vector Control System

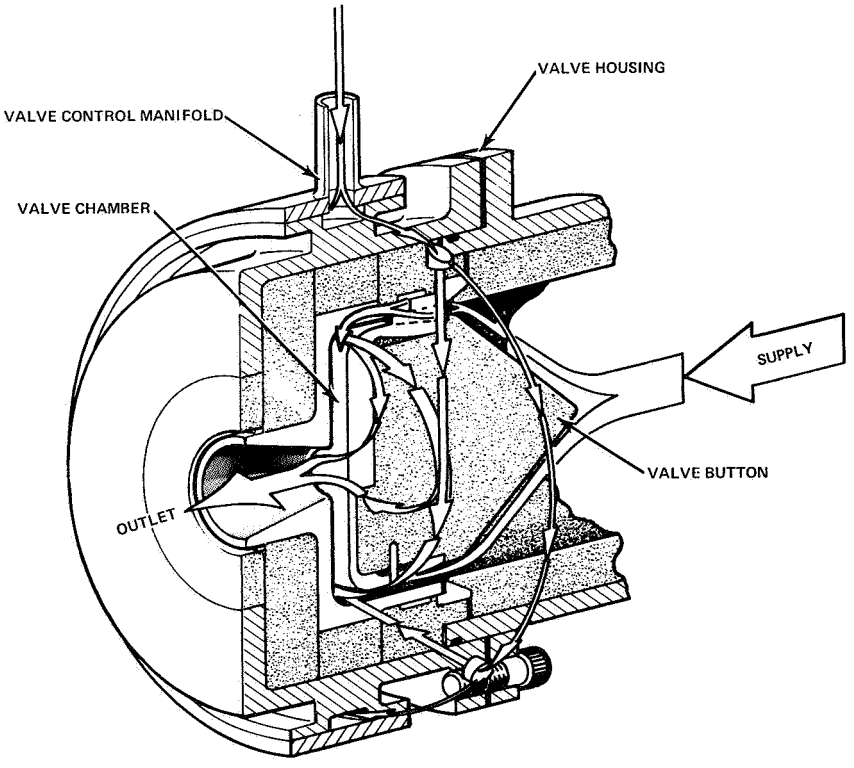

Figure 5 - 5500°F Vortex Valve

mode until thrust vectoring is commanded. When rocket engine thrust vectoring is required, the appropriate vortex valves or valve combinations would supply the proper amount of secondary injectant gas to obtain the desired thrust vector deflection. This technique will result in a SITVC system that is inherently simple and lightweight.

The main stage vortex valve and the simulated SITVC system were developed during a series of six hot gas tests. Before each hot gas test, the various systems and their components were cold gas tested on nitrogen to verify intended performance. Performance curves of the pilot stage vortex amplifier valves and the main stage vortex valves are shown in Figures 6 and 7.

The six hot gas tests consisted of one material and design evaluation test, two single vortex valve performance tests, and three complete single-axis system hot gas tests. Portions of the fourth hot gas test movies (Figures 8 and 9) graphically show the ability of the vortex valve to modulate the flow of 5500°F hot gas. These two test movie segments are from two different cameras operating at the same shutter speed. The frames of each strip are of the same system event and each frame exposure, starting from the top, occurred at essentially the same time. The film strips show a portion of a push-pull cycle of the two main stage vortex valves.

During the sixth hot gas test, the vortex valves modulated the flow of 5500°F hot gas at frequencies of 5, 10, and 15 cps. The maximum flow modulation obtained during the test was 3.46 to 1, which is comparable to the theoretical value of 3.56 to 1 (Appendix A). The best main stage vortex valve turndown performance curve is shown in Figure 10. The system controlled the flow of highly aluminized 5500°F solid propellant gas for 51 seconds with no component degradation.

System dynamic frequency response performance was only partially obtained during the hot gas tests because of plugging of the main stage vortex valve flow measurement system. The system functioned with little phase shift out to 15 cps while the amplitude ratio decreased to approximately 0.60. The flow measurement orifice plugged shortly after the 15 cps signal began, and the data are uncertain. Vortex valves used in this system are capable of high dynamic frequency response because other Bendix-developed vortex valves of approximately the same size have demonstrated a frequency response bandpass of 80 cps.

A system description and test results covering each of the six hot gas tests are provided in the following sections. The final configuration of the 5500°F vortex valve is shown in Figure 11, which includes the critical dimensions and tolerances used for the vortex valve.

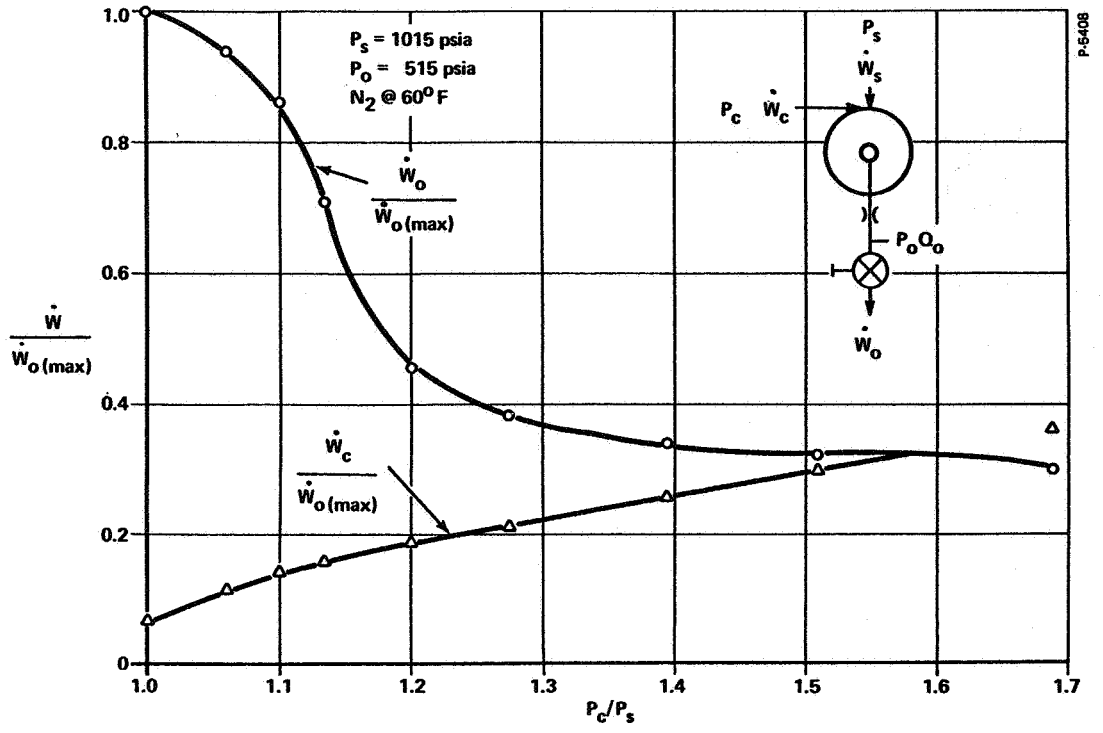

Figure 6 - Pilot Stage Vortex Amplifier Valve Turndown Characteristics

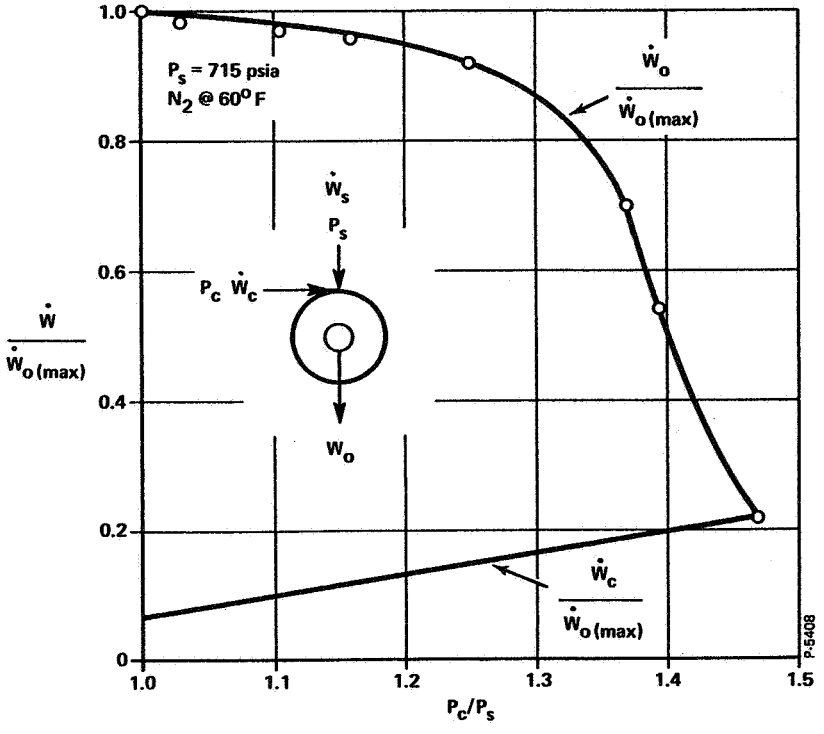

Figure 7 - Main Stage Vortex Valve Turndown Characteristics

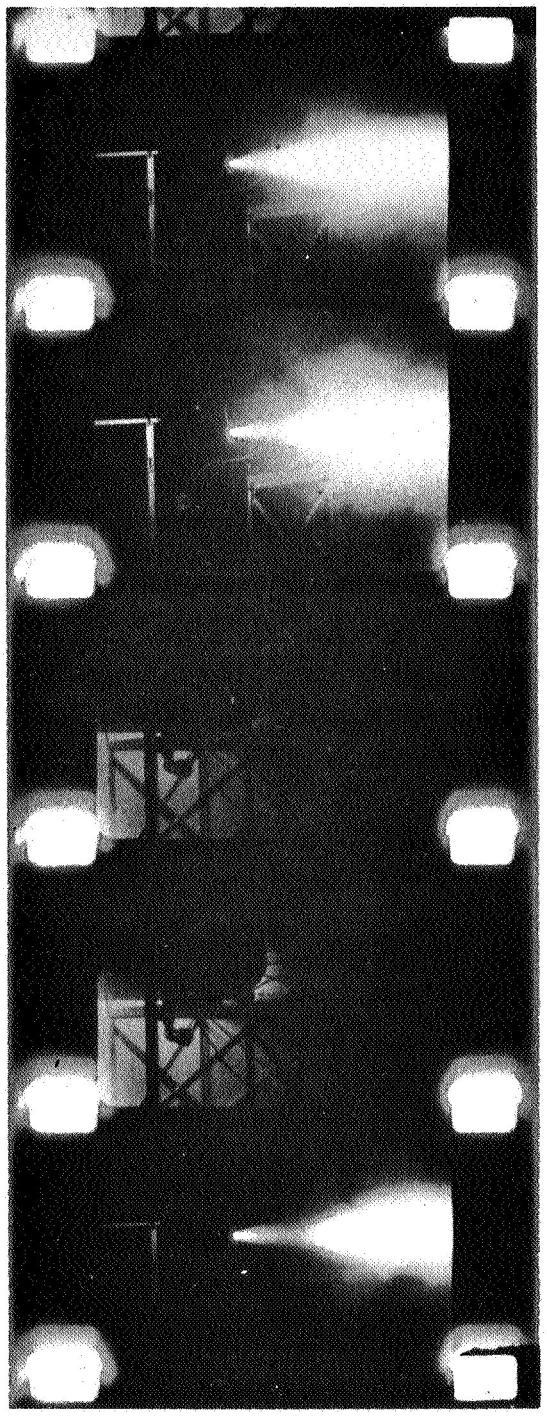

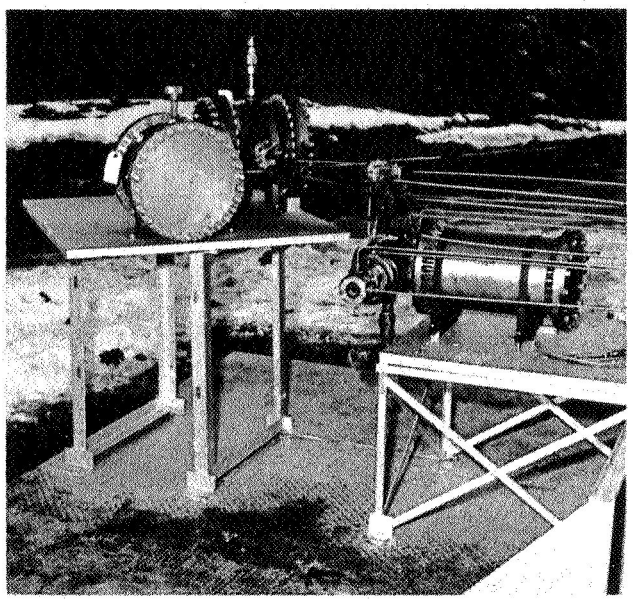

TEST
INSTALLATION

FILM CLIP
SHOWING
FLOW MODULATION

P-5408

Figure 8 - 5500°F Push-Pull System Main Stage Vortex Valve No. 1 During Operation (Hot Gas Test No. 4)

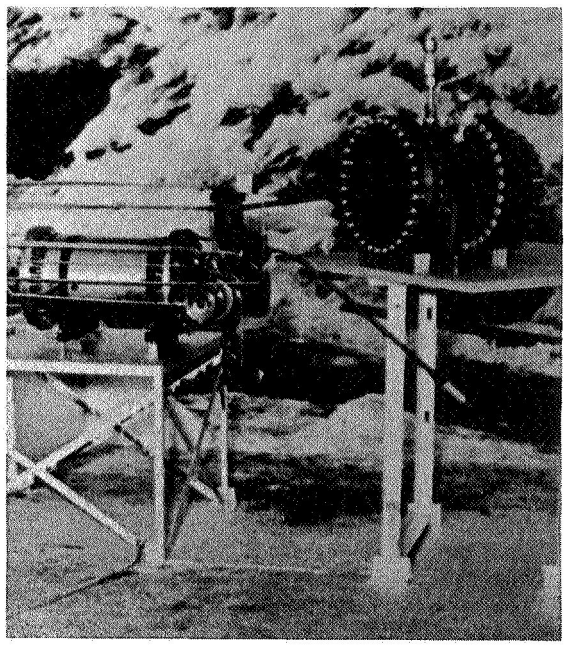

TEST
INSTALLATION

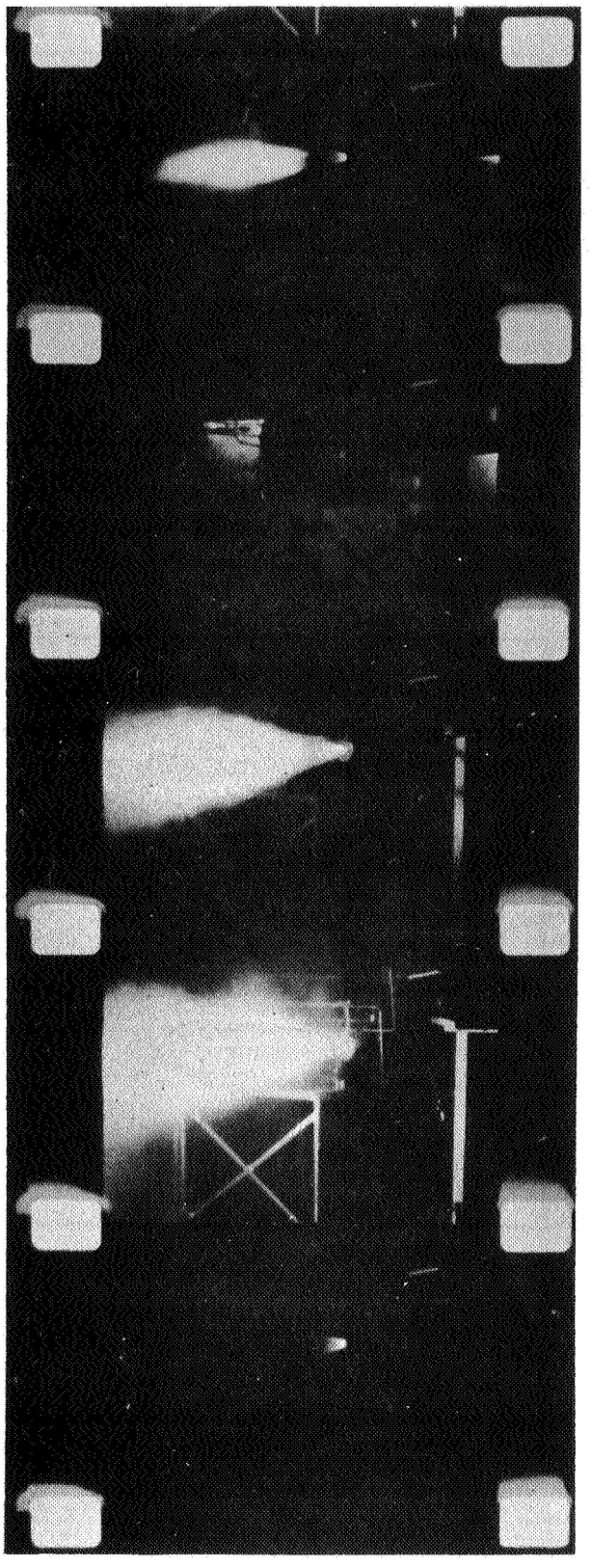

FILM CLIP
SHOWING FLOW
MODULATION

23623

Figure 9 - 5500°F Push-Pull System Main Stage Vortex Valve No. 2 During Operation (Hot Gas Test No. 4)

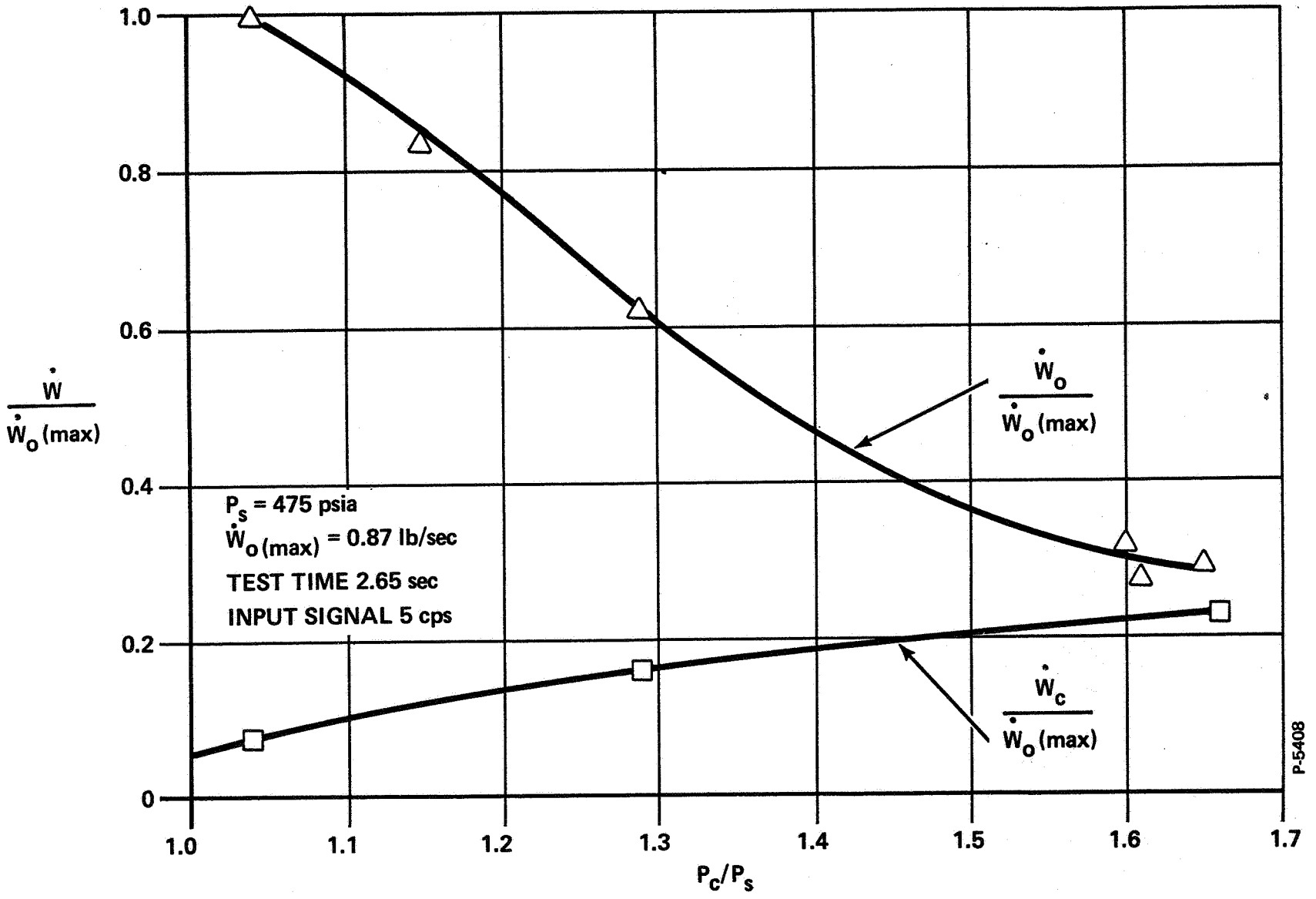

Figure 10 - Main Stage Vortex Valve No. 2 Hot Gas Turndown Characteristics
(Hot Gas Test No. 6)

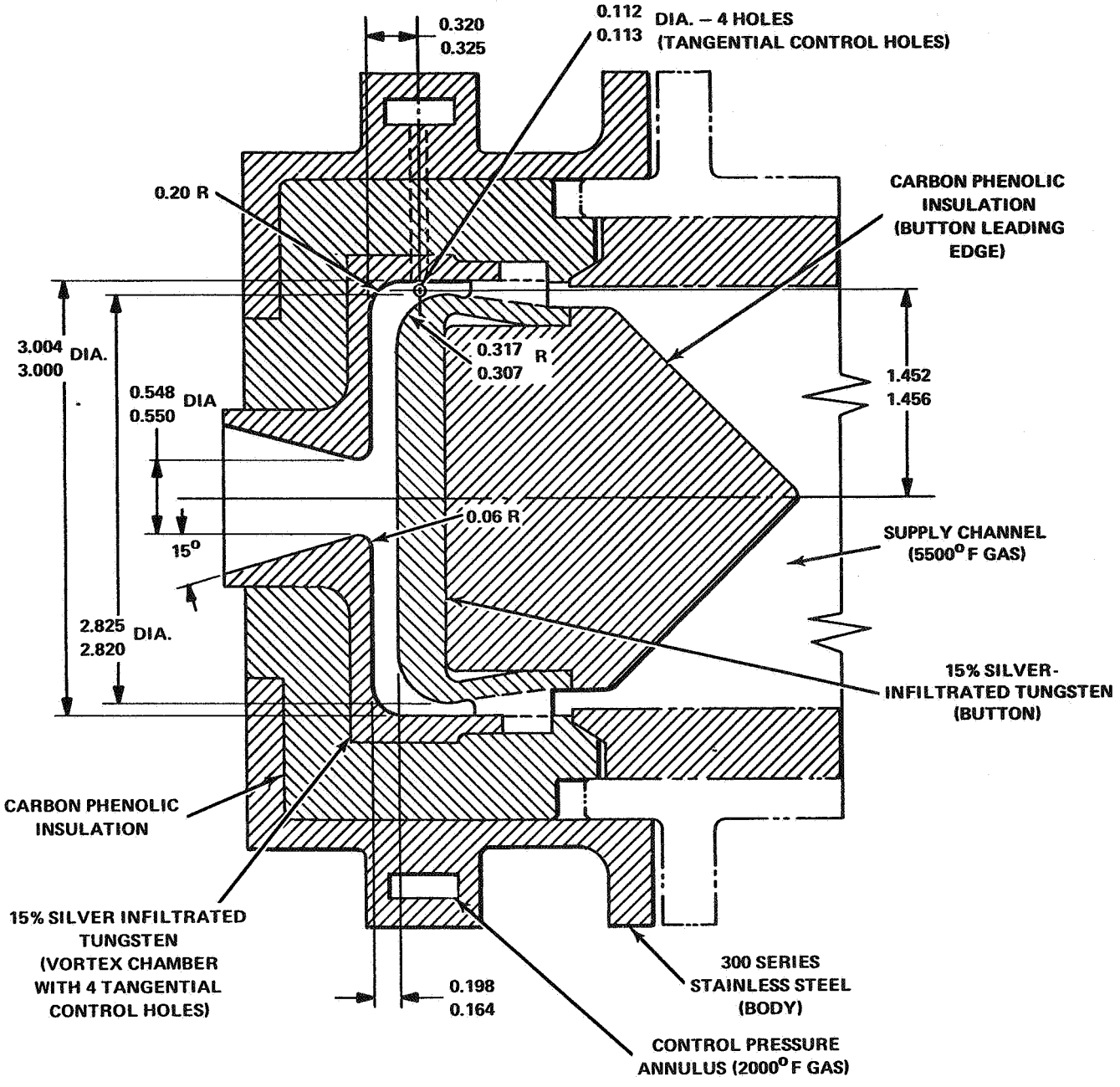

Figure 11 - 5500°F Vortex Valve Final Configuration,
Basic Dimensions and Materials

MATERIALS EVALUATION TEST

(Hot Gas Test No. 1)

Prior to the materials evaluation test, a transient heat transfer and thermal stress analysis was conducted to aid in selecting materials and establishing the design configuration for the 5500°F SITVC system. This thermal analysis is described in Appendix B. The system materials evaluation test included a 5500°F solid propellant gas generator, manifolds lined with various materials, a main stage vortex valve, and a system vent load orifice to simulate a vortex valve. The test objectives were to evaluate the materials selection and the system structural design, and to provide test data to support the thermal analysis conducted in conjunction with this program. The test also served to verify the 5500°F SPGG performance, which had not been fully demonstrated by the vendor before delivery.

The system design and the materials selected for this test were based on the Bendix thermal analysis and state-of-the-art technology.

System Description

The materials evaluation system tested in Hot Gas Test No. 1 is shown without the 5500°F SPGG in Figure 12. The main stage vortex valve consisted of a 303 stainless steel valve body and end cap; ATJ carbon inner liners; silicon phenolic insulation; Viton "O" rings; and

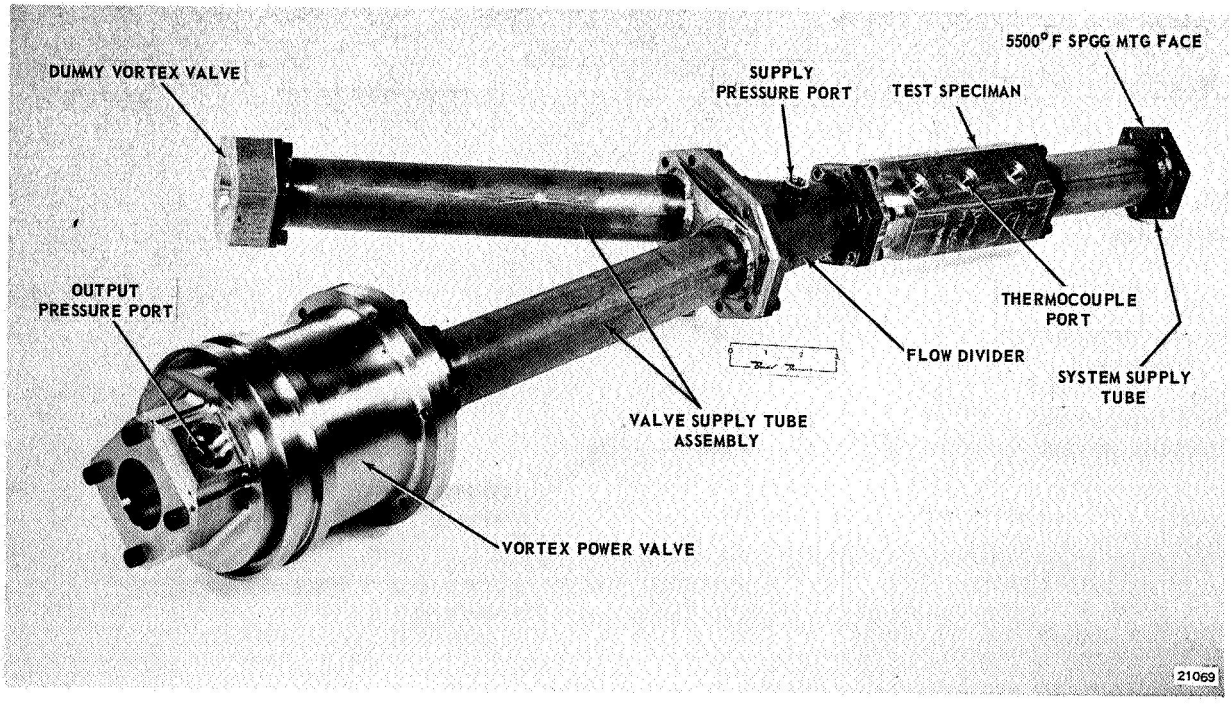

Figure 12 - 5500°F Materials Evaluation System

silver-infiltrated tungsten button assembly, vortex chamber, and load orifice. The button assembly was filled with lithium chloride to provide cooling for the button.

The system supply tube assembly and the vortex valve and vent orifice supply tube assembly were constructed from 303 stainless steel housings, silica phenolic insulation, and ATJ carbon liners.

The system vent orifice assembly and flow divider were constructed from 303 stainless steel housings, silica phenolic insulation, ATJ carbon inner liners, high density arc-cast tungsten (98W-2Mo) orifice, and a silver-infiltrated tungsten flow divider. The arc-cast tungsten was used to evaluate a backup material for the silver-infiltrated tungsten used elsewhere in the system.

The thermal analysis test specimen shown in Figure 13 was designed to verify the thermal analysis. The test specimen consisted of a 303 stainless steel housing and three sections of different laminate thickness of silica phenolic insulation, ATJ carbon intermediate liner, and silver-infiltrated tungsten inner liner. The test specimen was fitted with ten high-temperature thermocouples. The thermocouples were made from tungsten-rhenium wire and calibrated by the manufacturer to 4300°F.

Test Results

The materials evaluation system test consisted of a cold gas (nitrogen) test and a hot gas test. The cold gas testing was done to provide baseline data and instrumentation checkout. The thermal analysis test specimen was not used in the cold gas testing to minimize the handling damage to the specimen thermocouples.

The materials evaluation system hot gas test installation is shown in Figure 14, and the test schematic is shown in Figure 15. During the test the following data were recorded: generator pressure, pressure at the flow divider, main stage vortex valve outlet pressure, 10 test specimen temperatures, including the gas temperature, and 10 system skin temperatures.

The results of Hot Gas Test No. 1 are shown in Figures 16 through 19. The data plotted in Figure 16 versus time are SPGG pressure (P_g), system supply pressure (P_s), and main stage valve outlet pressure (P_o). The 5500°F SPGG ballistics performance, as obtained from the plot of P_g versus time, is given in Table 1. The SPGG test performance is compared with the predicted test performance and ballistics data as supplied by the SPGG vendor. The average SPGG operating pressure was 70 psi lower than the predicted value. This low operating pressure was the result of orifice size growth caused by erosion.

The plot of P_s and P_o versus time (Figure 16) shows the flow performance characteristics of the main stage valve and the vent orifice. After ignition, P_s increased in an irregular manner until at 11 seconds P_s reached a maximum pressure of 815 psia. It then dropped to 715 psia

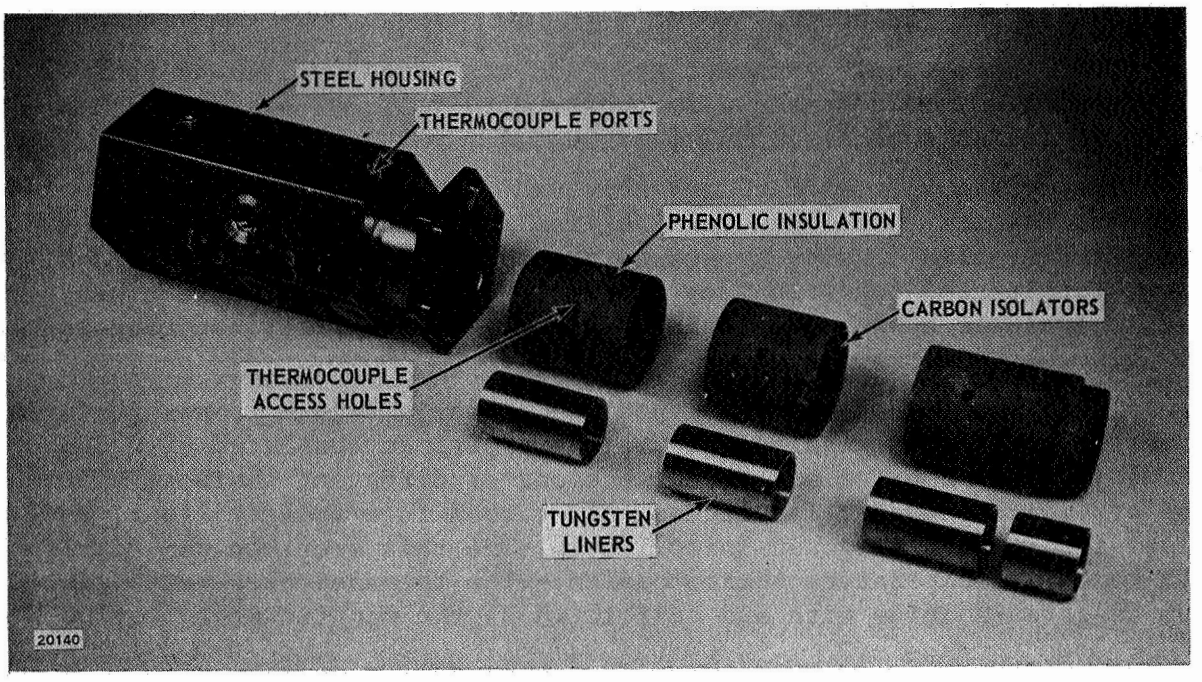

Figure 13 - Thermal Analysis Test Specimen

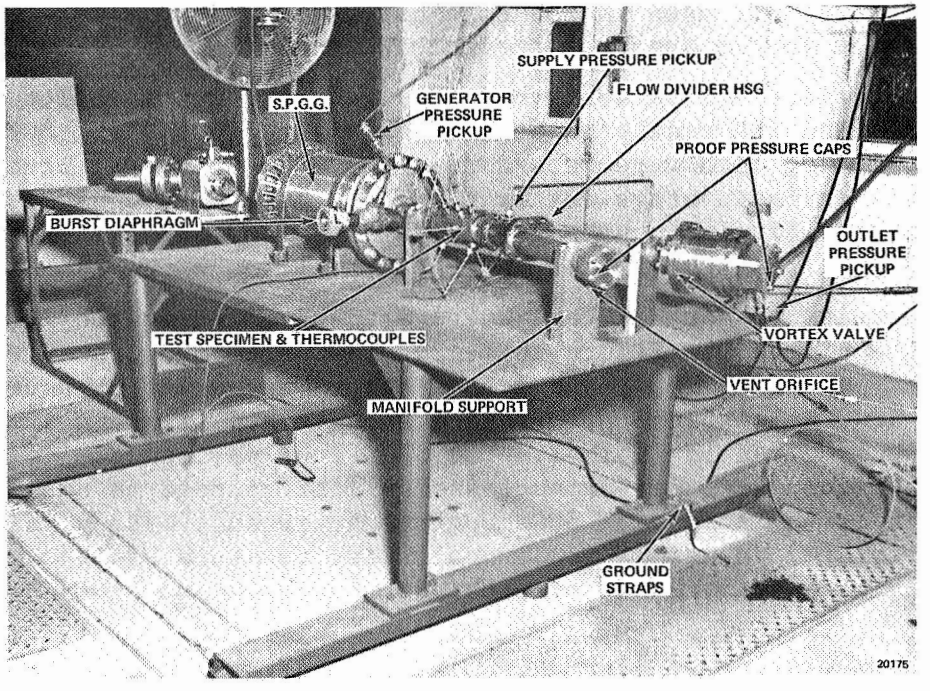

Figure 14 - Hot Gas System Test No. 1

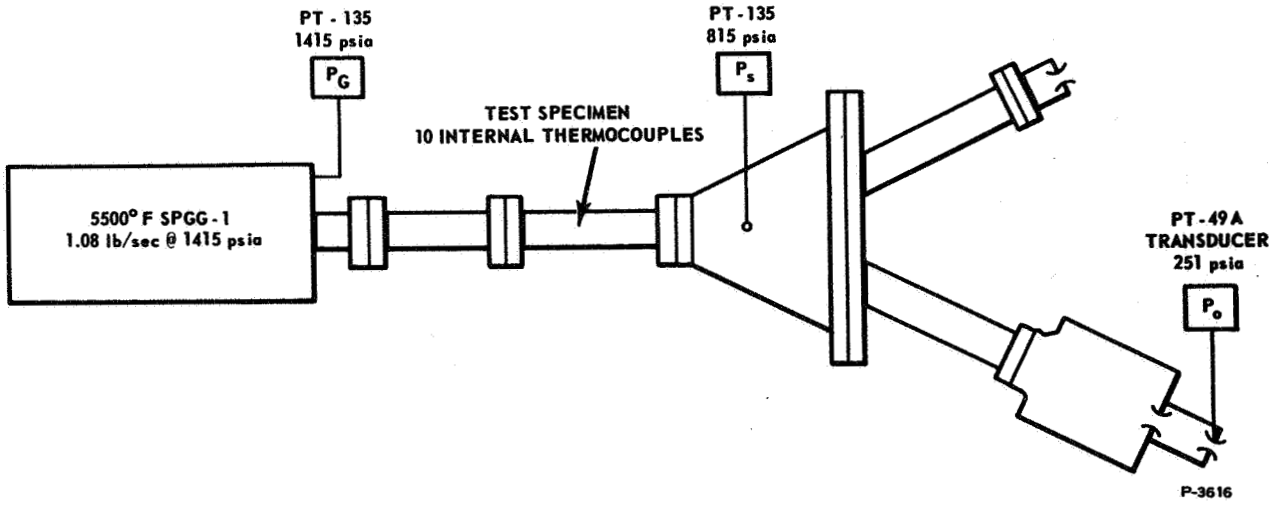

Figure 15 - 5500°F System Materials Evaluation Test

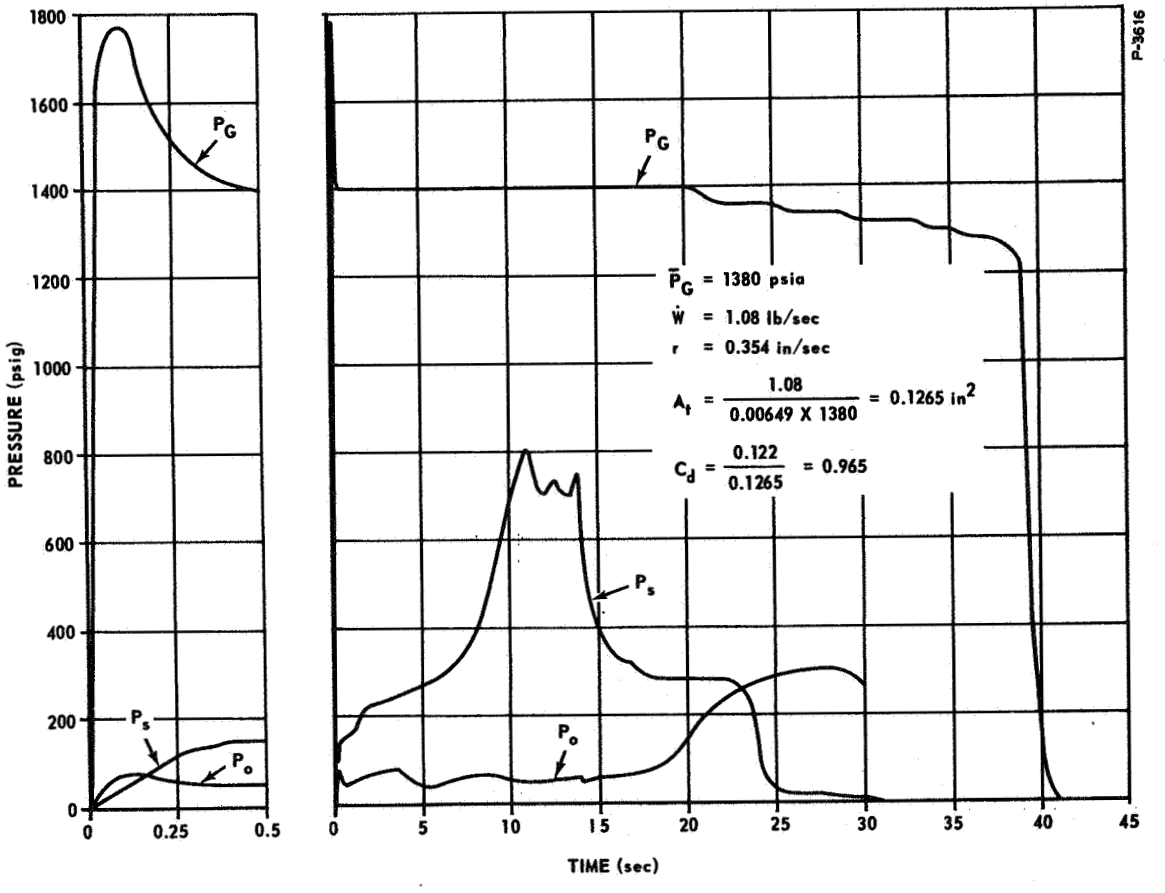

Figure 16 - 5500°F System Materials Evaluation
(Hot Gas Test No. 1)

Table 1 - SPGG Ballistic Performance

	Ballistic Test	Prediction	First Hot Gas Test
Breech Pressure (psia)	1600 avg.	1450 avg.	1380 avg.
Breech Temperature (°K)	3458	--	--
Burn Rate (in/sec)	0.380	0.359	0.354
Burn Surface (in^2)	48.0	48.0	48.0
Burn Time (sec)	37.4	38.5	38.0
Throat Diameter (in.)	0.3754	0.394	0.394
Flow Rate (lb/sec)	1.153	1.098	1.08

and fluctuated about 725 psia. The fluctuation is believed to be caused by alternate clogging and clearing of the aluminum oxide buildup in the main stage vortex valve. At 13.5 seconds, P_s dropped to 300 psia and held constant for about 4 seconds. The sudden drop in P_s at 13.5 seconds was caused by the failure of the system supply tube.

After the ignition spike, P_o oscillated between 65 psia and 95 psia. It increased to a maximum of 300 psia at 28 seconds; then the signal was lost.

Using the valve load orifice areas and the SPGG breech pressure, the theoretical values for P_s and P_o were calculated. When P_s was equal to 245 psia, the corresponding value for P_o should have been 82.5 psia. From Figure 16 at time 2.5 seconds, P_s was 245 psia and the corresponding value for P_o was 85 psia. The system was operating as expected at this time.

The temperature data for the thermal analysis test specimen are plotted in Figures 17, 18, and 19 as temperature versus time. The lack of data past 14 seconds was due to the failure of the system supply tube and the subsequent destruction of the thermocouple leads by the hot gas.

The data in each of the three figures represent temperature profiles of the three variations of laminate thickness. Figure 17 represents data from the upstream section. This section possessed the thickest carbon laminate and the thinnest silica phenolic laminate. In this section the backface of the tungsten liner (T_{12}) reached a temperature of approximately 3500°F at 9 seconds.

The data indicate that the temperature began to fall after this time, but this is not reasonable because the hot gas continued to flow through the test section. The heat transfer into the thermocouple junction was a combination of conduction and radiation. The conduction probably varied as thermal expansions caused relative motion between the junction and the surface under observation.

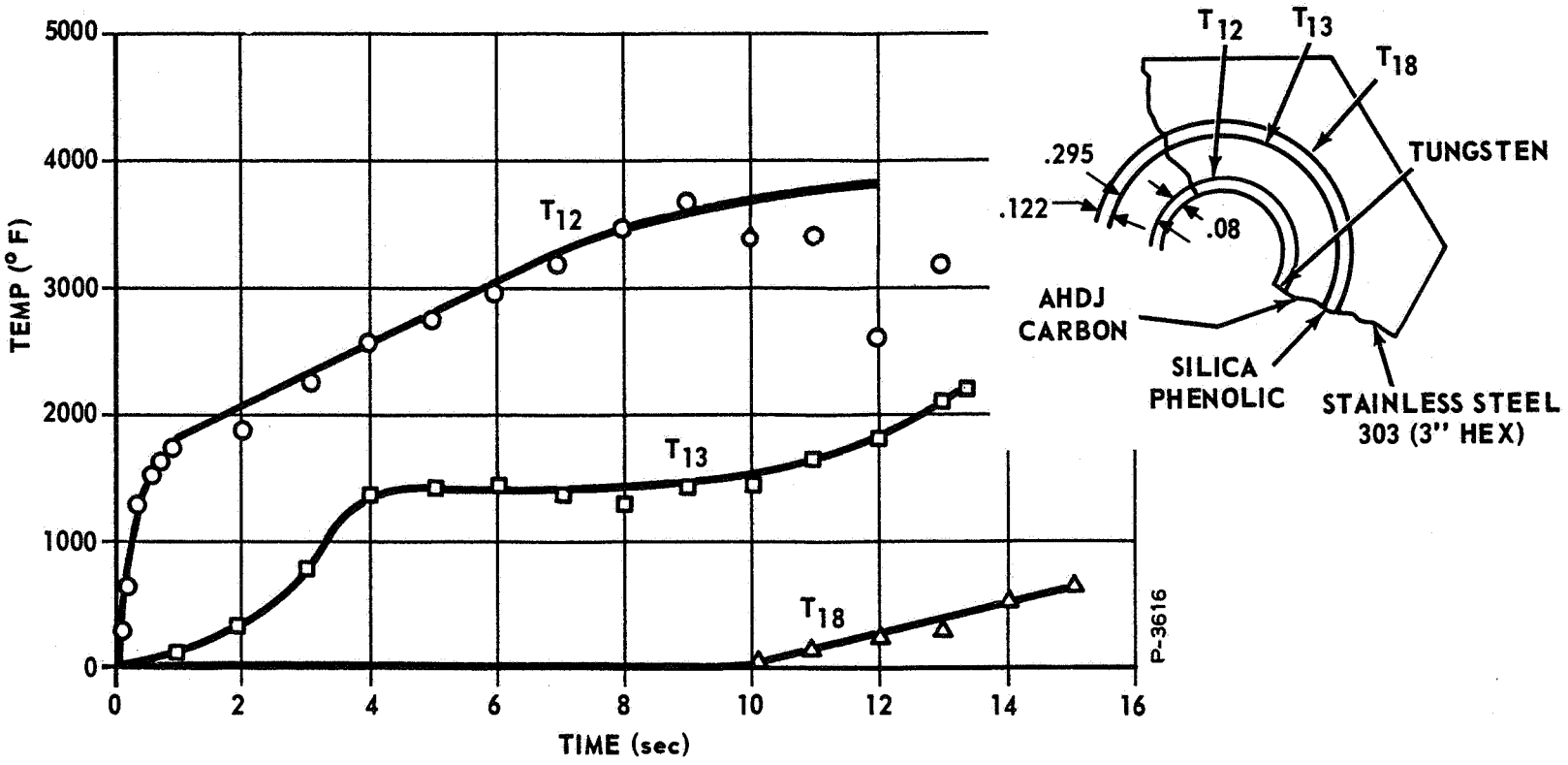

Figure 17 - Temperature Distribution Observed in a Laminated Cylinder
(Specimen No. 1)

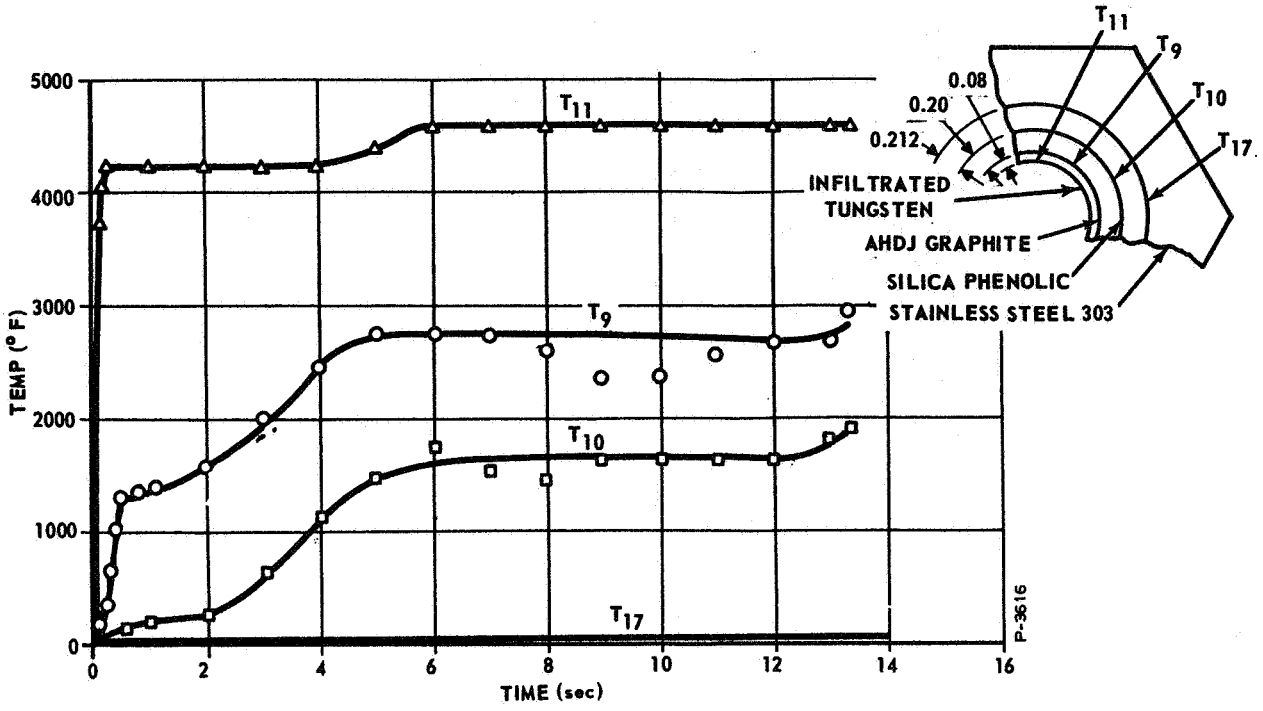

Figure 18 - Temperature Distribution Observed in a Laminated Cylinder (Specimen No. 2)

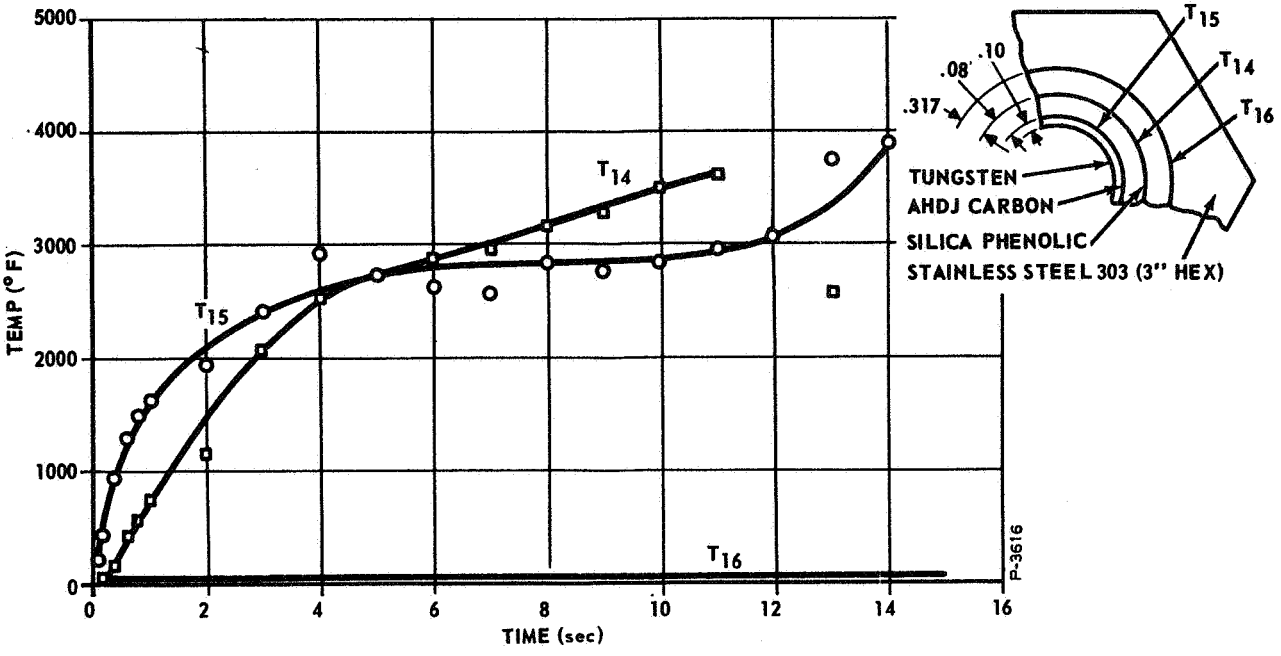

Figure 19 - Temperature Distribution Observed in a Laminated Cylinder (Specimen No. 3)

The data from the second section are shown in Figure 18. This section had carbon and silica phenolic laminates of approximately equal thickness. The tungsten liner backface temperature (T_9) in this section reached a temperature of 2800°F at 5 seconds. The temperature of the solid propellant hot gas (T_{11}) was also sensed and recorded in this section. The maximum recorded gas temperature was 4600°F.

The data from the third (downstream) section are shown in Figure 19. This section has the thinnest carbon laminate and the thickest silica phenolic laminate. The tungsten liner backface temperature (T_{15}) reached 2800°F at 10 seconds. The data indicate that the temperature at the carbon backface (T_{14}) exceeded T_{15} during part of the test; this condition is unreasonable and implies that the T_{14} thermocouple was not functioning properly at that time.

The post-test condition of the materials evaluation system and its components is shown in Figures 20, 21 and 22. The portion of manifold missing in Figure 20 is the system supply manifold. This manifold connected the thermal analysis test specimen to the 5500°F SPGG aft head. The system supply manifold failure was due to heavy erosion of the manifold's ATJ carbon and silica phenolic liners by the 5500°F solid propellant gas as it expanded from the SPGG load orifice.

The thermal analysis test specimen withstood the test well. The tungsten liners and insulation did not exhibit any erosion or distortion from the flow of hot gas.

The next element in the system manifolding was the flow divider. Heavy external erosion about the body and the flange was the result of the direct blast of solid propellant gas after the supply manifold failed. Internal erosion in the flow divider was not detectable.

The vent orifice was made from high density arc-cast tungsten. The condition of the orifice after the test indicated that arc-cast tungsten parts are adequate for this hot gas application.

The condition of the main stage valve after test is shown in Figures 21 and 22. The valve did not suffer from any structural failure such as erosion, cracking or warping but did accumulate considerable aluminum oxide. A solid core of aluminum oxide extended from the cone section, inside the end cap, through the valve supply tube. The conical section of the button was partially destroyed during disassembly. The aluminum oxide residue was thick, indicating low-velocity regions and cold surfaces.

Test Conclusions

The test data and hardware indicated that the main stage vortex valve started to plug with aluminum oxide at 2 seconds and was completely plugged at 11 seconds. The system supply manifold began to fail at 13.75 seconds and was completely severed into two sections 10 seconds later.

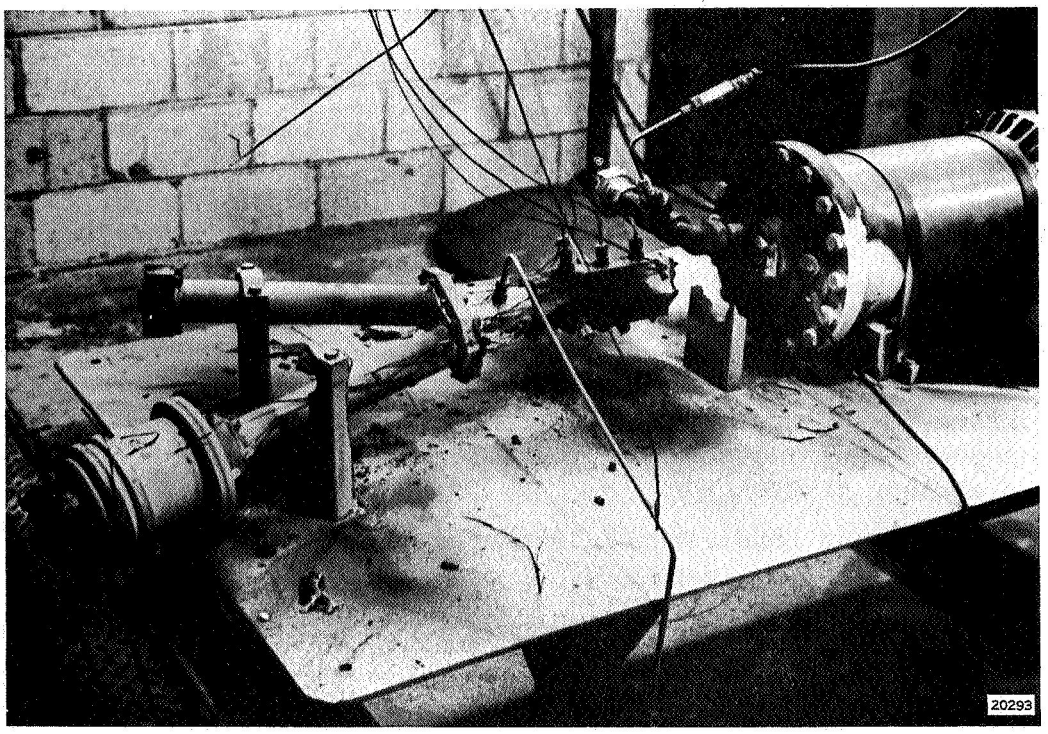

Figure 20 - Materials Evaluation System After Test (Hot Gas Test No. 1)

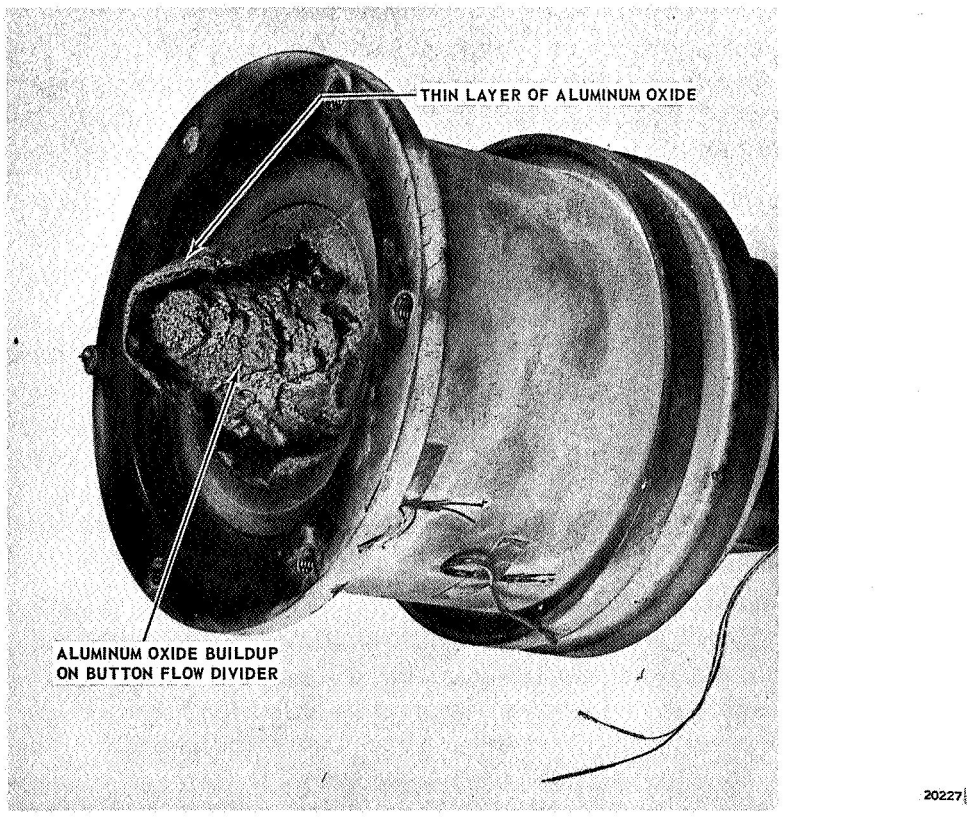

Figure 21 - 5500°F Vortex Power Valve Body and Internal Parts After Test

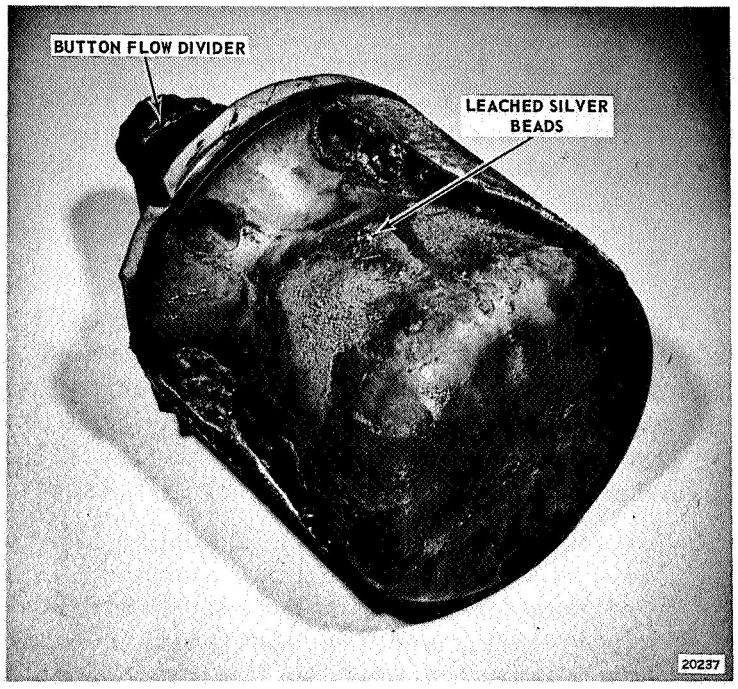

Figure 22 - 5500°F Vortex Power Valve Button Assembly After Test

The test results led to the following conclusions:

(1) The mass of the tungsten parts was too great and should be reduced to minimize the system heat sink.

(2) Carbon phenolic manifold liners should be utilized in place of carbon graphite liners to minimize heat transfer and to minimize manifold erosion.

(3) System Supply manifold lengths should be reduced to minimize heat loss from the hot gas.

SINGLE VORTEX VALVE SYSTEM PERFORMANCE TEST

(Hot Gas Test No. 2)

The system tested in Hot Gas Test No. 2 consisted of a single vortex valve system with a 2000°F pilot stage. The test objectives were to determine the structural integrity of the vortex valve design and its capability to modulate the flow of 5500°F aluminized gas using 2000°F nonaluminized gas for control.

System Description

The schematic of the system tested is shown in Figure 23, and the test setup is shown in Figure 24. The main stage vortex valve was supplied from a 5500°F SPGG which was fitted with a plenum chamber and vent orifice. The control gas for the main stage vortex valve was supplied by a 2000°F SPGG. The control gas flow and pressure were regulated by a vented poppet-type valve actuated by nitrogen controlled by a solenoid valve.

In the main stage vortex valve, the vortex chamber, the button assembly, the outlet orifice, and the valve plenum chamber liner all were made from silver-infiltrated tungsten. The material used for the orifice retaining plate, the valve port ring, end cap, and valve housing was 300 series stainless steel. The insulation used in the valve construction consisted of carbon phenolic, silica phenolic, and ATJ graphite. The control flow injectors were made from TZM molybdenum.

The plenum chamber and vent orifice assembly were fabricated by welding together a modified 5500°F SPGG aft closure and plenum chamber-supply tube assembly made from 1020 carbon steel. The face of the aft closure was lined with asbestos phenolic, and the plenum chamber was lined with silica phenolic. The supply tube liners and the vent orifice insulation were made from carbon phenolic. The orifice isolators were made from ATJ graphite, and the vent orifice was made from tungsten. All of the insulation and the vent orifice, except for the supply liners, were bonded in place with a high-temperature epoxy cement.

Test Results

Prior to the system hot gas test, the system and all components were cold gas performance tested. All of the system components functioned as predicted, and the main stage vortex valve had a turndown performance of 5.55 to 1 at a control-to-supply pressure ratio of 1.40.

The test schematic is shown in Figure 25. Modulation of the control pressure, P_C, was provided by a solenoid valve that opened and closed a vent control valve.

The results of the system cold gas test are shown in Figure 26. Variation of P_C by a square wave input to the solenoid valve caused the valve supply pressure, P_S, to vary as predicted from 965 psia to 515 psia,

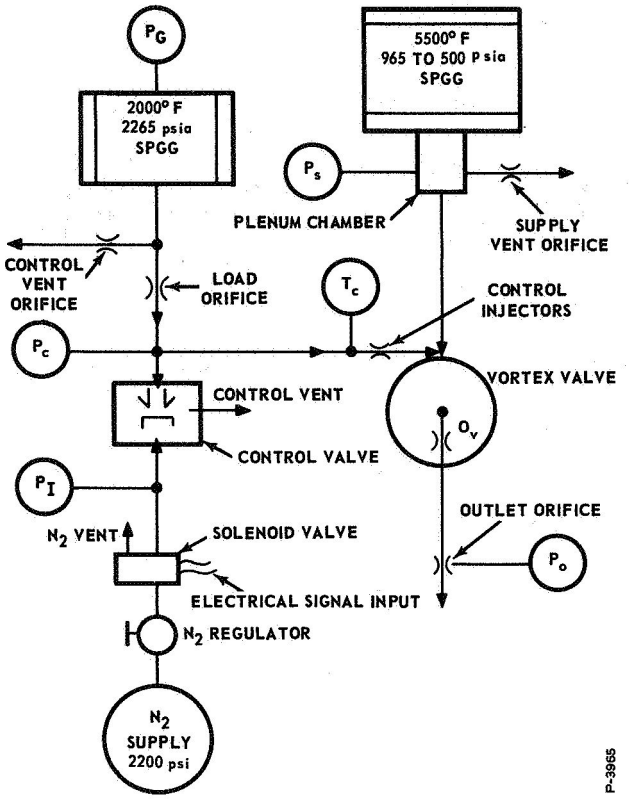

Figure 23 - Hot Gas Test Schematic of 5500°F Single Vortex Valve System

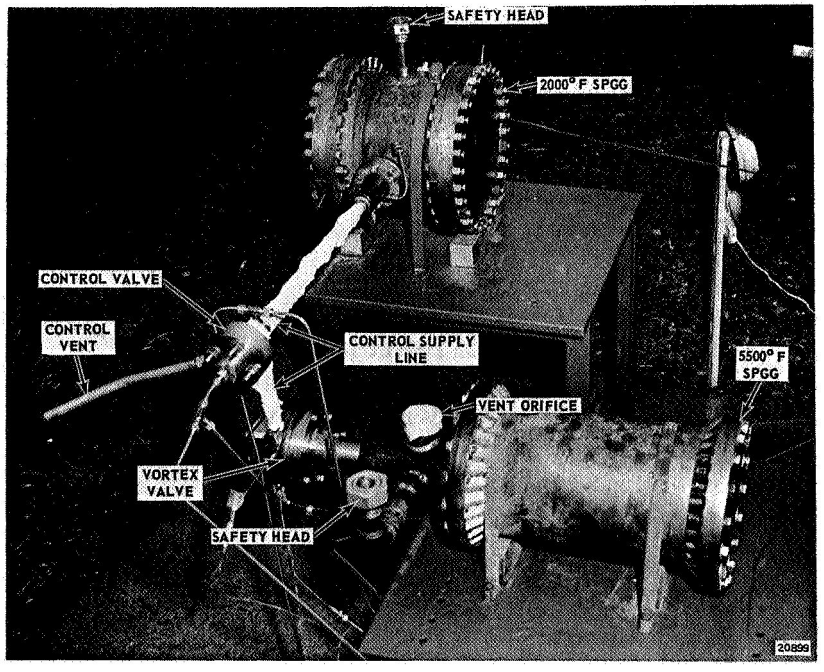

Figure 24 - 5500°F Single Vortex Valve System (Hot Gas Test No. 2)

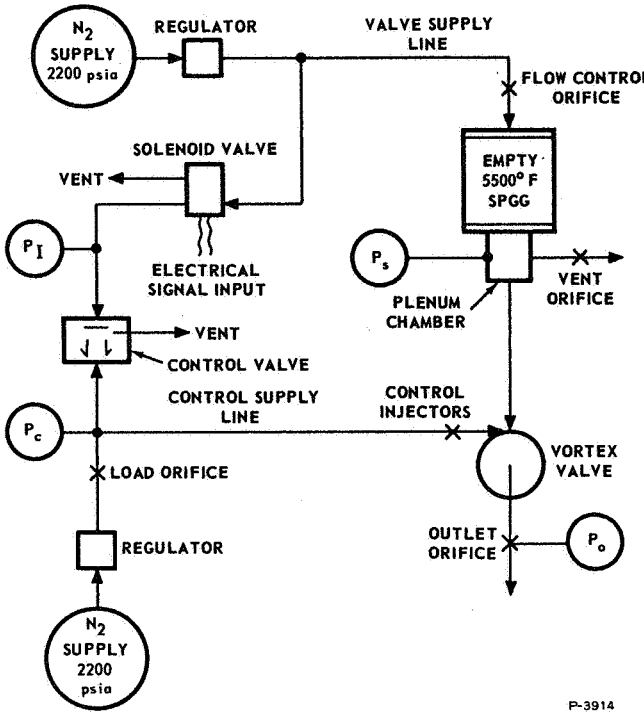

Figure 25 - Test Schematic for Cold Gas Test of 5500°F Single Vortex Valve System

with a resulting variation in P_o from 165 psia to 255 psia. The corresponding flow modulation from this test was 1.8 to 1. The lag in the non-square pressure outputs, P_s, P_o and P_c, from the square wave pressure input, P_I, was caused by the relatively large volume under compression in the valve supply line and the response characteristics of the vent control valve.

All of the hot gas test objectives were not met because of the misfire of the 2000°F SPGG, which was to provide the system's control flow. The misfire was caused by an open circuit in the 2000°F SPGG ignitor circuit. The hot gas test results were obtained with only the 5500°F SPGG in operation.

The test data are plotted in Figure 27. This is a plot of P_s and P_o versus time, starting with the ignition of the 5500°F SPGG as time zero. The low level of P_s for the first 2 seconds indicates that the 5500°F grain may not have been burning over the full face. At 2 seconds after ignition, P_s rose rapidly from 285 to 360 psia, indicating that the SPGG began operating normally at this point. An insufficient booster charge is believed to be the probable cause of this apparent partial face burning.

At time 3 seconds, the pressures stabilized at P_s = 360 psia and P_o = 150 psia. Using the values of P_s and P_o and cold gas flow calibration data, the flow through the vortex valve was found to be:

$$\dot{W}_o = 0.45 \text{ lb/sec} @ P_o = 150 \text{ psia}$$

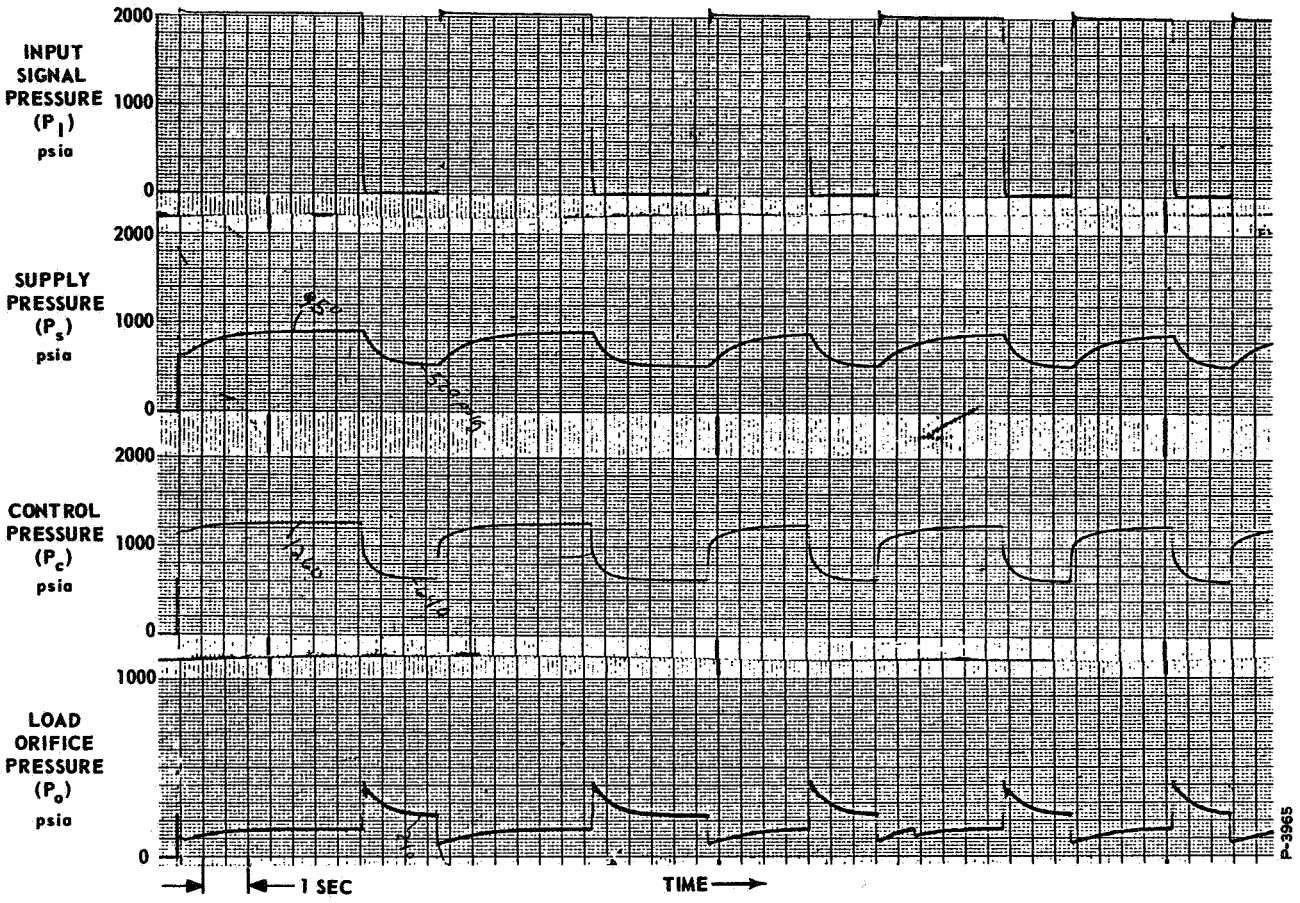

Figure 26 - Single Vortex Valve System Cold Gas Test Results

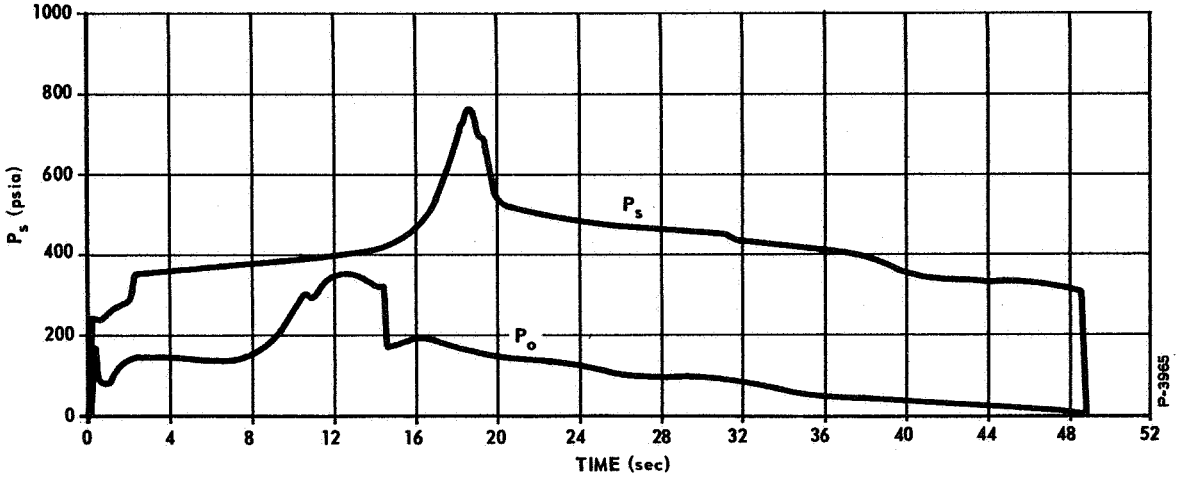

Figure 27 - 5500°F Single Vortex Valve System Test Results
(Hot Gas Test No. 2)

$$\dot{W}_o = 0.42 \text{ lb/sec} \; @ \; P_s = 360 \text{ psia}$$

This comparison indicates that P_o provided a good correlation of the vortex valve output flow rate. With P_s = 360 psia, the SPGG output, $\dot{W}_g$, and the vent orifice output, $\dot{W}_{v.o.}$, were found to be:

$$\dot{W}_g = 0.832 \text{ lb/sec}$$

$$W_{v.o.} = 0.35 \text{ lb/sec}$$

The SPGG output flow ($\dot{W}_g$ = 0.832 lb/sec) is the sum of the vent orifice flow and the flow to the vortex valve. Thus,

$$\dot{W}_g = \dot{W}_o + \dot{W}_{v.o.}$$

$$= 0.45 + 0.35$$

$$\dot{W}_g = 0.80 \text{ lb/sec}$$

This result indicates that the test data provided good flow correlation between all of the active system components.

At time 4 seconds, P_o started a slight decline while P_s began a moderate rise which lasted to 14 seconds. This condition appears to have been the result of a reduction in the flow area through the vortex valve caused by the forward displacement of the button face due to plastic deformation. As the space between the button and the outlet hole decreases, the flow is restricted and the resulting increase in pressure drop across the button face causes further forward motion and supply pressure rise.

At time 14 seconds, the rate of increase of P_s became more rapid until, at 18.6 seconds, P_s reached a maximum value of 760 psia and then began a rapid descent to 500 psia at 22 seconds. This rapid pressure rise was the result of the continued reduction in valve flow area caused by button face deflection. The rapid decrease in pressure was caused by the opening of a hole through the middle of the button, which relieved the restriction caused by thermal expansion.

The vortex valve body and end cap suffered no ill effects from the hot gas test. The valve control port ring was slightly eroded on the inner

surface from the backflow of 5500°F gas through the injectors. This backflow occurred because the control pressure, which would have prevented the backflow, was lost when the 2000°F SPGG failed to operate.

While the control ring was only slightly eroded, the control flow injectors were damaged extensively by the backflow of 5500°F gas. The evidence of backflow was seen by the aluminum deposits on the upstream end of the injectors and around the control port annulus. The plenum chamber and vent orifice housing remained in good general condition throughout the test.

The carbon phenolic insulation material used throughout the test system survived very well. The valve supply tube insulation successfully contained the flow of 5500°F aluminized gas for the duration of the test with only normal erosion. This supply tube was constructed in two sections, each with a different fabrication method. The upstream section was molded with the laminates perpendicular to the tube center line. The downstream section was molded with the laminates at a 30-degree angle to the center of the tube. From the appearances of tube cross-section, the tube section with laminates at 30 degrees to the tube center line provided the best resistance to erosion.

One unexpected result from the test was the high strength of carbon phenolic char. It was expected that as the carbon phenolic charred, and the mating tungsten parts tried to expand, the carbon phenolic char would crush and not resist the expansion of the tungsten parts. This did not happen, and the tungsten parts yielded plastically and were distorted. This distortion of the tungsten vortex chamber could have been one of the causes for the restriction in the vortex valve flow area, resulting in rapid supply pressure buildup prior to the button failure. The chamber distortion was attributed to the restraining of the outside diameter by the carbon phenolic during the heatup and the soft plastic condition of the tungsten material when it is at operating temperature.

The tungsten button assembly failed in two places. The hot gas burned a hole through the cone-shaped leading edge and through the flat face of the button assembly as shown in Figure 28. It appears that the cone-shaped leading edge failed first with a long delay before the trailing edge failed. This delay was deduced from evidence of erosion around the button body bleed holes as shown in Figure 29. This erosion pattern appears to have been produced when there was simultaneous flow through the bleed hole and over the outside of the button. This particular flow condition would be most prominent when there was a hole in the button leading edge and when the trailing edge was intact.

One major objective of the valve design tested was that the critical gas flow passages should remain free from undesirable aluminum oxide buildup. This objective was accomplished as is indicated by the open flow passages shown in Figure 28. The outlet portion of the valve remained in good general condition, with only a small aluminum accumulation in the bottom of the valve plenum chamber. Aluminum also was deposited at the control injectors by the backflow of 5500°F gas through the injectors.

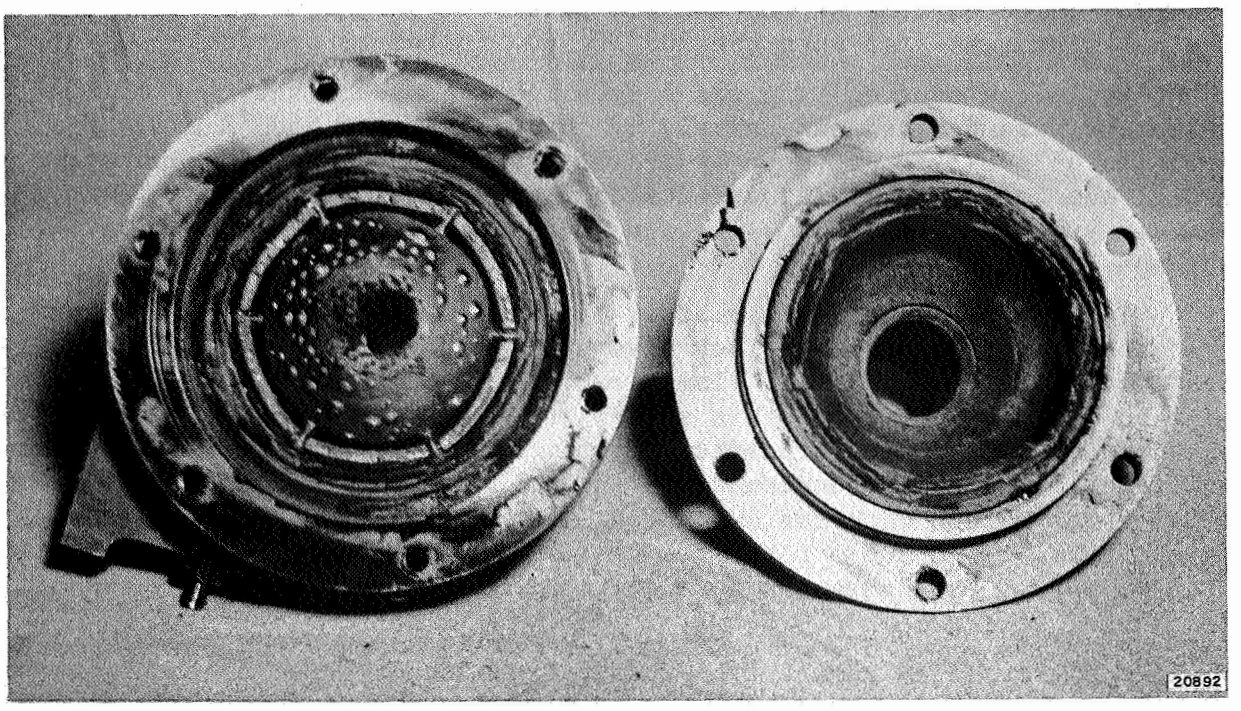

Figure 28 - Valve End Cap, Body, and Button

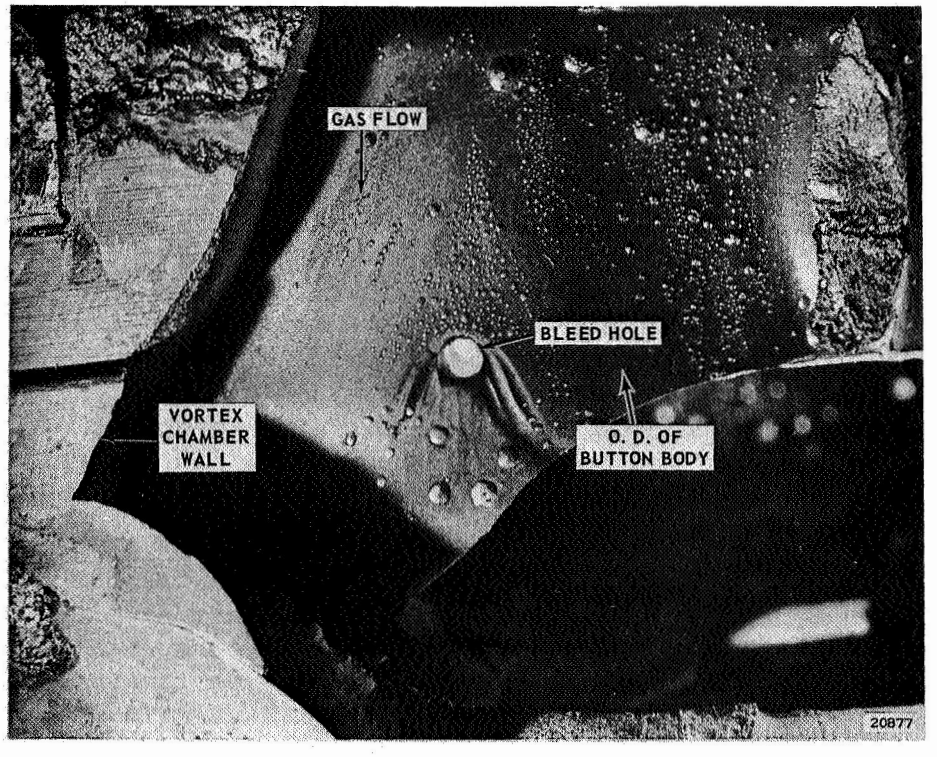

Figure 29 - Valve Button Body Air Bleed Hole

Test Conclusions

The following conclusions were drawn from Hot Gas Test No. 2.

(1) The redesigned vortex valve eliminated the aluminum oxide buildup about the button, the vortex chamber, and the approach section to the vortex valve.

(2) The plastic condition of the tungsten parts and the lack of aluminum oxide deposit indicate that the system operating temperature was achieved early in the test.

(3) The orientation of the insulating fabric lay does affect erosion resistant properties.

(4) Design modifications of the vortex valve are required to prevent tungsten part distortion and button burnthrough.

SINGLE VORTEX VALVE PERFORMANCE TEST

(Hot Gas Test No. 3)

The system tested in Hot Gas Test No. 3 consisted of a single vortex valve and a 2000°F pilot stage. The test objectives were to demonstrate the modulation of 5500°F highly aluminized hot gas flow and to evaluate the third design configuration of the main stage vortex valve.

System Description

The system tested (Figures 30 and 31) in the third hot gas test was basically the same system as tested in the second hot gas test except for the redesigned main stage vortex valve. The vortex chamber, the button body, the valve load orifice and plenum chamber, and the support ring were all made from silver-infiltrated tungsten. All of the insulation used in the valve construction was carbon phenolic. The materials used for the orifice retaining plate, the valve end cap, the valve housing, and the outlet pressure pickup adaptor were 300 series stainless steel. The valve button assembly consisted of the carbon silica phenolic button cap retained to the silver-infiltrated tungsten button body by two press-fit forged tungsten pins. The vortex valve control injectors were made from TZM molybdenum.

Test Results

The cold gas tests of the system and components were as predicted. The cold gas test results were the same as obtained in the previous cold gas tests.

During the hot gas test, all of the single-vortex-valve system components performed their intended functions for the duration of the test. Hot gas flow modulation performance of the system was less than expected. The test data obtained are shown in Figures 32 and 33. Figure 32 is a reproduction of the actual data as recorded on a strip chart. Figure 33 is a plot of vortex valve control pressure, P_c, supply pressure, P_s, and outlet pressure, P_o, versus test time, t.

The 5500°F SPGG performance for this test was compared with the SPGG performance of the two previous Bendix hot gas tests and with the manufacturer's ballistics test and projected performance. This comparison was made by plotting grain burn rate, r, versus SPGG mean burn pressure, $\bar{P}$, on log-log coordinates as shown in Figure 34. This comparison indicates that the 5500°F SPGG varies from the manufacturer's predicted performance at low burn pressures.

At recorded time of 1.6 seconds, the 2000°F SPGG ignited. After 1.8 seconds of burning, the SPGG pressure, P_g, dropped to 1900 psia and remained relatively constant at this value. The SPGG average burn pressure was 1900 psia for a total burn time of 33.4 seconds. The average

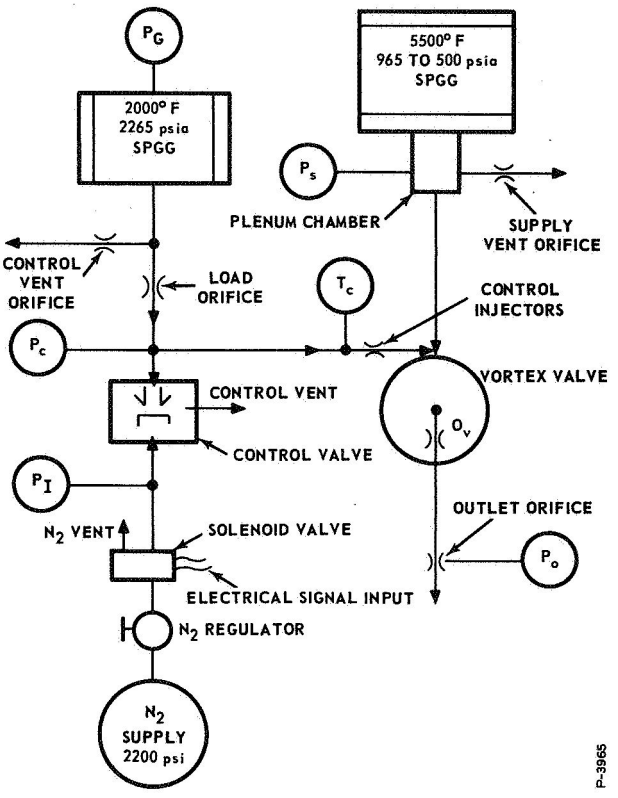

Figure 30 - Test Schematic, Hot Gas Test No. 3, 5500°F Single Vortex Valve System

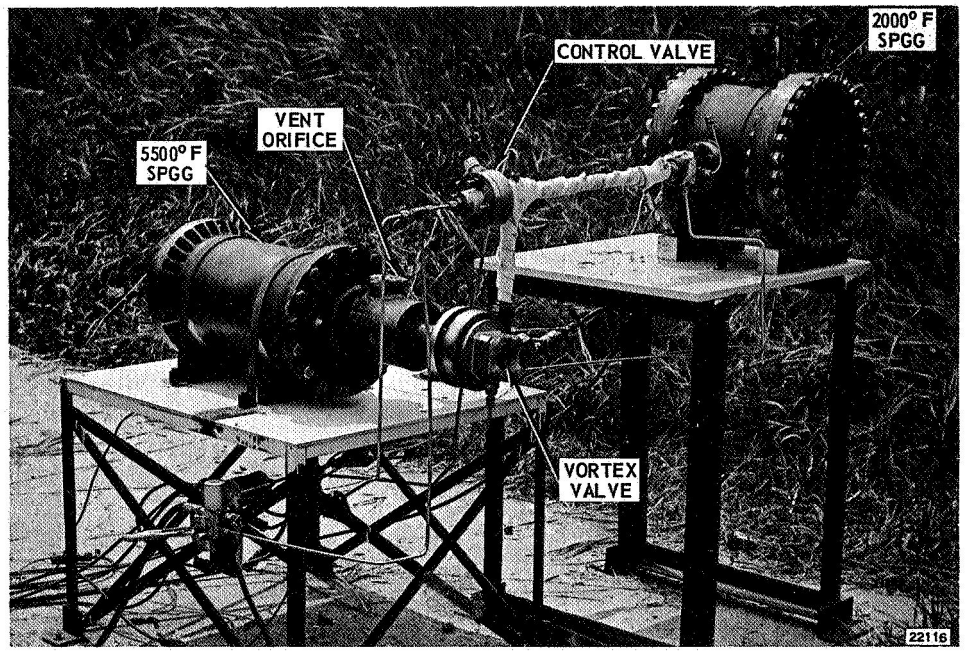

Figure 31 - 5500°F Single Vortex Valve System Hot Gas Test Arrangement (Hot Gas Test No. 3)

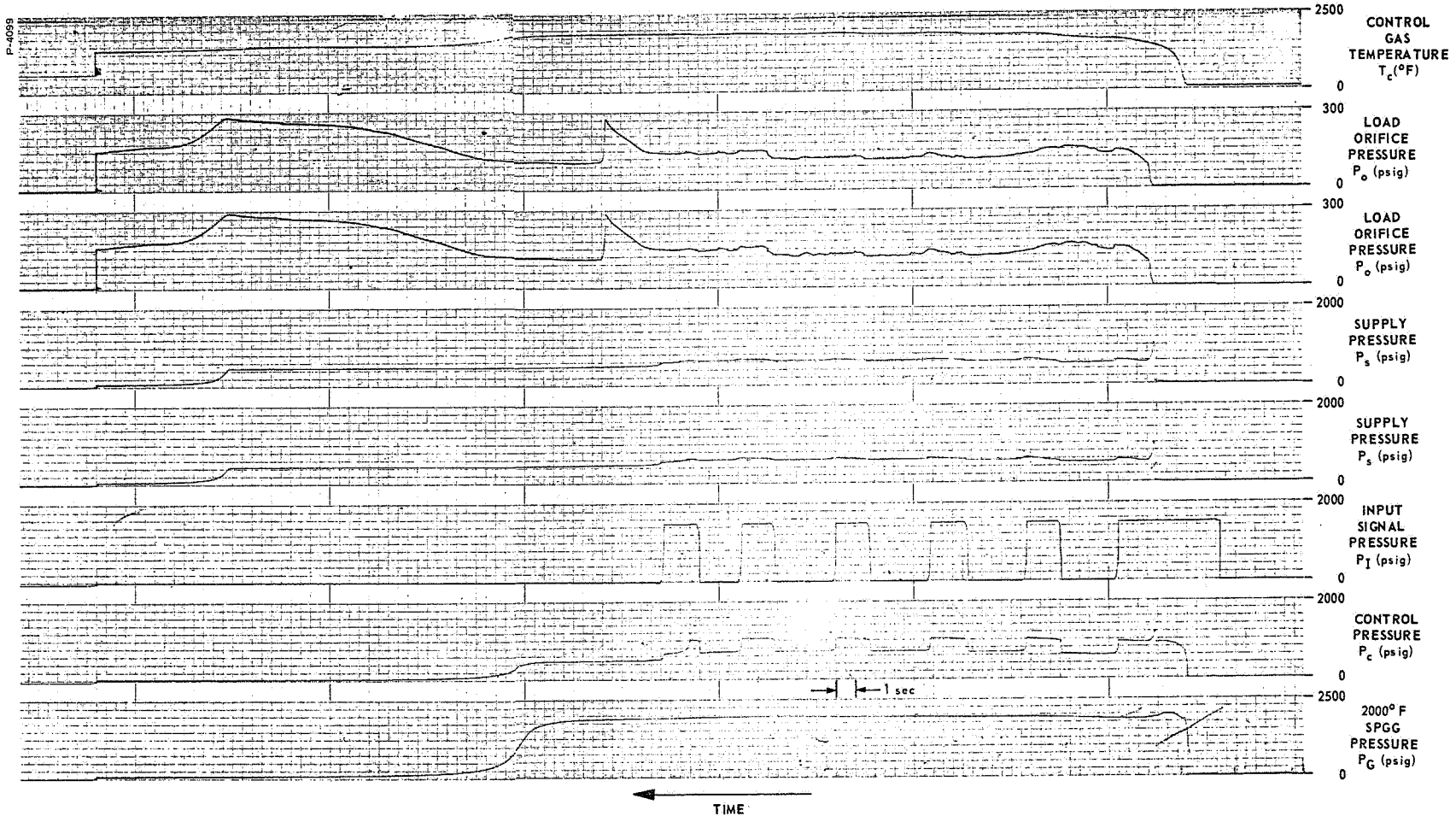

Figure 32 - Recording of 5500°F Single Vortex Valve System Test Results (Hot Gas Test No. 3)

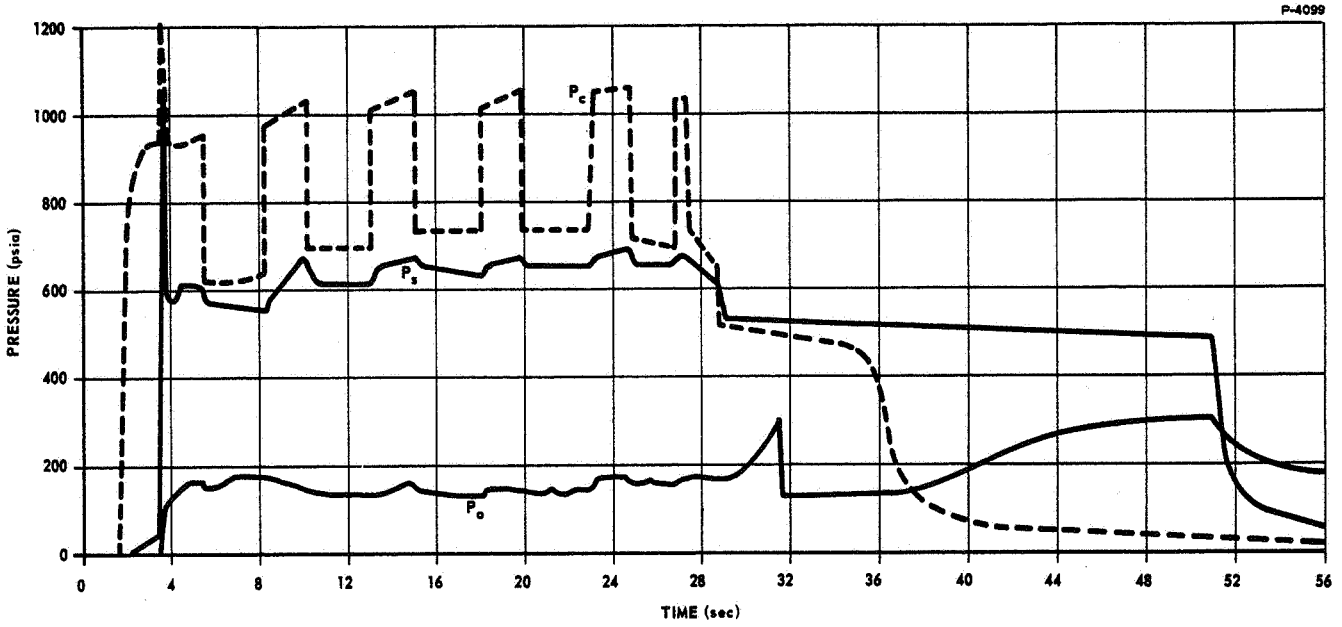

Figure 33 - Pressure-Time Plot of 5500°F Single Vortex Valve System Test Results (Hot Gas Test No. 3)

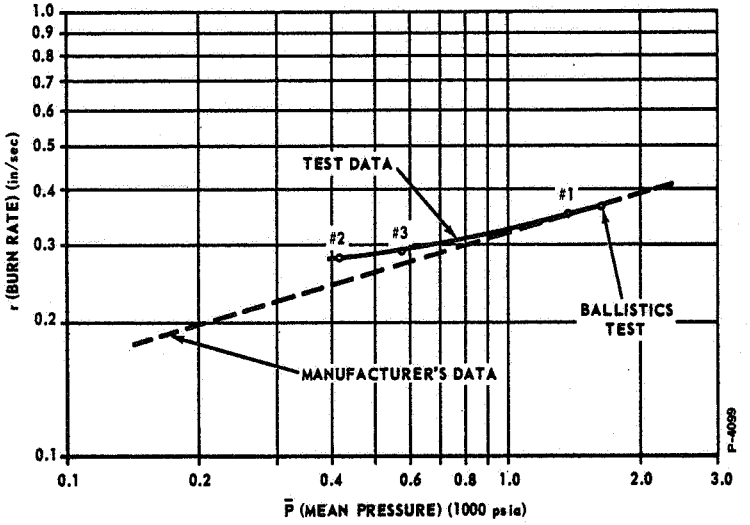

Figure 34 - 5500°F SPGG Performance

SPGG pressure, P_g, was lower than the intended pressure of 2265 psia. This lower SPGG pressure, P_g, was the reason that the vortex valve control pressure, P_c, never reached its calculated value of 1235 psia.

At 3.4 seconds, the 5500°F SPGG ignited and produced a pressure spike of 1050 psia. At 5.4 seconds, the system started its first modulation cycle, which lasted 10 seconds. The remaining four cycles were similar to the first cycle.

In compiling a flow balance between the system's various components at various test times, the fact became apparent that P_o did not provide satisfactory flow correlation for the vortex valve. This is illustrated by reviewing the test data at time 8 seconds. At this time, the 5500°F SPGG had an outlet flow of 0.87 lb/sec and the vent orifice was flowing 0.52 lb/sec. These figures indicate that the vortex valve was receiving 0.35 lb/sec of hot gas. The cold-gas test data indicated that the vortex valve flow for P_o = 175 psia should be 0.96 lb/sec. Thus, P_o as an indicator of valve flow did not correlate with the other flow measurements.

The first modulation cycle, from time 5 seconds to 11 seconds, is reproduced in Figure 35. Also shown in the figure is the theoretical value of P_s for corresponding test values of P_c. At time 8 seconds, the actual P_c/P_s ratio was 1.14 and the apparent vortex valve turndown was 1.43 to 1. At this time, a P_c/P_s ratio of 1.25 was predicted and the corresponding valve turndown should have been 1.54 to 1. Thus, the hot gas turndown was 7% less than the theoretical turndown at this time.

At time 10 seconds, P_c/P_s (actual) was equal to 1.5 and the resulting apparent valve flow turndown was 1.42 to 1. The calculated value for P_c/P_s was 1.3, which would have resulted in a predicted turndown ratio of 4.05 to 1. Thus, the hot gas turndown was 65% less than the theoretical turndown at this time. This low main stage vortex valve performance is attributed to the hot gas erosion of the valve control injectors as indicated by a post-test examination.

The generally good post-test condition of the vortex valve is shown in Figure 36. The vortex valve load orifice and the vent orifice remained open with no distortion. The only exterior portion to suffer any ill effects from the hot gas test was the vortex valve control port ring. This part burned through in two places and distorted into a barrel shape. This failure was due to backflowing of the 5500°F vortex valve supply gas through the control injectors after the burnout of the 2000°F SPGG. Evidence of this supply gas backflow was aluminum oxide buildup on the upstream side of the injectors.

The interior of the main stage vortex valve was in far better condition than after the previous hot gas tests. The valve button did not suffer burnthrough but did show some erosion. None of the tungsten parts experienced expansion distortion or burnthrough, and the valve remained free from aluminum oxide buildup. The only parts of the valve

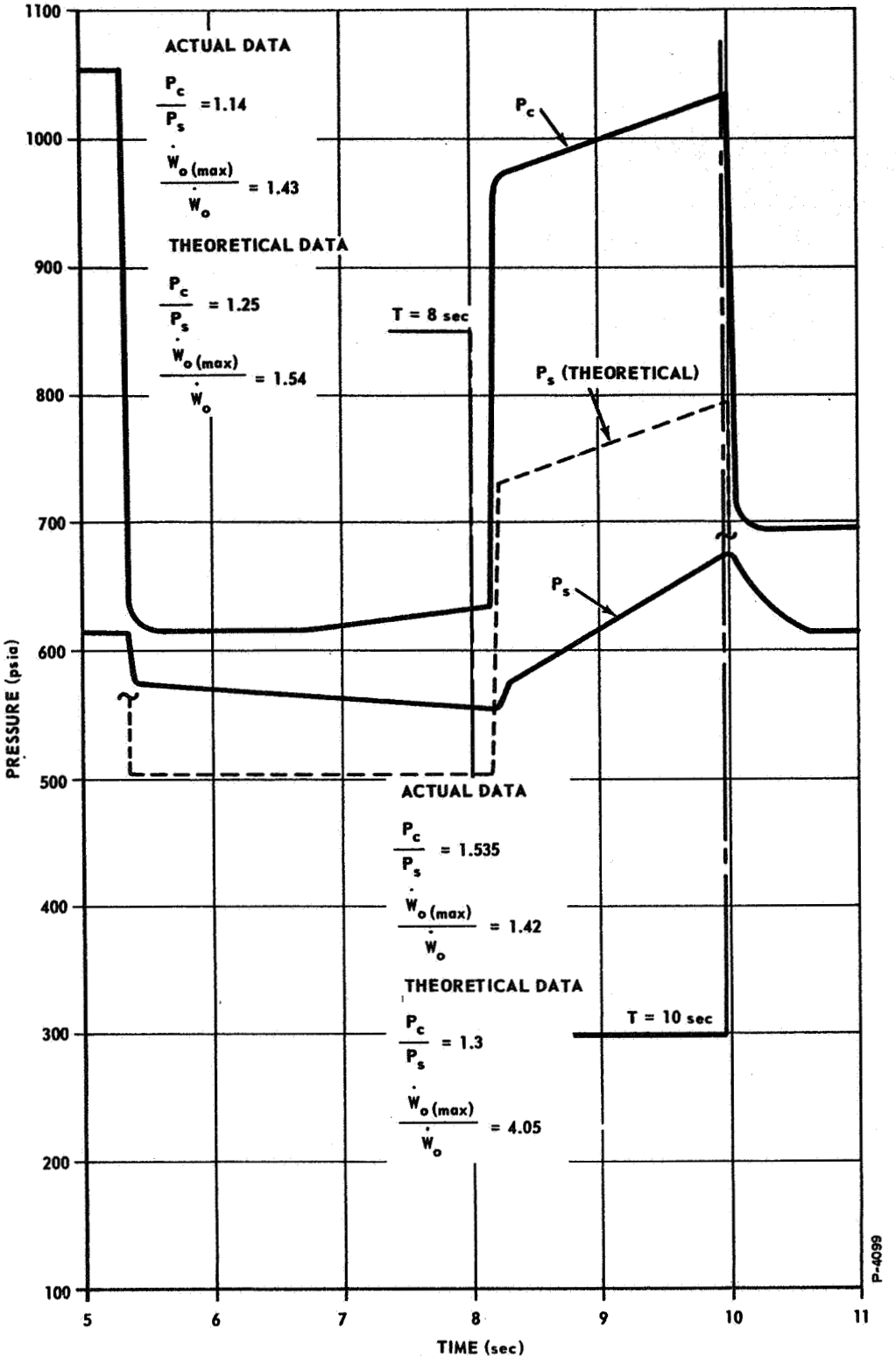

Figure 35 - First Modulation Cycle of Hot Gas Test No. 3

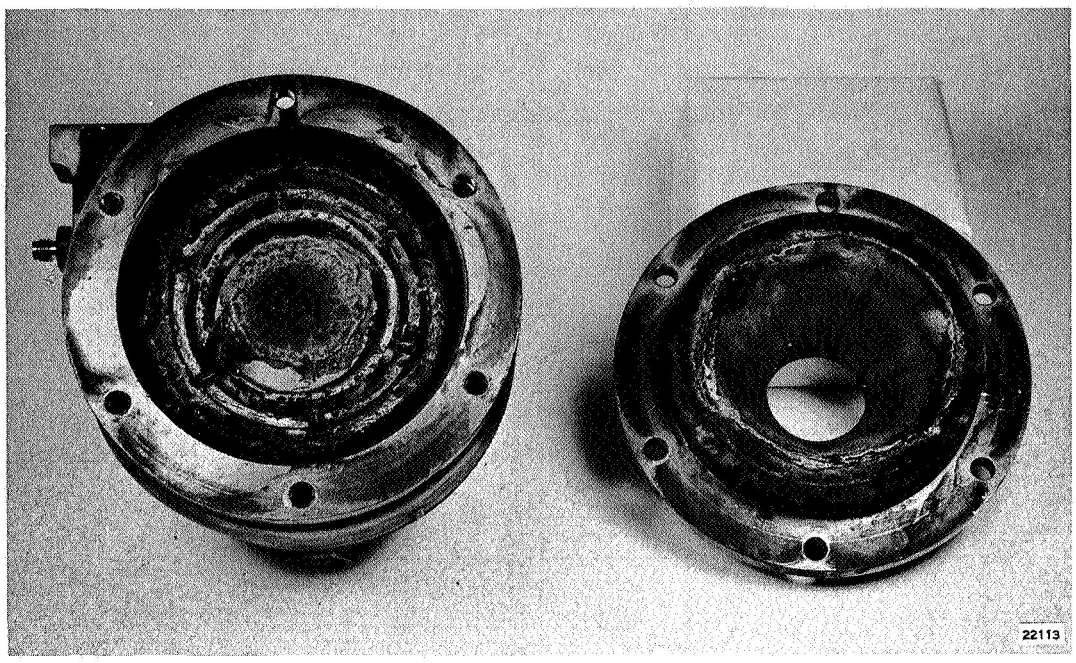

Figure 36 - Vortex Valve and End Cap

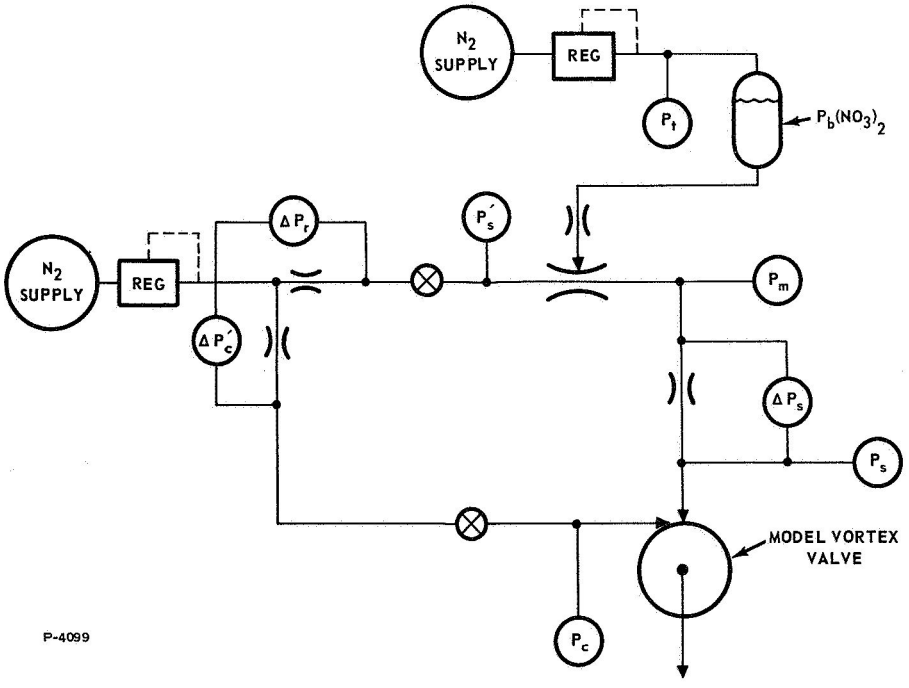

Figure 37 - Test Schematic

to fail were the control injectors. The injectors were eroded approximately 0.75 inch back from the vortex chamber wall. The cause of the loss of the injectors is that molybdenum has too low a melting temperature for this application.

Post-Test Evaluation

After Hot Gas Test No. 3, a post-test evaluation was made to determine the reasons for the low hot gas performance of the main stage vortex valve. Two possible reasons for the low performance were investigated.

(1) The loss of control injectors may have caused sufficient degradation of the interaction of the control and supply flow momentums to produce low vortex valve performance.

(2) The 2000°F control gas may not have imparted sufficient control momentum to the aluminum oxide particles in the supply gas to produce the desired flow modulation. It was possible that the 2000°F control gas acted only on the gaseous products and not on the droplets of molten aluminum oxide in the 5500°F supply gas.

These possibilities were investigated by a computer simulation of vortex valve performance and by cold gas tests.

The vortex valve computer simulation as shown in Appendix A, Figure 80, indicates how the temperature of the control gas affects the vortex valve performance. The main stage vortex valve as tested should have produced a flow modulation of at least 3.56 to 1.

Two cold gas tests were run to evaluate the possible reasons for low hot gas vortex valve performance. The first test was run to determine the effect of heavy particles in the supply gas. This was accomplished by operating a representative model of the main stage vortex valve and comparing performance, first, with nitrogen as both the control gas and supply gas and, second, with the supply gas being a mixture of nitrogen and lead nitrate solution. The lead nitrate was introduced into the nitrogen supply gas to simulate the aluminum oxide particles in the 5500°F hot gas. It was not clear what effect the heavy aluminum oxide particles had on the vortex flow field. A distinct possibility existed that the particles would not follow the vortex field streamlines because of their inertia.

The test was run utilizing the schematic shown in Figure 37. The results of the test and a base line test conducted with pure nitrogen control and supply gas are shown in Figure 38. These tests indicated that heavy particles in the vortex valve supply gas had little effect on the valve performance.

The second test was conducted to evaluate the effect of eroded control injectors. This test was run with pure nitrogen control and supply gas and utilized a vortex valve with control injectors modified as shown in Figure 39. The results of this test, which also are shown

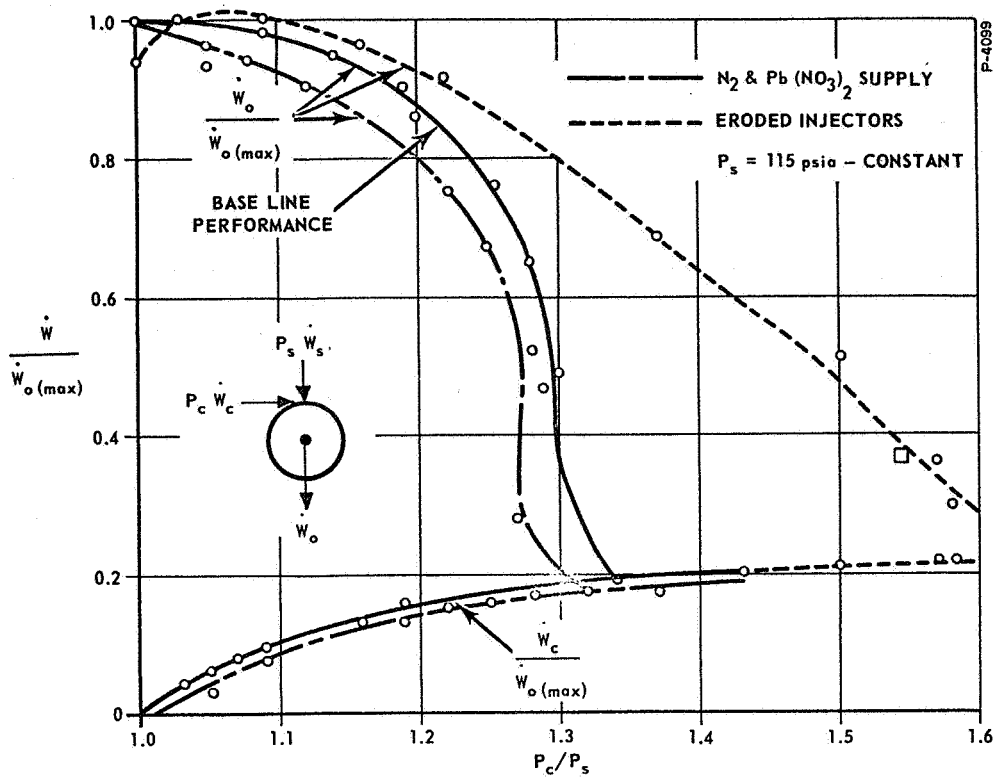

Figure 38 - Performance Characteristics of a Model Vortex Valve

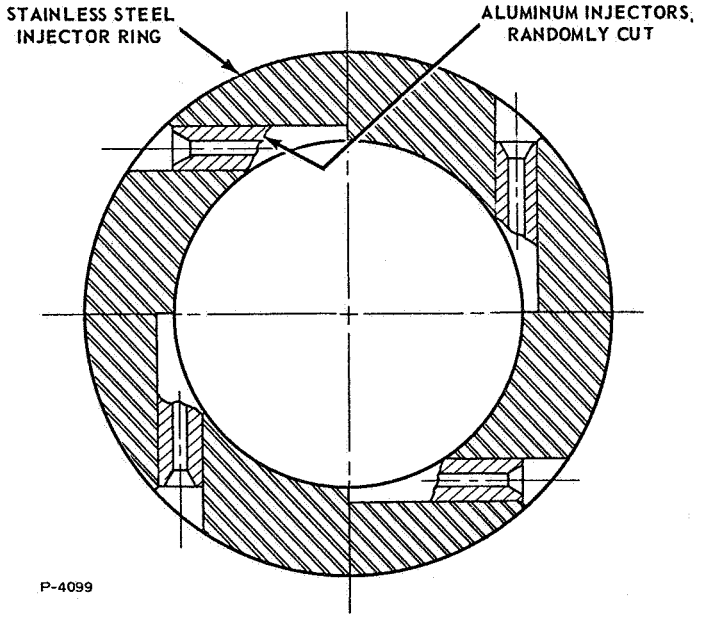

Figure 39 - Model Vortex Valve Injector Modification

in Figure 38, indicate that the eroded control injectors seriously affect vortex valve performance and increase the required control pressure to turn down the vortex valve.

The conclusion is that the low main stage vortex valve performance observed was due to the erosion of the valve control injectors.

5500°F PUSH-PULL SYSTEM TEST

(Hot Gas Test No. 4)

The fourth hot gas test was conducted to demonstrate the flow modulation of highly aluminized 5500°F solid propellant gas with vortex valve controlled push-pull system hardware (as might be employed in a SITVC system), and to verify the structural integrity of the system design.

System Description

The 5500°F push-pull system schematic, shown in Figure 40, consisted of one 5500°F and two 2000°F solid propellant gas generators, a pilot stage comprising two vortex amplifier valves controlled by a torque motor and flapper-nozzle valve, two main stage vortex valves, a specially designed check valve, a relief valve, and plenum chambers and manifolding

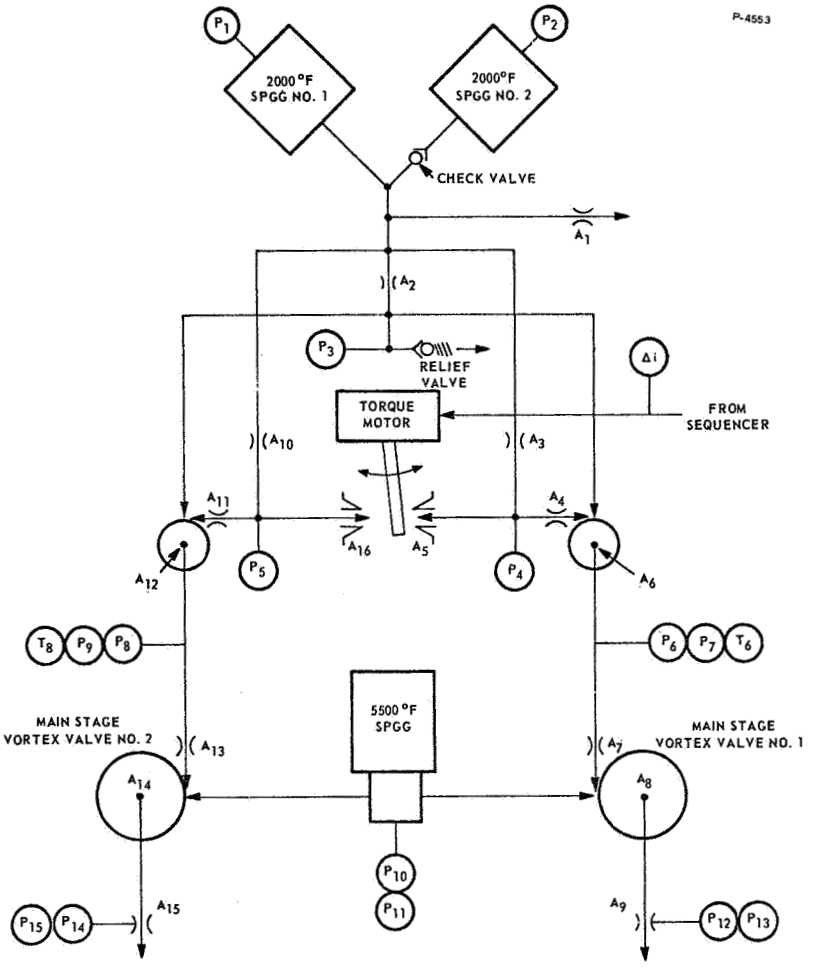

Figure 40 - Test Schematic for 5500°F Push-Pull System
(Hot Gas Test No. 4)

The two main stage vortex valves were mounted 180 degrees apart on opposite sides of the 5500°F SPGG plenum chamber. The pilot stage was mounted above the 5500°F SPGG plenum chamber and connected to the main stage vortex valves with tube manifolds. The pilot stage was supplied from the two 2000°F SPGG's, which were fired in sequence in order to extend the pilot stage operating time beyond the 5500°F SPGG operating time to prevent the backflow of hot gas into the pilot stage.

The configuration of the two main stage vortex valves as utilized in Hot Gas Test No. 4 is shown in Figure 41. The valve component materials are: 303 stainless steel housing; RA-330 (AMS-5716) stainless steel control flow annulus rings and control manifold; carbon phenolic and graphite phenolic insulation; Viton "O" rings; and 15% silver-infiltrated tungsten liners and control injectors.

The system was operated by firing 2000°F SPGG No. 1 with the pilot stage torque motor flapper in null position. After 2 seconds, the 5500°F SPGG was ignited. The pilot stage was pressurized first to prevent the backflowing of the 5500°F aluminized gas into the pilot stage. After 2 seconds of 5500°F SPGG operation, the torque motor began receiving its pre-programmed operation signals. The torque motor controlled the pilot stage vortex amplifier valves, which, in turn, controlled the main stage vortex valves.

Test Results

The cold gas tests of the system and its components were conducted with the test arrangement diagrammed in Figure 42. The tests verified the predicted performance. On nitrogen gas the main stage vortex valves demonstrated a flow modulation range of 5 to 1 at a control-to-supply pressure ratio of 1.4. A portion of the system cold gas test data with a system input signal of 0.5 cps is shown in Figure 43.

The main stage vortex valve output flow was determined by P_8 and P_9. The fact that the system outputs, P_8 and P_9, were distorted sine waves was due to the characteristic nonlinear shape of the main stage vortex valve turndown curve.

The 5500°F push-pull system duty cycle used for the fourth hot gas test is shown in Figure 44.

The capability of the vortex valve to modulate the flow of highly aluminized 5500°F gas is shown in the form of film strips in Figure 45. These film strips show a portion of a cycle of each main stage vortex valve operation. The film strips are segments of the test movies, from different cameras, and both segments have a common time base. The complete test movies indicated that each main vortex valve modulated the flow of 5500°F gas through 14 cycles of operation at a rate of 5 cps. During the remainder of the test, the vortex valves flowed equal amounts of 5500°F gas.

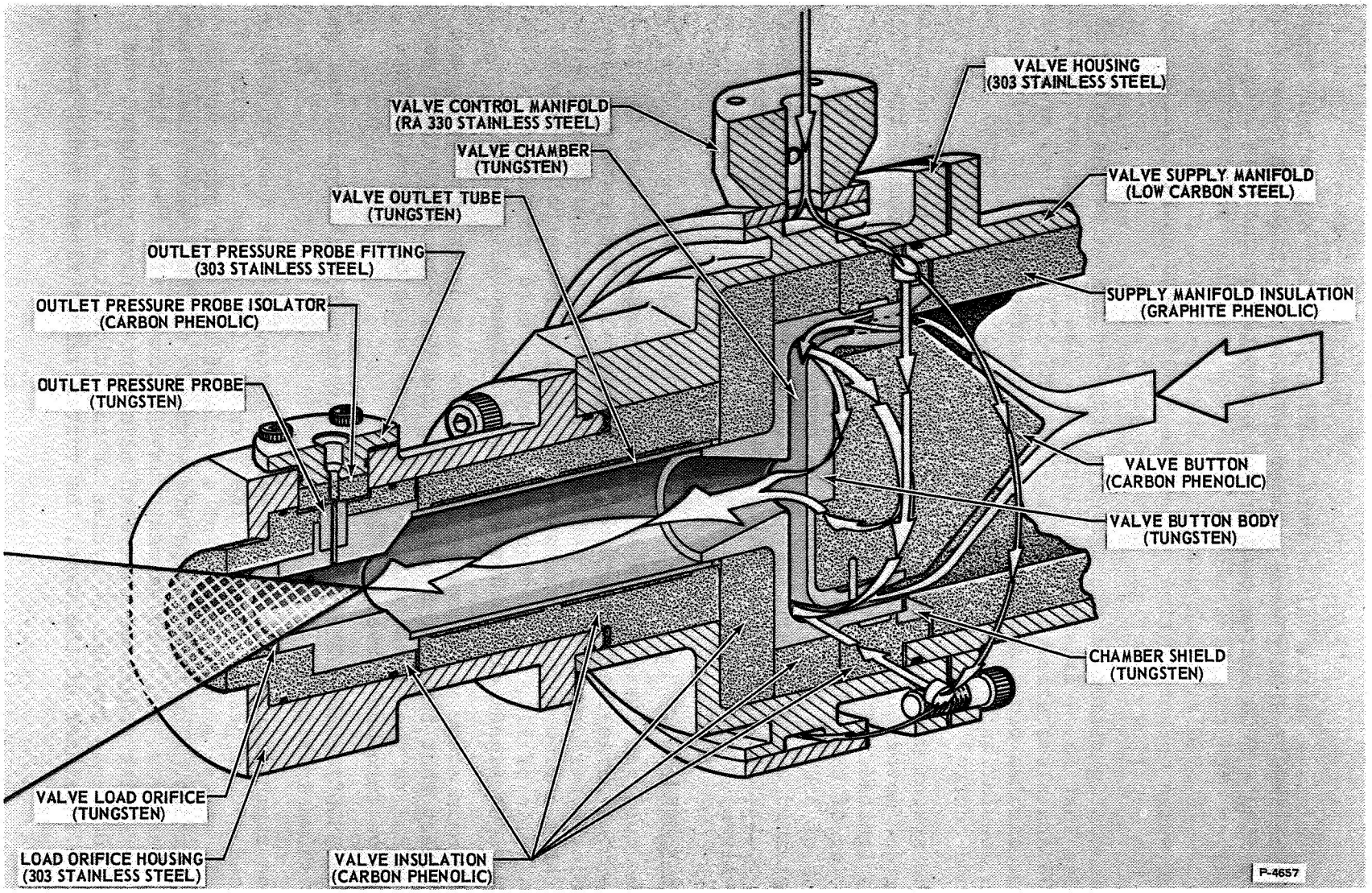

Figure 41 - 5500°F Vortex Valve with Flow Measurement Orifice

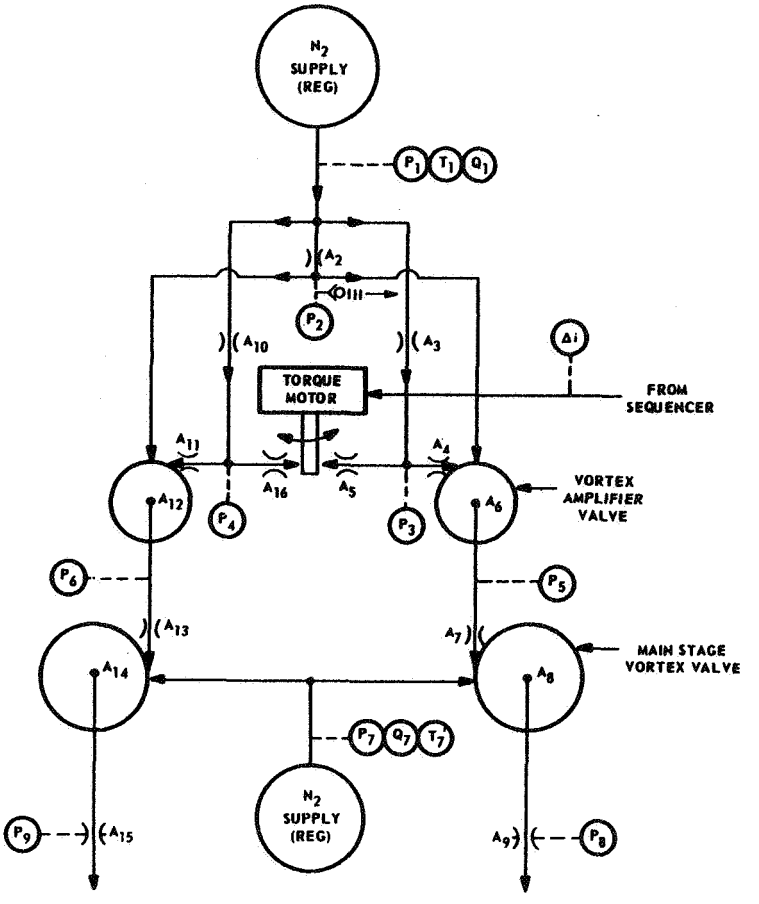

Figure 42 - Test Schematic for Cold Gas Test of 5500°F Push-Pull System

The recorded test data are shown in Figures 46 and 47. A portion of the data was not obtained during the test because of instrumentation malfunction. The data lost were the main stage vortex valve supply and outlet pressures, P_{10} through P_{15}. The loss of this data prevented the calculation of the main stage vortex valve actual hot gas turndown performance. The cause of the instrumentation malfunction was that instrument grease in the pressure transducer lines became too viscous during the pre-test preparation because of the low ambient temperature. This grease had been used in all previous tests to protect the pressure transducers during system startup, and no problems were encountered when ambient test temperatures were higher than at the time of this test.

The reason the main stage vortex valves ceased to modulate the flow of 5500°F gas after 14 cycles of operation was the development of leaks in the pilot stage. The leaks initially occurred in the control section of the pilot stage vortex valves. These leaks produced a decrease in the pressure level of P_4 and P_5 (see Figure 40) at test time 4 seconds. The decrease in P_4 and P_5, or the loss of the pilot stage control pressure,

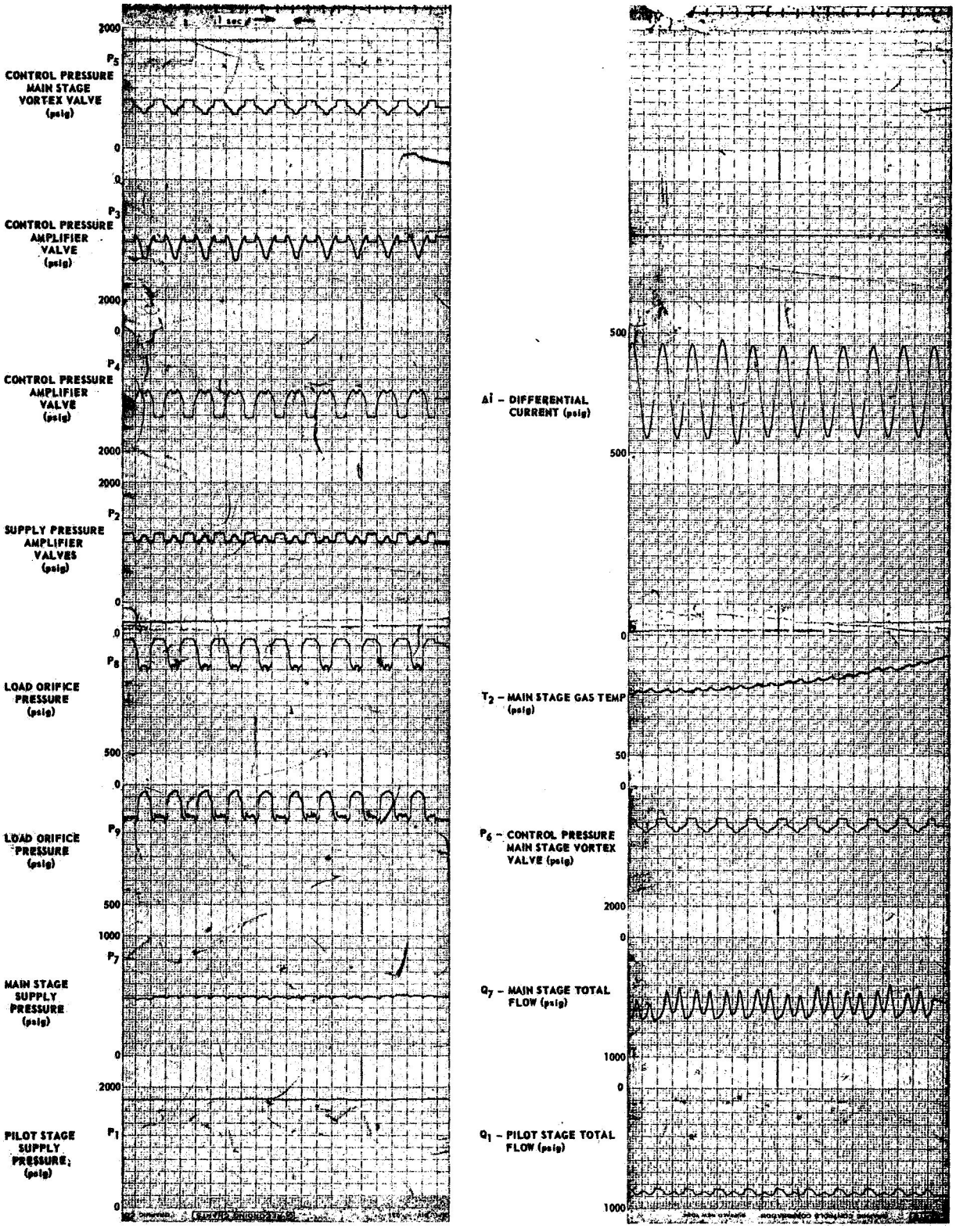

Figure 43 - 5500°F Push-Pull System Cold Gas Test Results

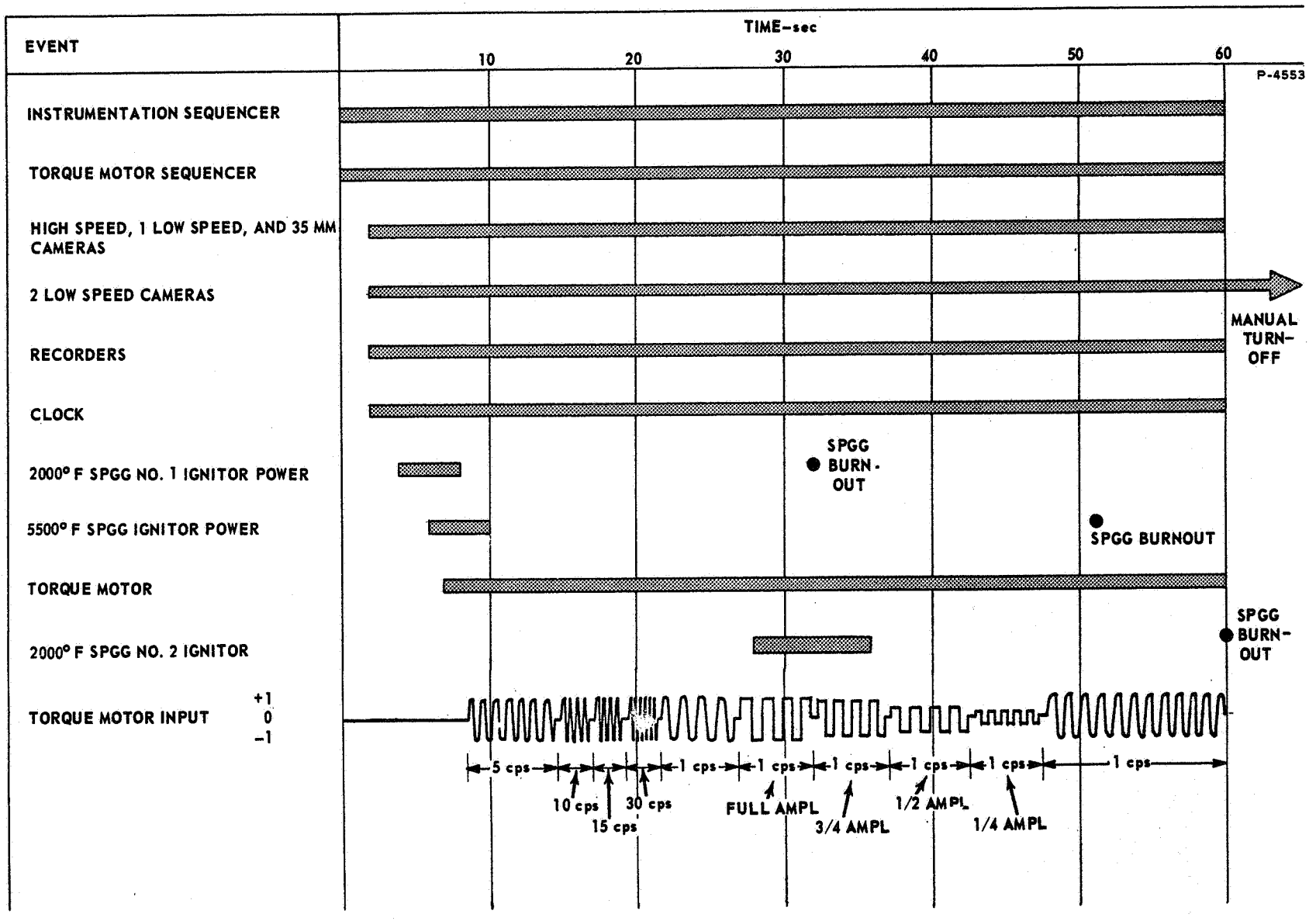

Figure 44 - Duty Cycle for Hot Gas Test No. 4

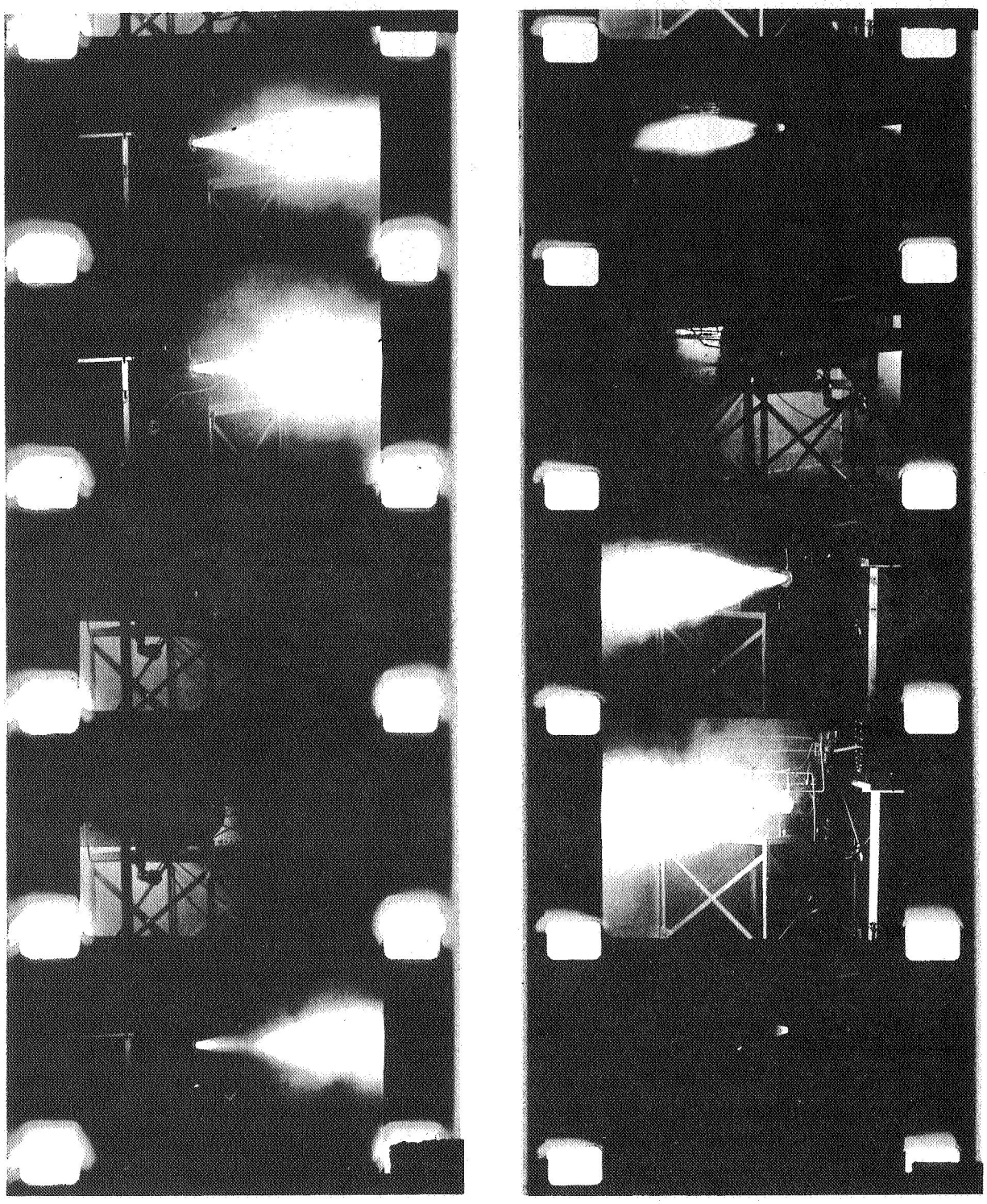

MAIN STAGE VORTEX VALVE NO. 1

MAIN STAGE VORTEX VALVE NO. 2

Figure 45 - 5500°F Push-Pull System During Operation

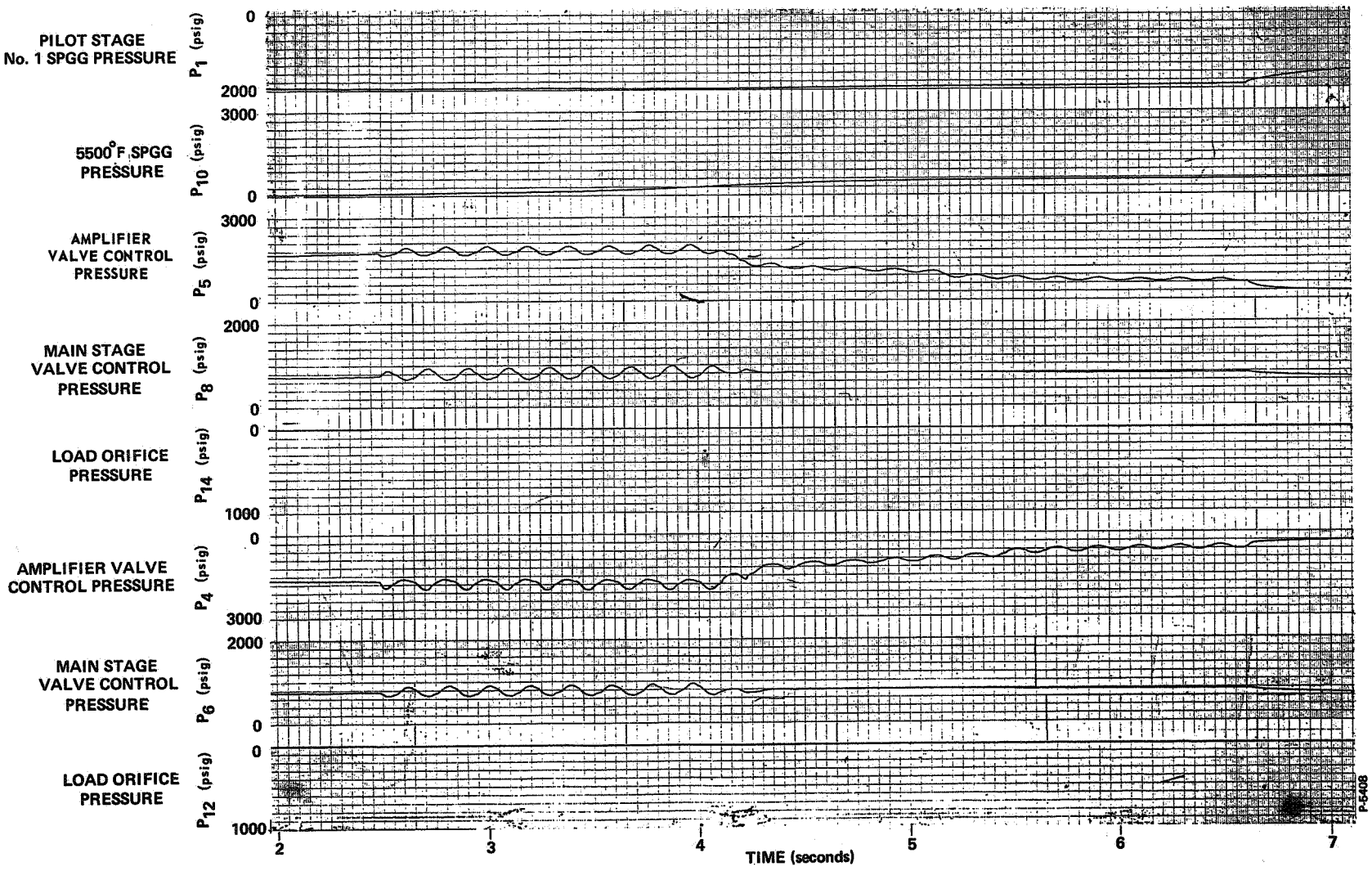

Figure 46 - Recorded Data of 5500°F Push-Pull System Hot Gas Test No. 4
(Sheet 1)

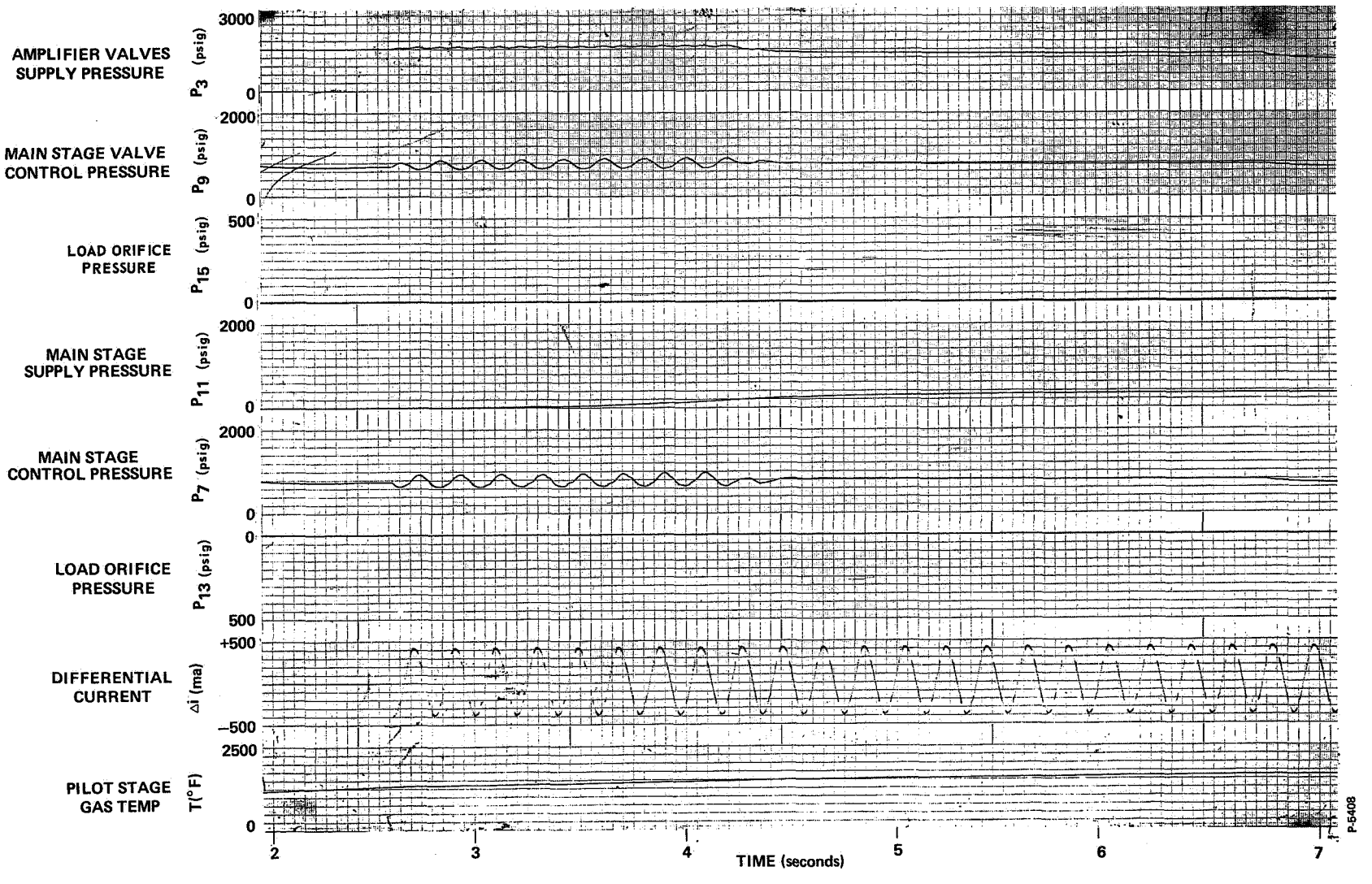

Figure 47 - Recorded Data of 5500°F Push-Pull System Hot Gas Test No. 4
(Sheet 2)

caused the pilot stage outputs, P_6 and P_8, to remain constant. With the pilot stage outputs constant, the main stage vortex valves ceased to modulate the flow of 5500°F gas, but continued to flow the hot gas in a partial turndown mode until the No. 1 2000°F SPGG burned out.

By utilizing the available recorded test data and the test movies, the sequence of test events of the system was concluded to be:

Time	Event
0 sec	2000°F SPGG No. 1 ignited.
1.5 sec	5500°F SPGG ignited.
2.5 sec	First main stage valve turndown cycle began.
4.0 sec	Pilot stage vortex valve control pressure began to drop because of a leak between orifices A_3 and A_5, and between orifices A_{10} and A_{16}.
5.3 sec	Last of the main stage vortex valve turndown cycles. The valves began to flow equal amounts of 5500°F gas in a partial turndown mode.
6.5 sec	2000°F SPGG breech pressure began dropping because of a leak upstream of orifices A_3 and A_{10}. This leak was the result of the loss of two threaded plugs in the pilot stage housing.
32 sec	2000°F SPGG No. 1 began its burnout, and 2000°F SPGG No. 2 ignited but burst its safety head and failed to pressurize the pilot stage because the check valve stuck.
34 sec	The control manifold for the main stage vortex valve No. 1 began to burn through because 5500°F gas was backflowing into the control manifold as the result of low pressure in the pilot stage after the burnout of 2000°F SPGG No. 1.
45 sec	The 5500°F SPGG began its burnout

Hot Gas Test No. 4 provided evidence of the main stage vortex valve structural integrity. Figures 48 and 49 show one of the main stage vortex valves during disassembly. Figure 49 shows a cross-section of the inside of one of the vortex valves. These pictures show that the main stage vortex valves were able to contain the flow of 16% aluminized 5500°F solid propellant gas for 43.5 seconds of test time without any tungsten distortion, burnthrough, excessive aluminum oxide buildups, or excessive insulation erosion.

Test Conclusions

The 5500°F SITVC System Hot Gas Test No. 4 demonstrated the ability of the vortex valve to contain and modulate the flow of 16% aluminized 5500°F solid propellant gas.

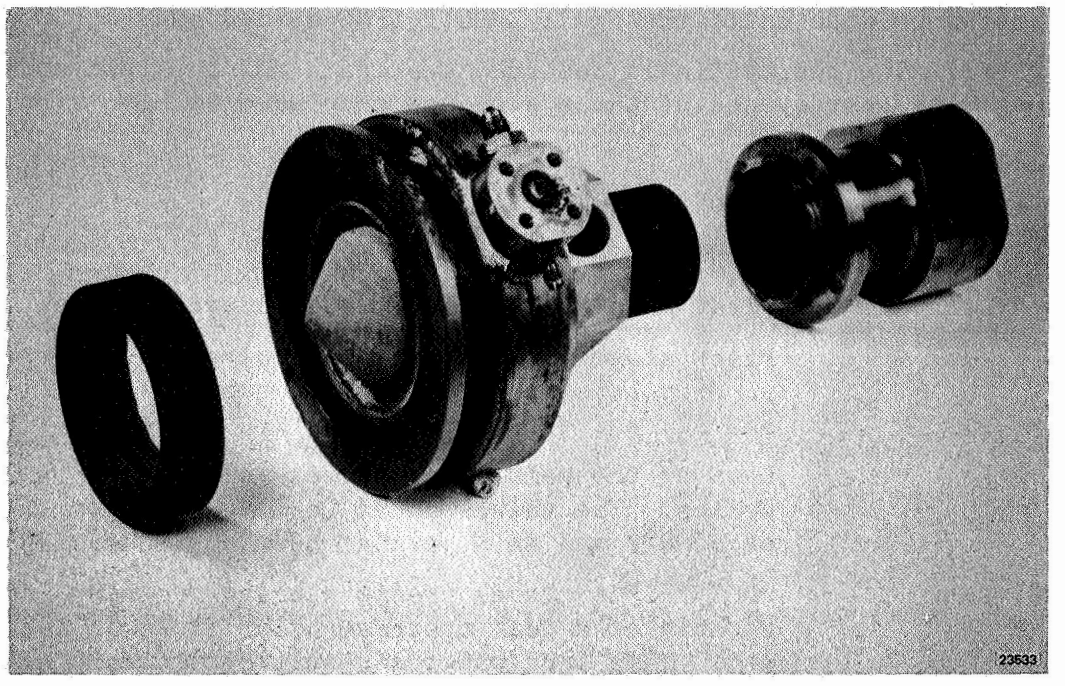

Figure 48 - 5500°F Push-Pull System Vortex Valve No. 1 (Post-Test Disassembly)

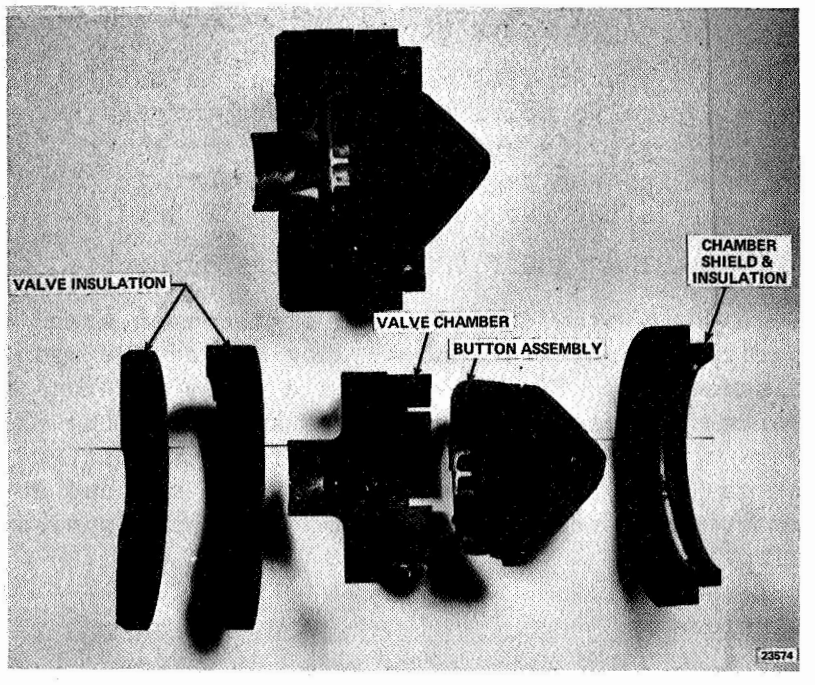

Figure 49 - 5500°F Vortex Valve Button and Chamber (Post-Test Disassembly)

From the available test information, the performance results of Hot Gas Test No. 4 were concluded to be:

(1) The main stage vortex valves are able to modulate the flow of 5500°F highly aluminized solid propellant gas from 0.95 lb/sec to zero.

(2) The vortex valves modulated the flow of 5500°F gas through 14 cycles of operation at a rate of 5 cps.

(3) The vortex valves operated in a partial turndown mode for 26 seconds after the valves' control signal stopped modulating.

(4) The 5500°F SPGG burned for 45 seconds at an average pressure of 1000 psig and an average flow rate of 0.95 lb/sec.

(5) The 2000°F SPGG No. 1 burned for 32 seconds at an average pressure of 2240 psia and an average flow rate of 1.01 lb/sec.

5500°F PUSH-PULL SYSTEM TEST

(Hot Gas Test No. 5)

The fifth hot gas test was conducted to determine the hot gas performance of the 5500°F push-pull system and the main stage vortex valves, and to verify the system capability of handling highly aluminized 5500°F solid propellant gas.

System Description

The system tested was basically the same as that tested in the fourth hot gas test. The system pilot stage contained a torque motor, a flapper-nozzle valve assembly, and two vortex amplifier valves. The pilot stage orifices, flapper, nozzles, and the vortex amplifier valves were constructed from molybdenum. The pilot stage body and manifolds were made from a high nickel content stainless steel, and all of the pilot stage seals were annealed copper crush-type ring seals.

Test Results

The complete 5500°F push-pull system was cold gas tested utilizing the schematic shown in Figure 50. Nitrogen was supplied to the pilot stage valves at 1815 psia, and to the main stage valves at 520 psia. The system cold gas tests were run at pressures lower than the expected hot gas test pressures because of pressure limitations of the cold gas source. The results of the test are shown in Figures 51 and 52. A tabulation of the test results at various frequencies, which compares the design values with the observed test results and the projected test results, is shown in Table 2. The cold gas test data was modified by the ratio of P_1 (cold gas test) to P_1 (theoretical) and recorded as projected data for comparison with hot gas test results. The test results indicated that the observed pressures were very close to the predicted design values. The test schematic and duty cycle for the fifth hot gas test are shown in Figures 53 and 54, respectively.

Hot Gas Test No. 5 demonstrated the ability of the system to modulate the hot gas flow and to withstand the highly erosive gas. Movies of the test show that the output flow of each main stage valve was being modulated. However, the data which would have shown the output flow variation of the main stage valves were not recorded because the pressure ports became plugged by the aluminum oxide present in the hot gas.

The recorded test data are shown in Figures 55 and 56. The test data indicate that the 5500°F SPGG and 2000°F SPGG No. 1 both operated at lower pressures than expected (Figures 57 and 58), and that 2000°F SPGG No. 2 was spontaneously ignited one-half second after 2000°F SPGG No. 1 was correctly ignited. The cause of the low SPGG burn pressures and the early ignition of SPGG No. 2 was due to a leak in the check valve

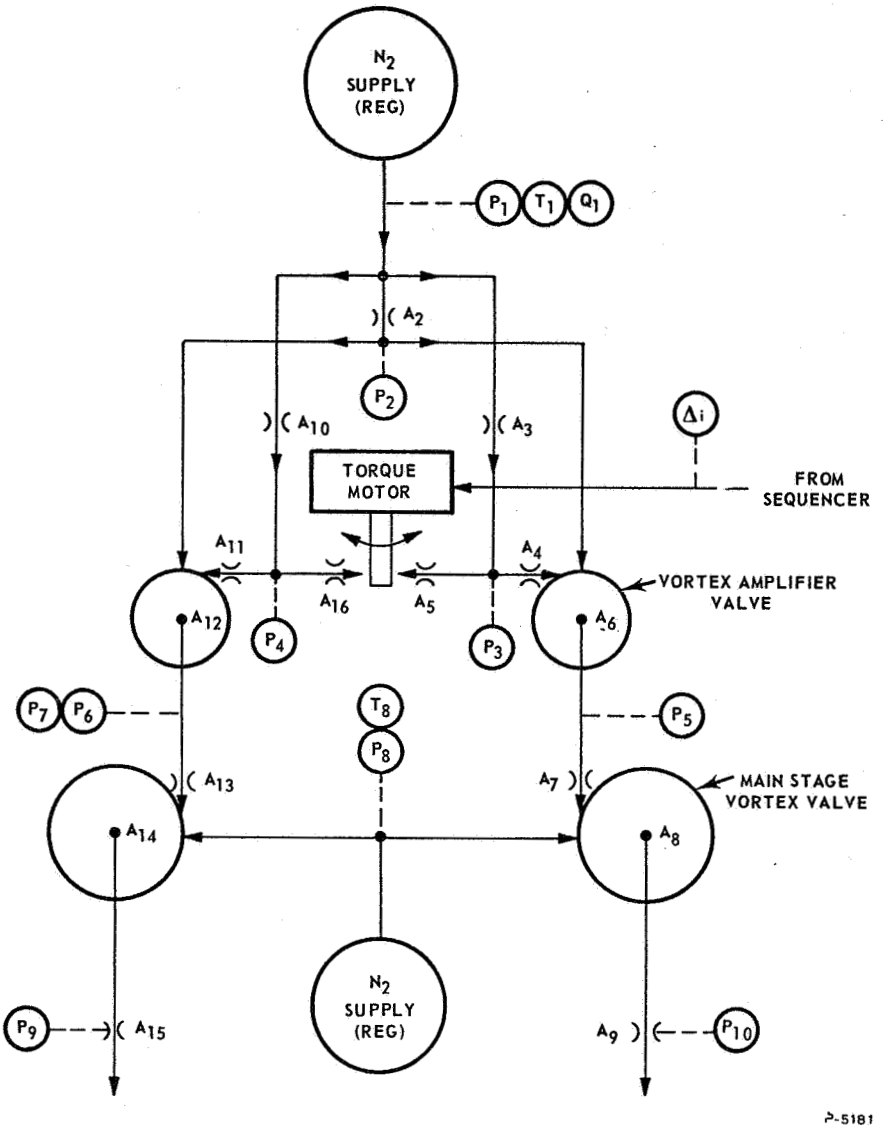

Figure 50 - Test Schematic for Cold Gas Test of 5500°F Push-Pull System

which separated the two 2000°F SPGG's. This same check valve leak also appears to have exhausted the gas that was not consumed by the pilot stage, via the SPGG No. 2 breech and ruptured burst diaphragm.

A tabulation of the various recorded test pressures with the pertinent pressure ratios is shown in Table 3. Since 2000°F SPGG No. 1 burned at a pressure that was low by 600-700 psia, the tabulated test pressures were modified by a ratio of P_1 (design value) versus P_1 (test value) and these numbers are listed as projected test results. The projected test results provided a means of comparing the system performance with design predictions. Most of the projected pressures were close to their design values, indicating that the system was functioning satisfactorily and only lacked sufficient supply pressure.

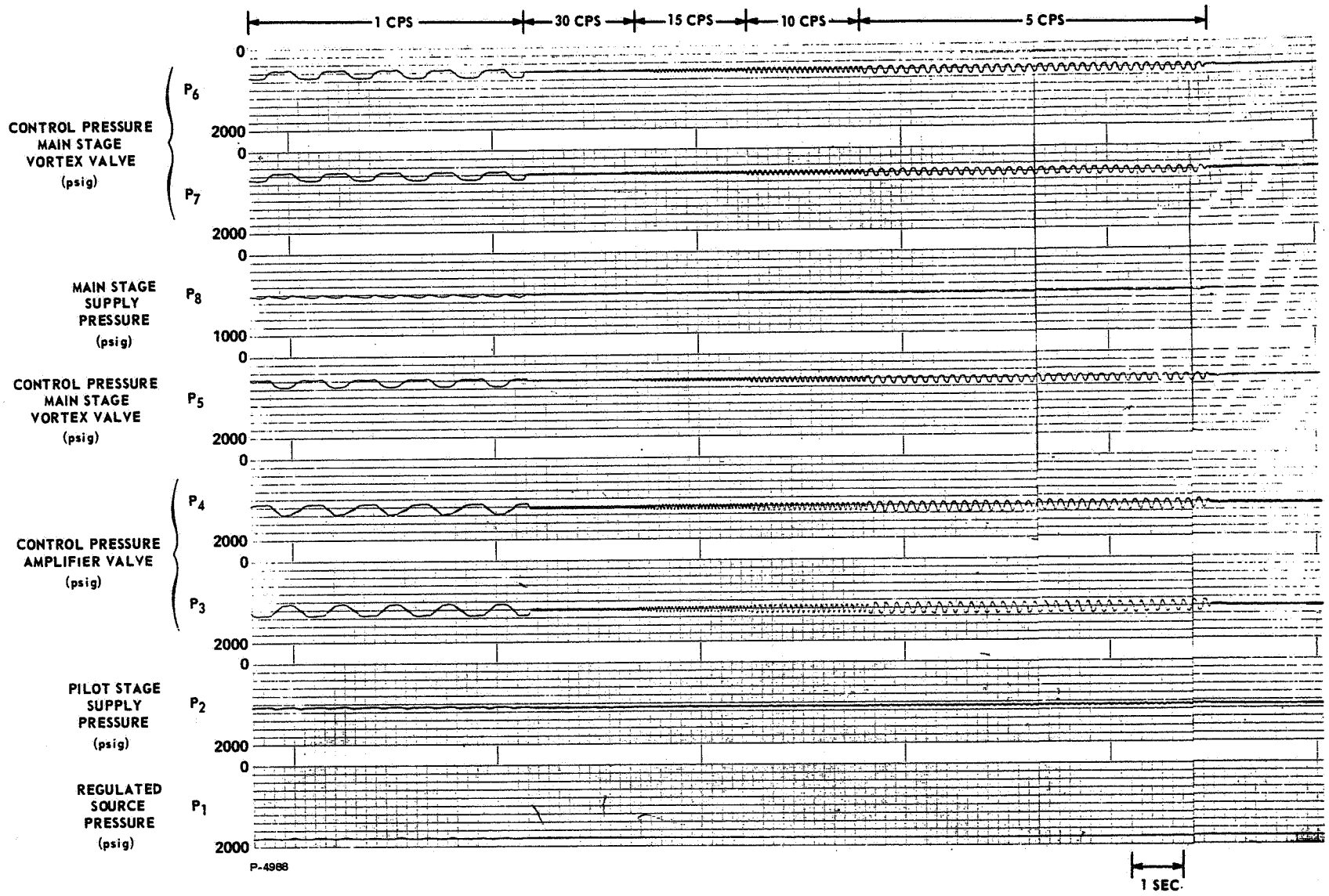

Figure 51 - 5500°F Push-Pull System Cold Gas Test Results (Sheet 1)

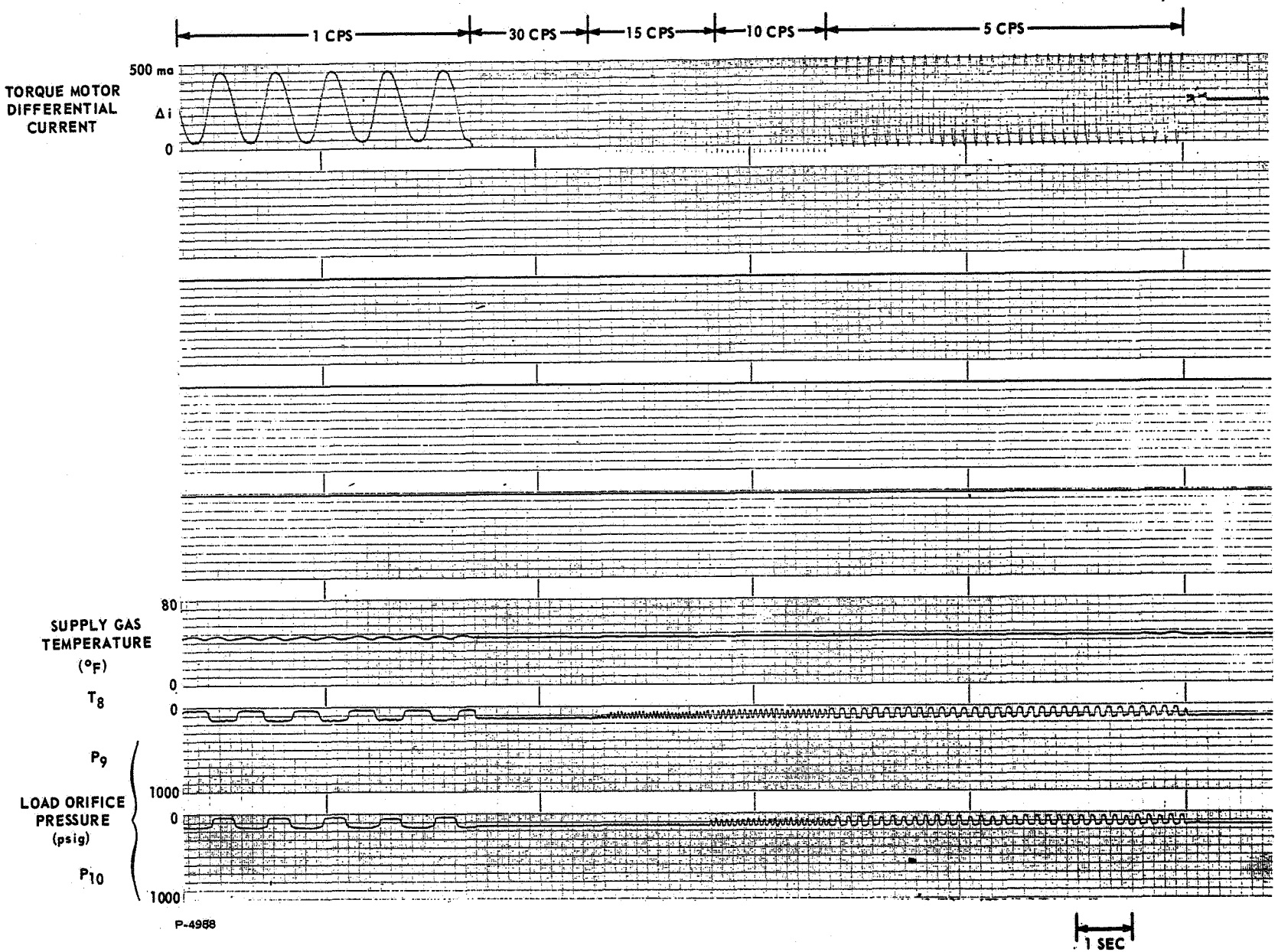

Figure 52 - 5500°F Push-Pull System Cold Gas Test Results (Sheet 2)

Table 2 - Cold Gas Test Results of the 5500°F Push-Pull System

	Input Signal	P_1 psia	P_2 psia	P_3 psia	P_4 psia	P_5 psia	P_6 psia	P_{10} psia	P_9 psia	P_8 psia	Valve No. 1		Valve No. 2	
											Pilot Stage $P_c/P_s=P_4/P_2$	Main Stage $P_c/P_s=P_6/P_8$	Pilot Stage $P_c/P_s=P_3/P_2$	Main Stage $P_c/P_s=P_5/P_8$
Design Value		2600	1515	1590-2050	1590-2050	787-1120	787-1120			750	1.05-1.35	1.05-1.50	1.05-1.35	1.05-1.50
Test Result	5 cps Sine Wave	1815	1115	1095-1360	1150-1395	575-755	550-725	55-165	45-165	520				
Projected Test Result		2600	1600	1570-1950	1650-2000	824-1080	788-1040	79-236	64.5-236	745	1.03-1.25	1.06-1.40	0.98-1.22	1.11-1.45
Test Result	10 cps Sine Wave	1815	1115	1135-1335	1170-1360	575-730	555-675	86-160	65-160	520				
Projected Test Result		2600	1600	1625-1910	1675-1950	823-1045	795-966	122-229	93-229	745	1.047-1.22	1.07-1.30	1.015-1.195	1.105-1.4
Test Result	15 cps Sine Wave	1815	1115	1165-1295	1185-1305	600-670	570-635	145-160	85-155	515				
Projected Test Result		2600	1600	1670-1855	1700-1870	860-960	817-910	208-229	122-222	737	1.06-1.17	1.11-1.235	1.045-1.16	1.17-1.3
Test Result	30 cps Sine Wave	1800	1115	1185-1250	1215-1285	630	600	160	150	515				
Projected Test Result		2600	1610	1710-1805	1755-1855	910	867	231	217	744	1.09-1.15	1.165	1.06-1.12	1.22
Test Result	1 cps Sine Wave	1815	1115	1075-1360	1135-1395	575-760	535-725	55-175	50-165	530				
Projected Test Result		2600	1600	1540-1950	1625-2000	824-1090	767-1040	788-251	71.6-236	760	1.015-1.25	1.01-1.37	0.96-1.22	1.085-1.435

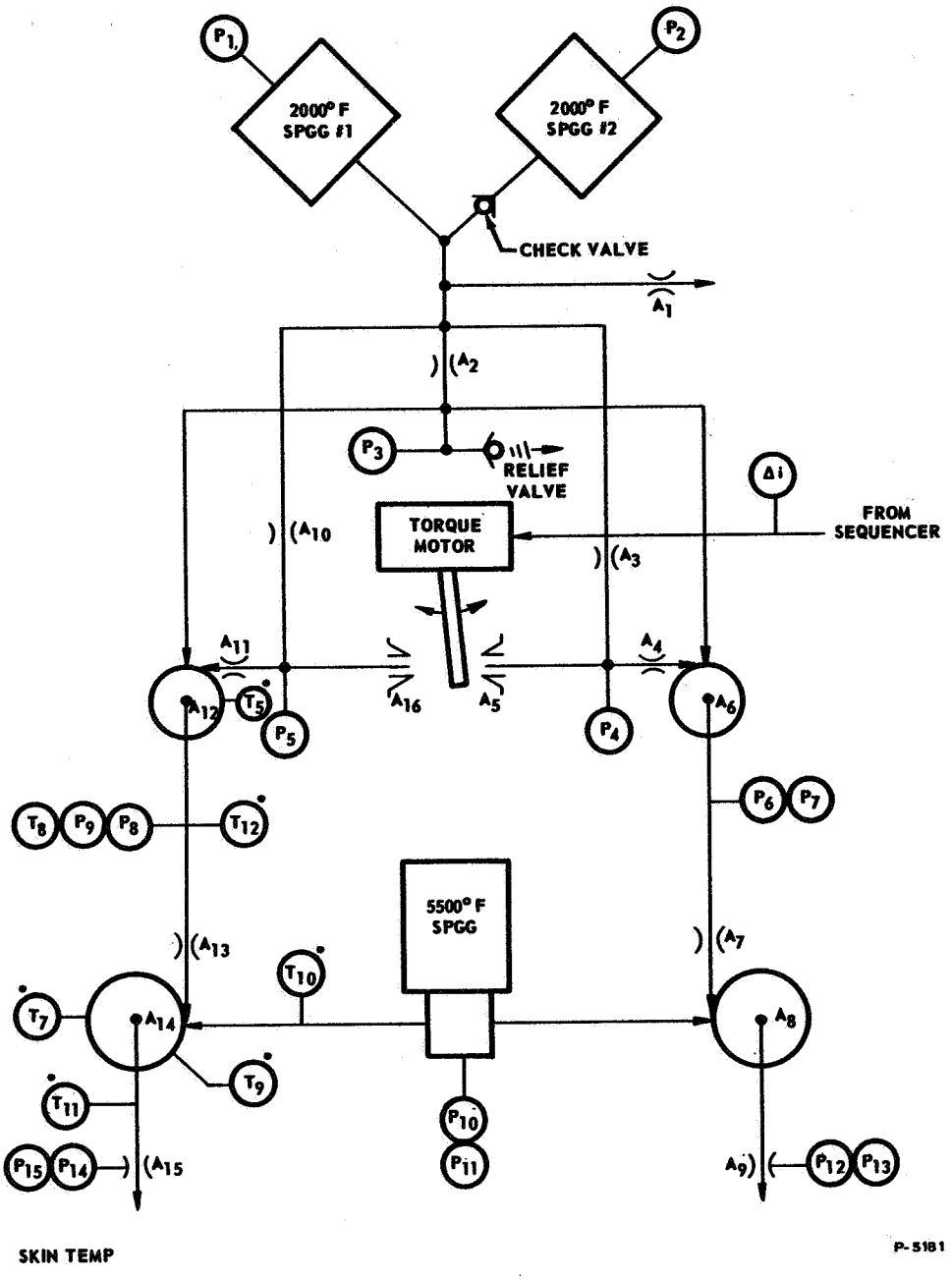

Figure 53 - Test Schematic for 5500°F Push-Pull System (Hot Gas Test No. 5)

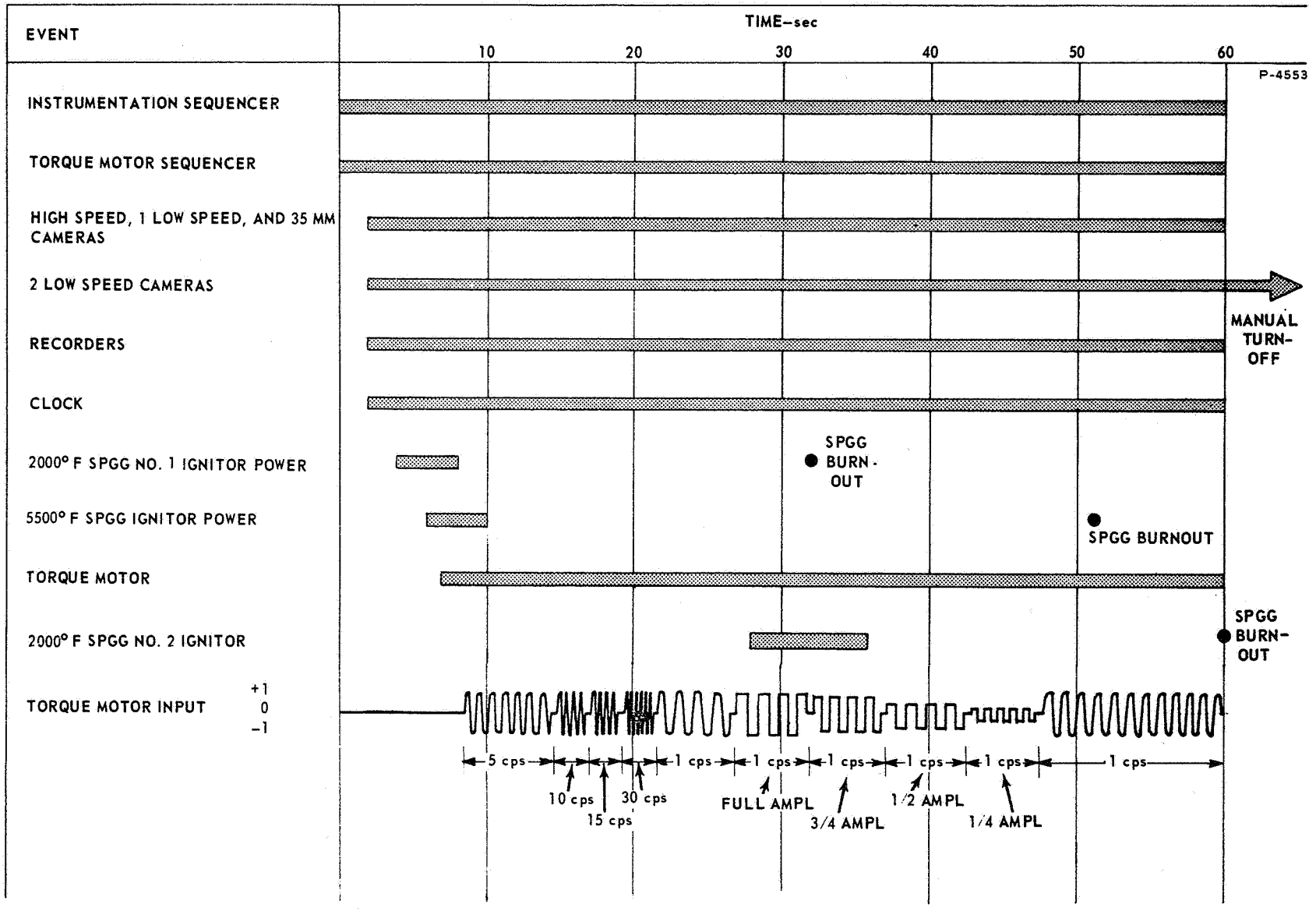

Figure 54 - Duty Cycle for Hot Gas Test No. 5

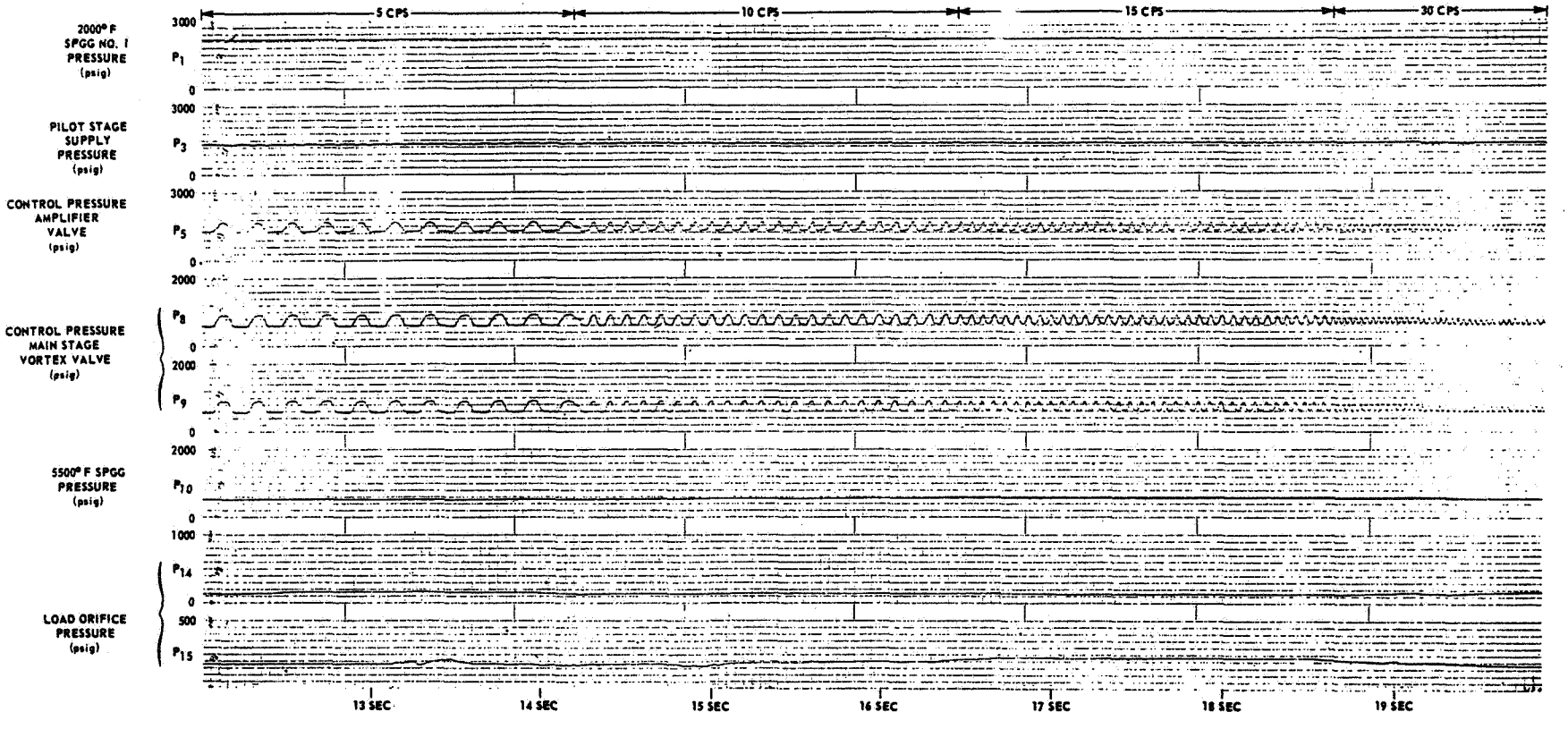

Figure 55 - Test Data From Hot Gas Test No. 5 (Sheet 1)

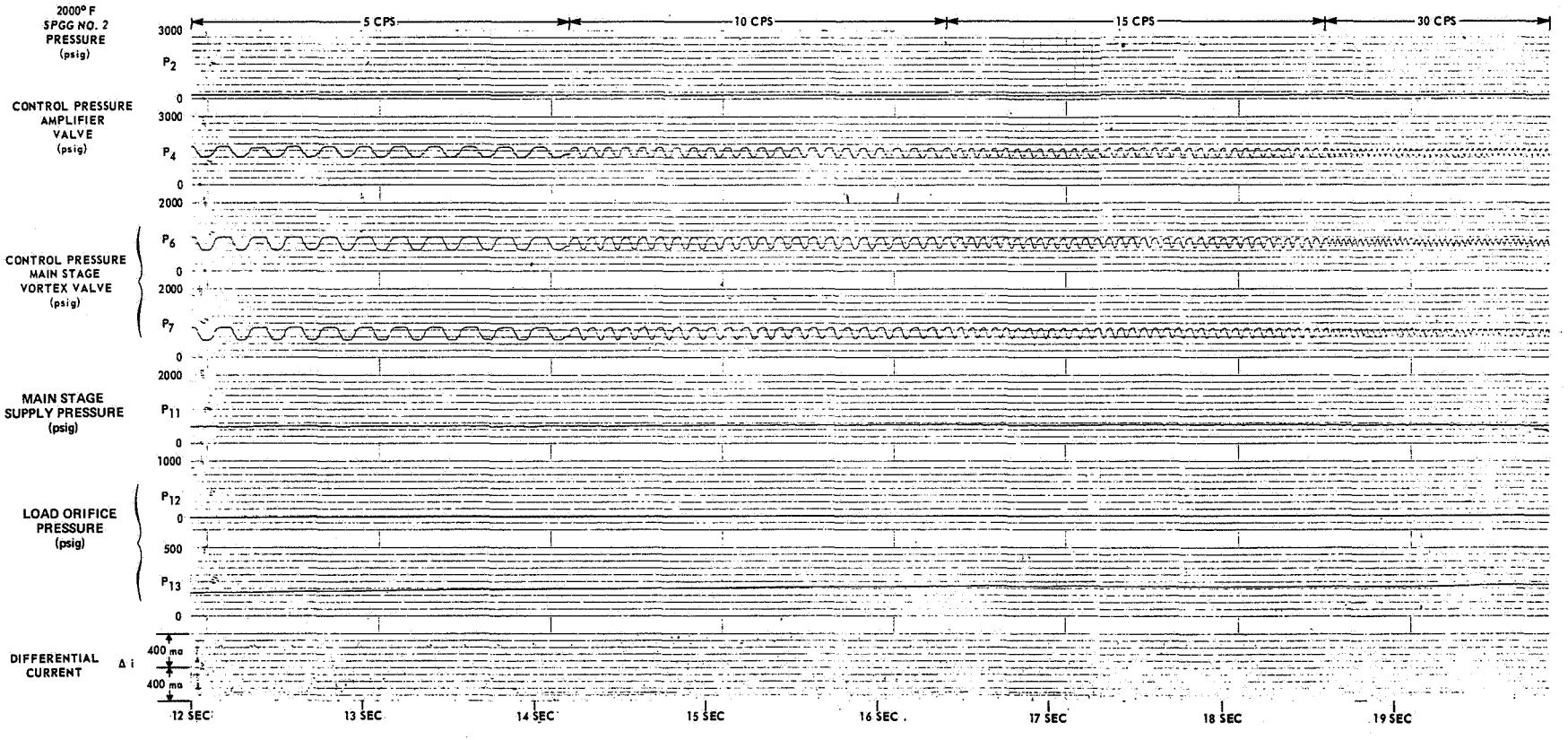

Figure 56 - Test Data From Hot Gas Test No. 5 (Sheet 2)

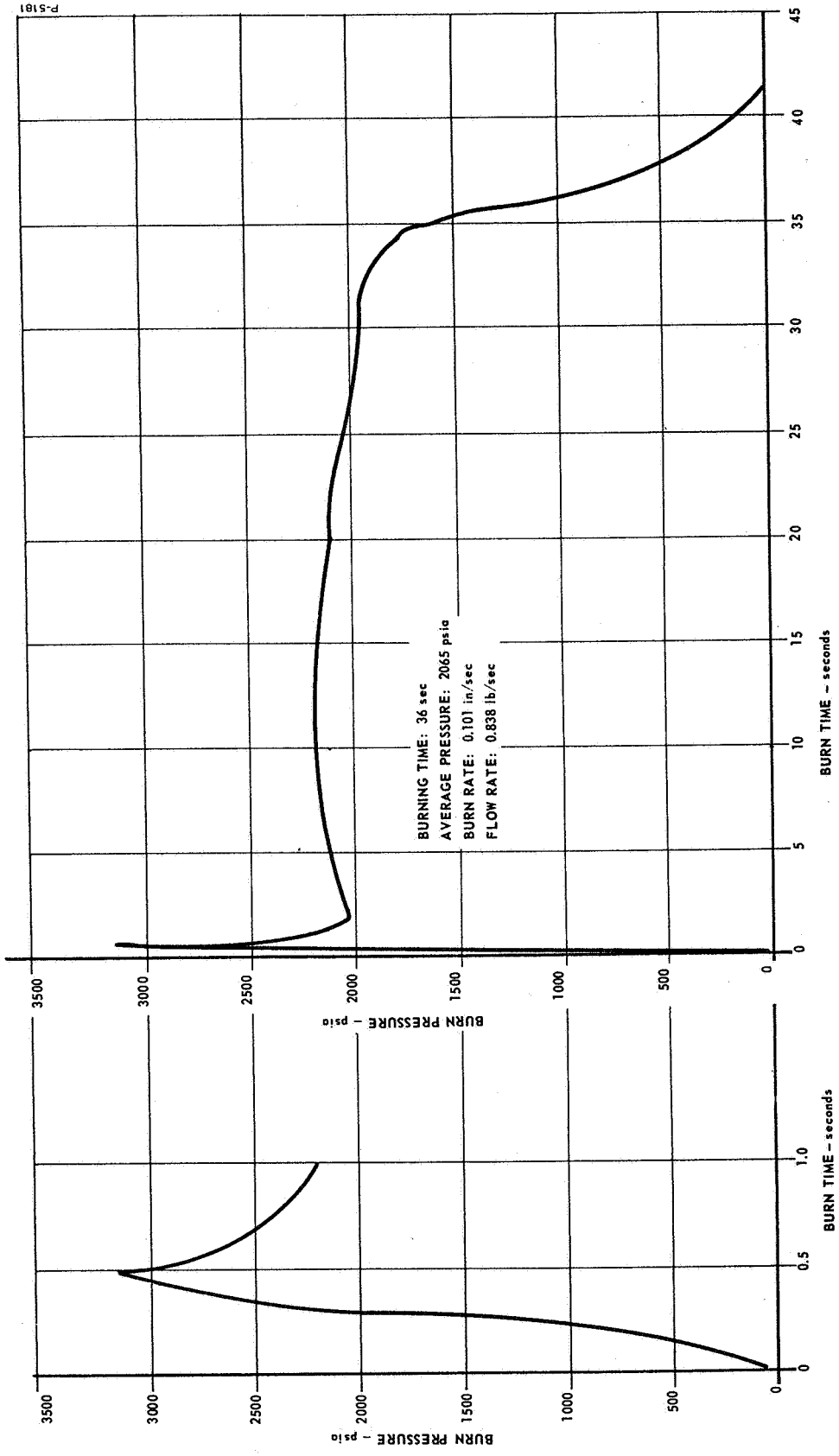

Figure 57 - 2000°F SPGG No. 1 Performance (Hot Gas Test No. 5)

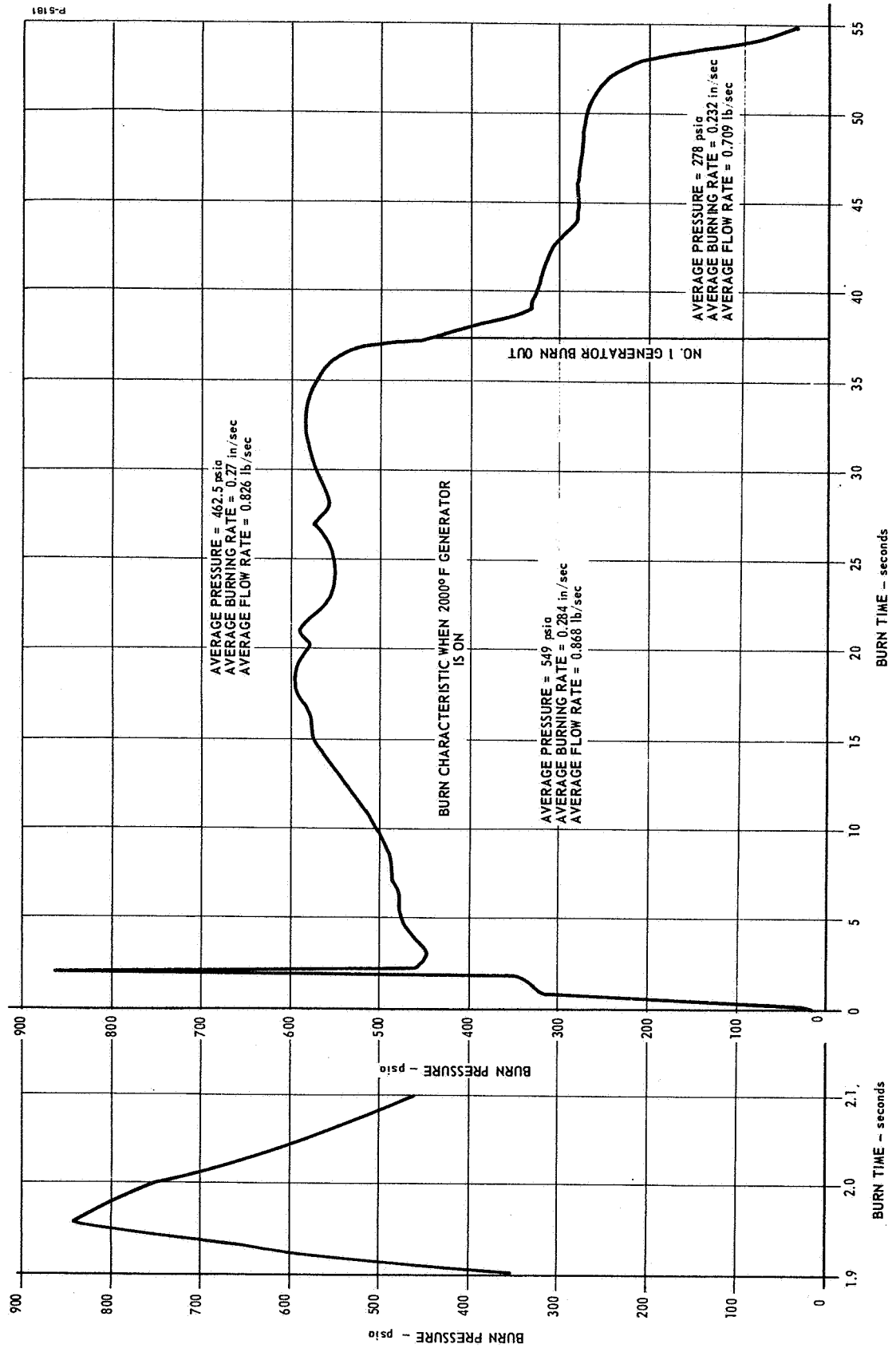

Figure 58 - 5500°F SPGG Performance (Hot Gas Test No. 5)

Table 3 - Test Results of 5500°F Push-Pull System Hot Gas Test No. 5

	Frequency	P_1 psia	P_3 psia	P_5 psia	P_8 psia	P_{10} psia	P_2 psia	P_4 psia	P_7 psia	Valve No. 1		Valve No. 2	
										Pilot Stage $\frac{P_c}{P_s} = \frac{P_5}{P_3}$	Main Stage $\frac{P_c}{P_s} = \frac{P_8}{P_{10}}$	Pilot Stage $\frac{P_c}{P_s} = \frac{P_4}{P_3}$	Main Stage $\frac{P_c}{P_s} = \frac{P_7}{P_{10}}$
Design Value		2600	1515	1590-2050	787-1120	750	2600	1590-2050	787-1120	1.05-1.35	1.05-1.50	1.05-1.35	1.05-1.50
Test Result	1 cps Rect. Wave	1945	1245	1285-1475	615-755	575	180	1215-1485	575-775				
Projected Test Result		2600	1665	1720-1970	822-1010	768	241	1625-1985	768-1035	1.03-1.18	1.07-1.315	0.977-1.19	1-1.35
Test Result	1 cps Sine Wave	2055	1305	1315-1655	600-895	555	180	1160-1590	525-825				
Projected Test Result		2600	1650	1665-2090	759-1130	702	228	1470-2010	664-1045	1.01-1.27	1.08-1.61	0.89-1.22	0.947-1.49
Test Result	5 cps Sine Wave	2175	1335	1285-1665	555-905	505	165	1245-1695	515-875				
Projected Test Result		2600	1597	1540-1990	664-1080	604	197	1490-2030	616-1046	0.965-1.25	1.1-1.79	0.933-1.27	1.02-1.73
Test Result	10 cps Sine Wave	2145	1345	1295-1665	620-915	565	170	1215-1665	560-885				
Projected Test Result		2600	1630	1570-2020	752-1110	685	206	1475-2020	678-1075	0.964-1.24	1.1-1.98	0.905-1.24	0.99-1.57
Test Result	15 cps Sine Wave	2135	1345	1280-1635	650-895	590	170	1215-1625	570-875				
Projected Test Result		2600	1640	1560-1990	792-1090	718	207	1480-1980	694-1065	0.952-1.21	1.1-1.52	0.903-1.21	0.965-1.48
Test Result	30 cps Sine Wave	2115	1335	1290-1535	635-775	575	180	1265-1595	635-815				
Projected Test Result		2600	1640	1585-1885	780-952	707	221	1555-1960	780-1000	0.967-1.15	1.1-1.35	0.95-1.195	1.1-1.415

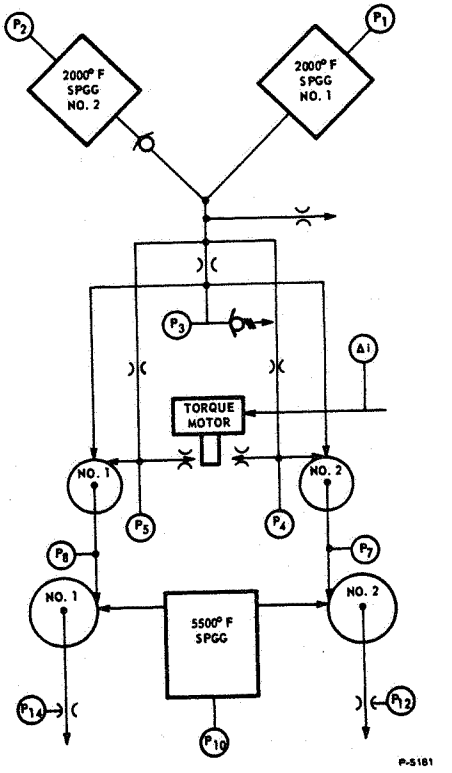

The results of the various temperatures recorded during the test are shown in Figures 59 and 60. The temperature data indicate that the maximum skin temperature reached by the main stage valves and manifolds was 800°F. These parts are insulated from the hot gas. The data appearing in Figure 60 show that the main stage vortex valve control gas was at 1840°F and that the control manifold also reached 1840°F.

Post-test hardware inspection showed that the output pressure tap and control injectors of the main stage valves were plugged by aluminum oxide. Aluminum oxide deposits were found in the pilot stage control injectors; all of these deposits were due to the backflow of the 5500°F gas when the 2000°F gas generator burned out.

The post-test condition of the main stage valves and plenum chamber is shown in Figure 61. The picture indicates that the materials were still in good condition after the hot gas test.

Test Conclusions

The post-test examination of the system hardware and the evaluation of the recorded data allow the following conclusions to be drawn concerning the 5500°F Push-Pull System Hot Gas Test No. 5.

(1) The main stage vortex valves, manifolds, and pilot stage materials are adequate for the test period.

(2) The main stage vortex valves modulated the 5500°F gas flow (based on the film coverage).

(3) The 2000°F SPGG No. 2 fired prematurely because of leakage in the check valve, and the premature firing ruptured the burst disk on that generator.

(4) The system operating pressures were less than predicted because the 2000°F SPGG ran low and thereby unloaded the main stage gas generator.

(5) Flow data for the main stage valves were not recorded because aluminum oxide plugged the pressure tap ports.

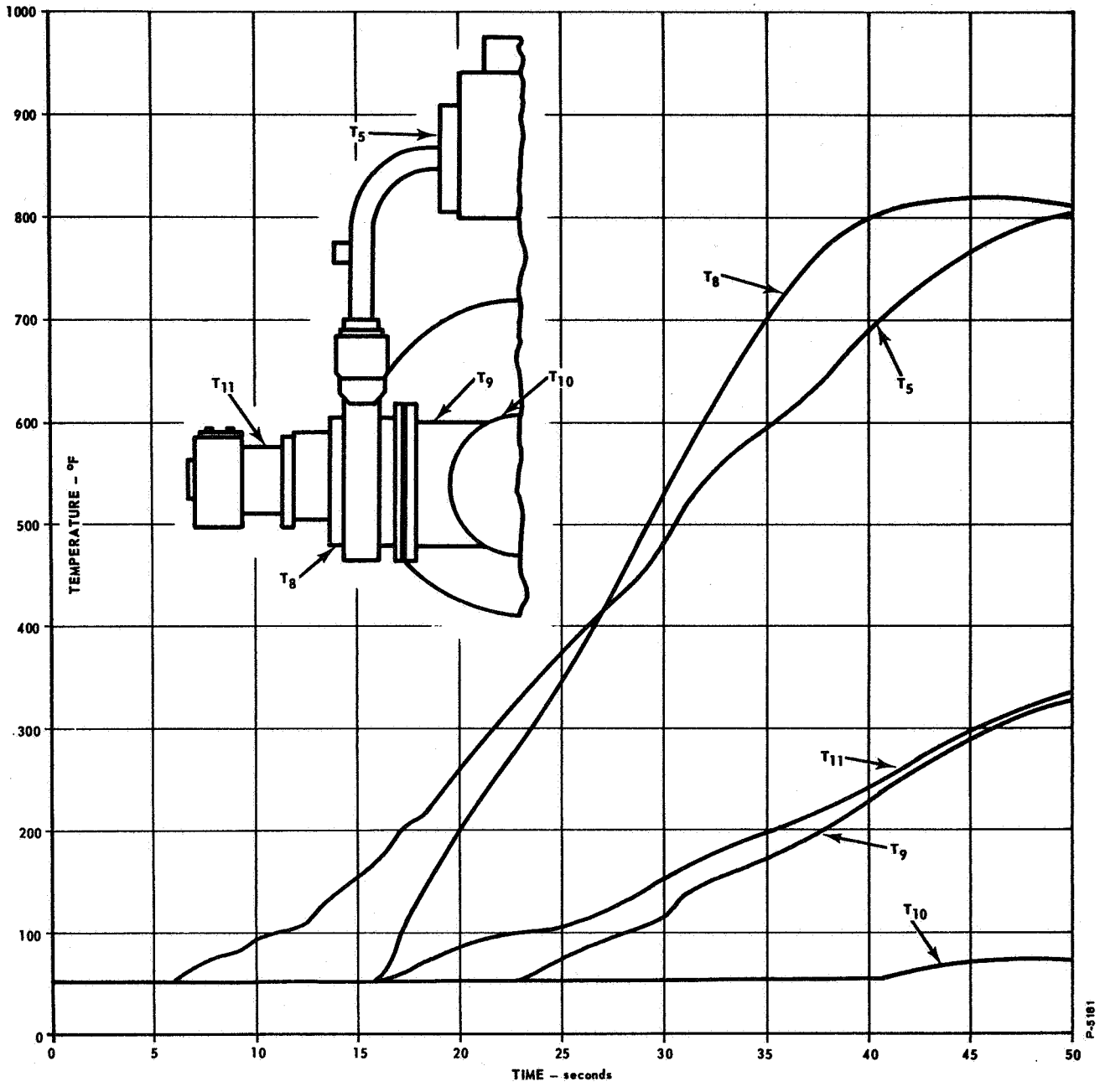

Figure 59 - Skin Temperature Variation as Function of Time
(Hot Gas Test No. 5)

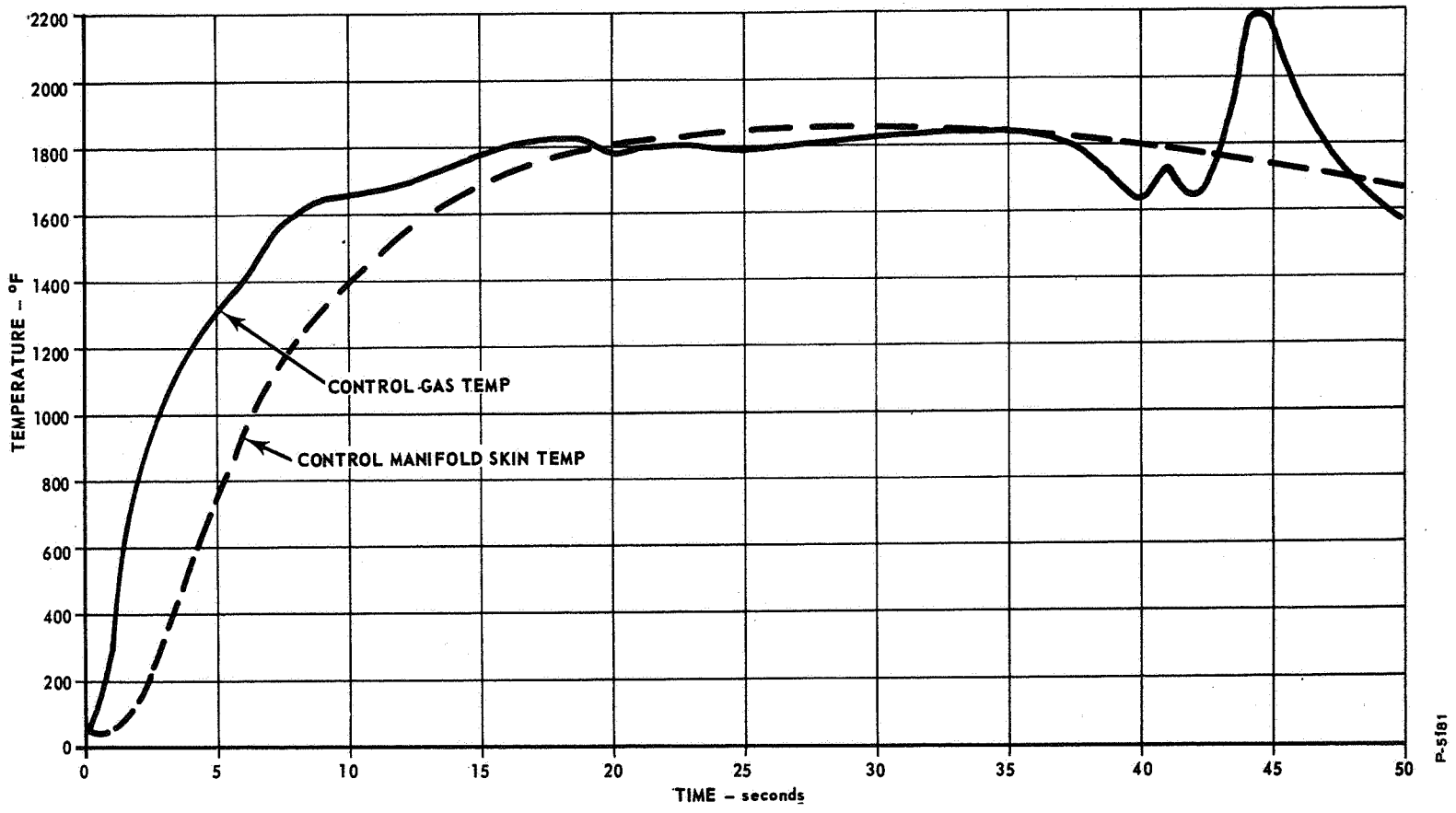

Figure 60 - Control Gas and Manifold Skin Temperatures

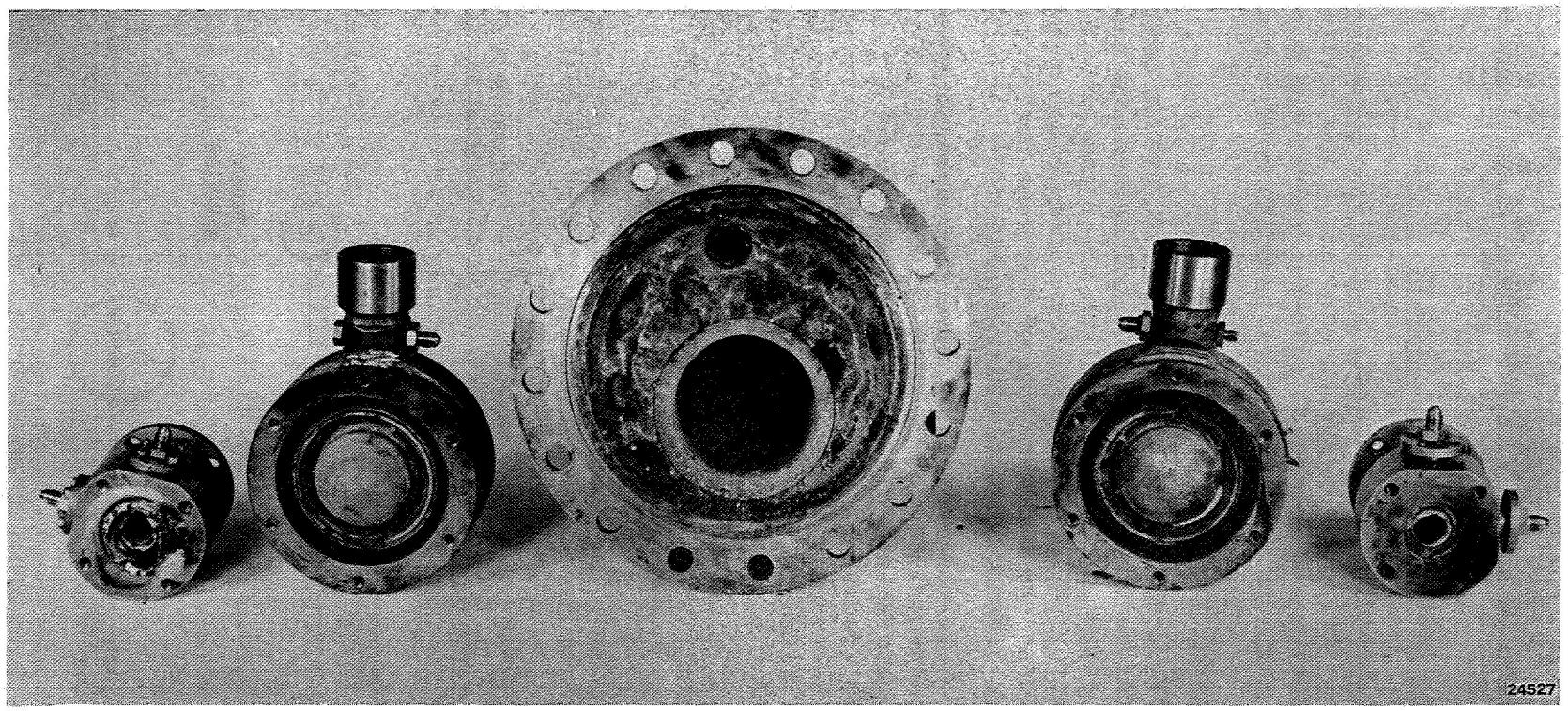

Figure 61 - 5500°F Main Stage Vortex Valves, Plenum Chamber and Load Orifices After Test

5500°F SITVC SYSTEM TEST

(Hot Gas Test No. 6)

The system tested in Hot Gas Test No. 6 was a 5500°F vortex valve controlled SITVC system mounted on a simulated rocket motor. The test objective was to obtain flow modulation of highly aluminized 5500°F solid propellant gas with the SITVC system hardware. The testing was conducted in two parts, system and component cold gas tests, and a system hot gas test.

System Description

The 5500°F vortex valve controlled SITVC system consisted of two main stage vortex valves, a 5500°F SPGG for main stage supply, a 2000°F SPGG for pilot stage supply, and a pilot stage containing two vortex amplifier valves controlled by a torque motor driven flapper-nozzle valve. All of the SITVC system hardware was of the same design as utilized in Hot Gas Test No. 5 except for the flow measurement technique.

In addition to the conventional sensing port in the main stage vortex valve load orifice, a "weeping" orifice system, Figure 62, was used for flow measurement. The system used the vortex valve load orifice pressure port as a subsonic orifice, which was fed by an upstream sonic orifice from a nitrogen gas supply. The sonic orifice was sized to provide a constant nitrogen flow out of the port under all test conditions

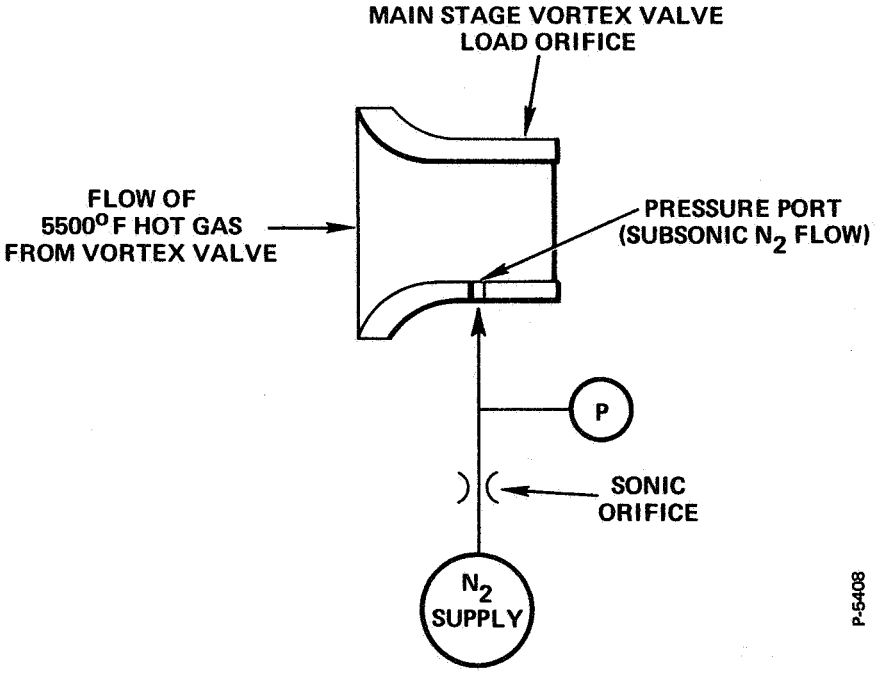

Figure 62 - Main Stage Vortex Valve Weeping Orifice Flow Measurement System

with the nitrogen source regulated at 2000 psia. The change in hot gas flow through the valve's load orifice caused a variation in flow impedance of nitrogen through the pressure port. This variation of flow impedance produced a change in pressure upstream of the pressure port. This pressure variation was calibrated to provide the measurement of flow through the vortex valve.

Cold Gas Test Results

The main stage vortex valves, the pilot stage vortex valves, and the complete SITVC system were cold gas tested to verify their intended performance. A portion of the cold gas test results are shown in Figures 63, 64, and 65. Figure 63 is the typical turndown performance of the pilot stage amplifier vortex valves, and Figure 64 is the typical cold gas performance of the main stage vortex valve.

Figure 65 shows the typical flow calibration curve for the main stage vortex valve flow measurement system. The calibration curve is a plot of total valve outlet flow ($\dot{W}_O$) versus valve outlet pressure (P_O or P_{OW}). The results show that the valve outlet flow was proportional to outlet pressure when the control flow was zero, but the flow was not proportional to outlet pressure when the valve control pressure was greater than the supply pressure (i.e., during valve turndown). The lack of proportionality between valve outlet flow and outlet pressure during valve turndown was caused by the swirl that was imparted to the gas that passed through the vortex valve. The gas that enters the load orifice retains this vortex swirl action, which produces a cross-section of gas across the orifice that is not of uniform static pressure. The gas at the outside periphery of the orifice is at a higher pressure and density than the gas at the center. This condition changes with the amount of vorticity in the vortex valve, thereby producing a characteristic curve as shown in Figure 65.

Cold gas test results were similar to the results attained in previous testing and indicated that the system and components would operate as intended in the hot gas test.

Hot Gas Test Results

The 5500°F vortex valve controlled SITVC system schematic and duty cycle utilized in the hot gas test are shown in Figures 66 and 67, respectively. A photograph of the setup on the test bench before firing is shown in Figure 68. Note that this is a heavyweight test setup and that the large manifolds would not be required for a direct engine chamber bleed system as shown in Figure 1. Two pictures of Hot Gas Test No. 6 in operation are shown in Figures 69 and 70. The outlets of the two main stage vortex valves, which contained the flow of hot gas, were mounted 90 degrees apart with one valve exhausting vertically downward and the other exhausting horizontally. The direction of the combined exhaust plume from the two vortex valves depended on the relative flow modulation of the valves.

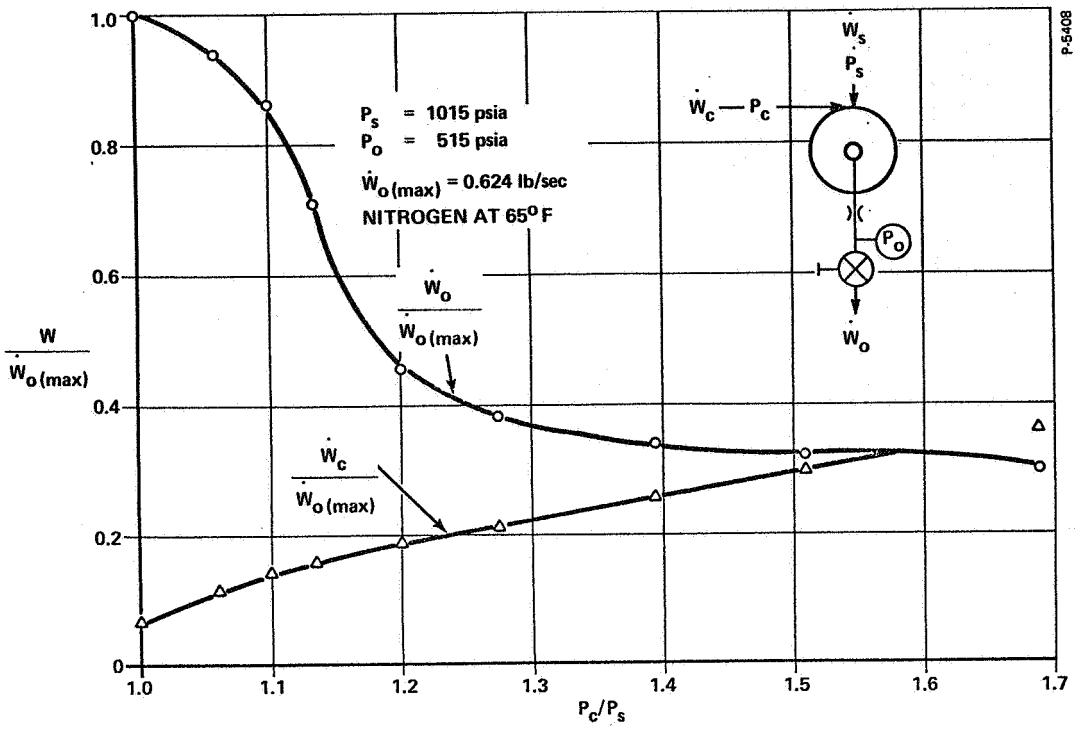

Figure 63 - Pilot Stage Vortex Amplifier Valve No. 1
Turndown Performance on Cold Gas

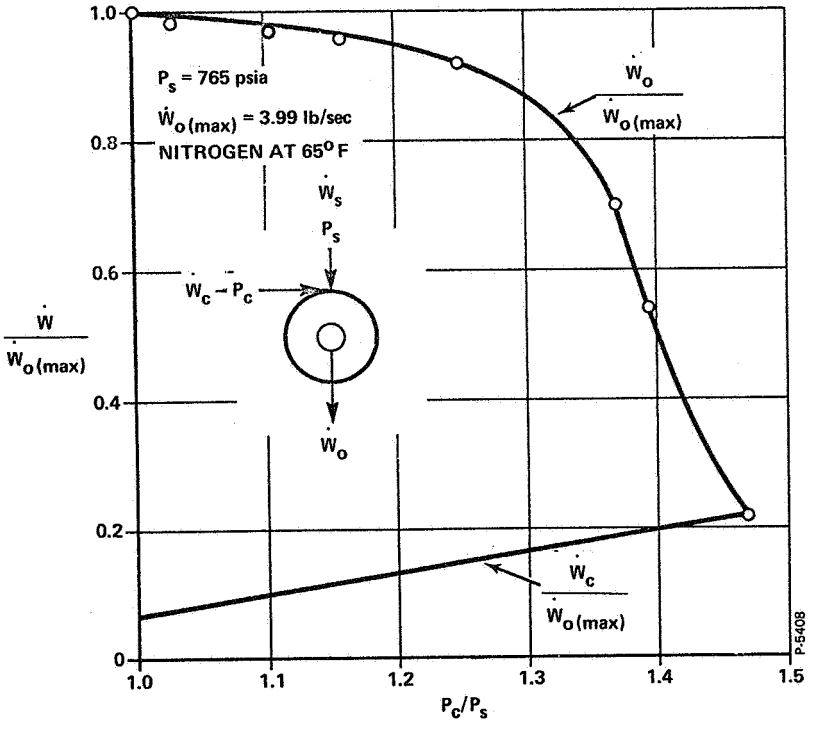

Figure 64 - Main Stage Vortex Valve No. 1
Turndown Performance on Cold Gas

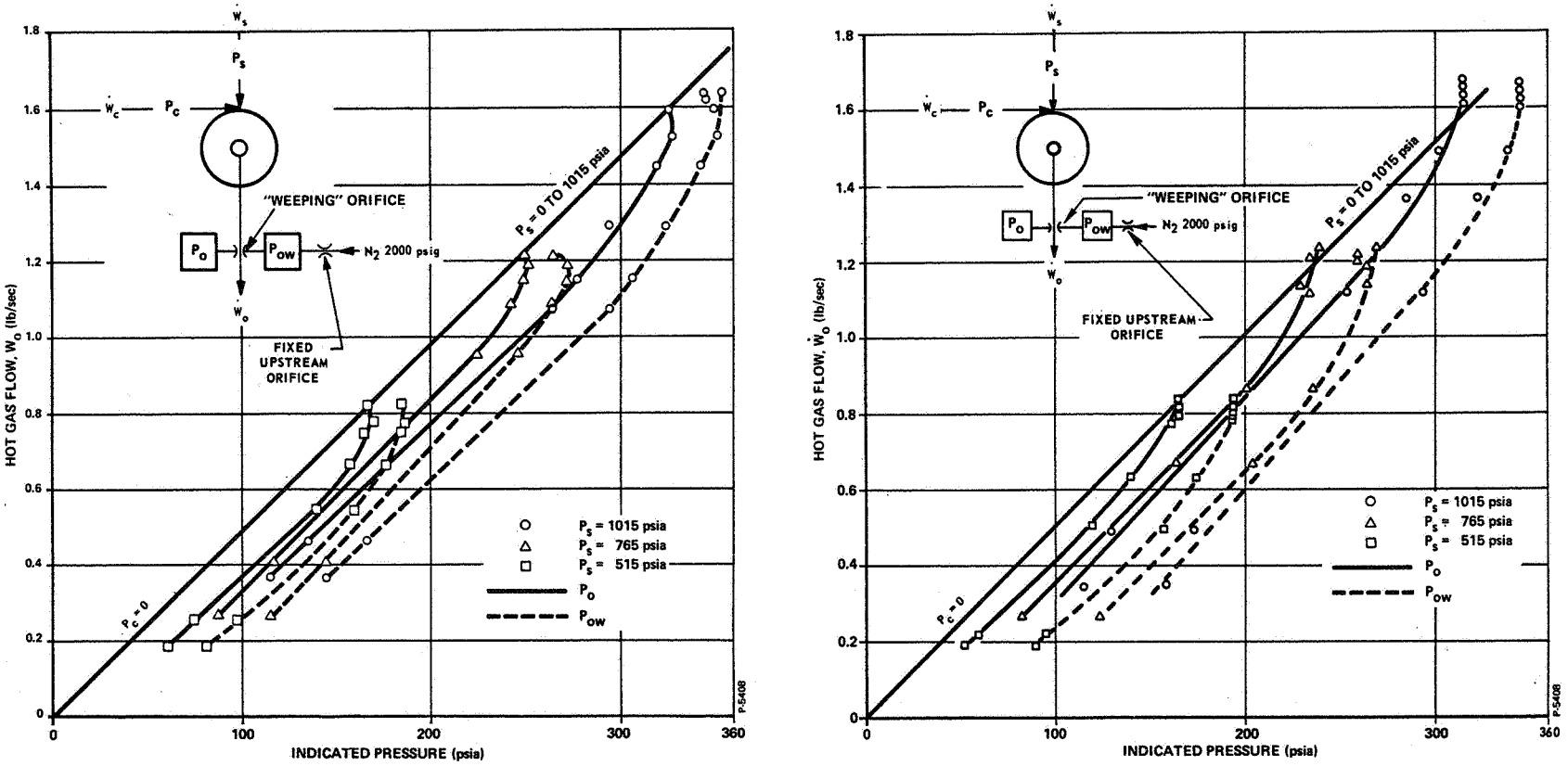

(a) Main Stage Vortex Valve No. 1

(b) Main Stage Vortex Valve No. 2

Figure 65 - Pressure Tap and Weeping Orifice Cold Gas Flow Calibration (Corrected to Hot Gas Flow)

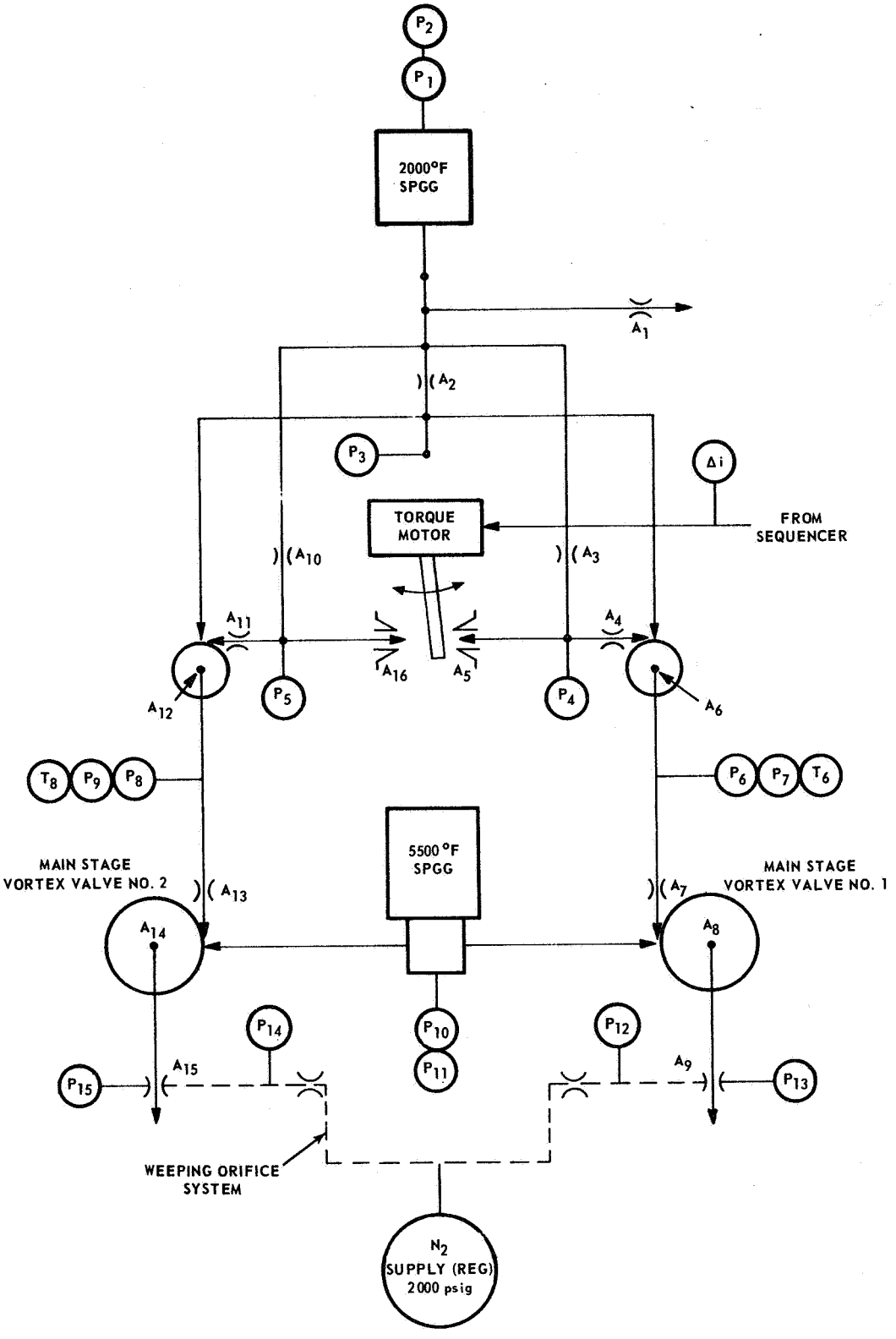

Figure 66 - Test Schematic for Hot Gas Test of 5500°F SITVC System (Hot Gas Test No. 6)

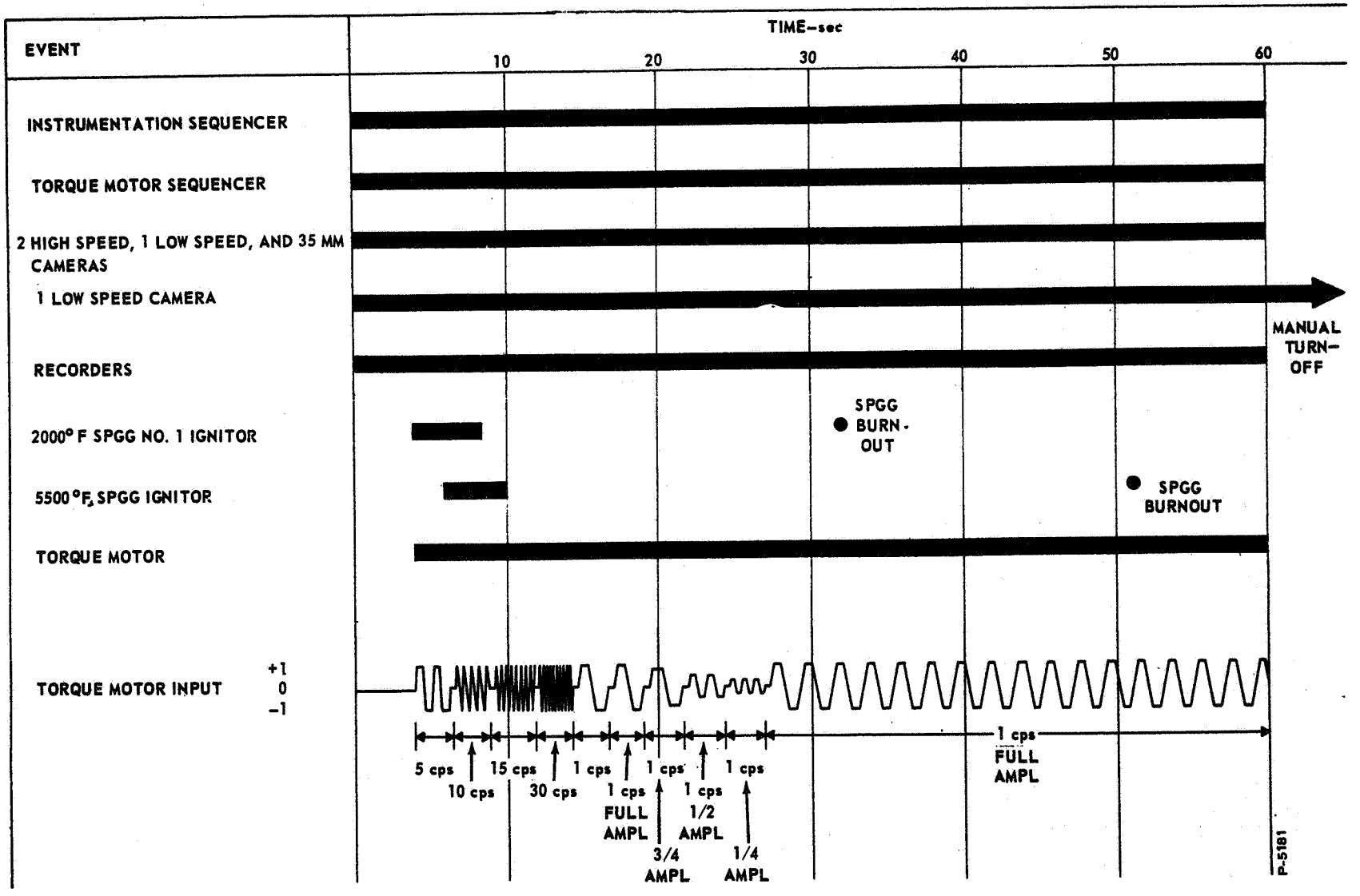

Figure 67 - Duty Cycle for Hot Gas Test No. 6

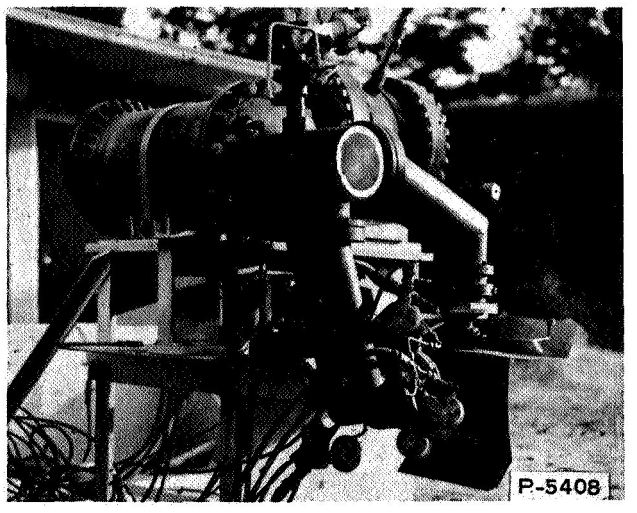

Figure 68 - Test Setup for Hot Gas Test No. 6

A portion of the data recorded during the hot gas test is shown in Figures 71 and 72. The data recorded in these figures cover the first ten seconds of system operation, during which the system sine wave input signal varied from 5 to 30 cps. The remainder of the 51 seconds of test data contained the type of information as shown at time 9 seconds, with all of the pressures showing modulation except the main stage flow measurement pressures. These flow measurement pressures ceased to record pressure modulation because of plugging of the pressure ports with aluminum oxide from the 5500°F solid propellant. The weeping orifices should not have plugged during operation because any plugging would increase the pressure upstream of the plug, which in this case could be as high as 2000 psi. It is believed that this pressure would blow out the plugging material even if the material was very viscous as the aluminum oxide is thought to be under these test conditions. However, if charring of the insulation material began to provide leak paths, the pressure rise upstream of the weeping orifice caused by plugging could be severely limited. The end result could be insufficient pressure available to clear the weeping orifice. Because of thermal soakback and subsequent charring of the insulation, it was impossible to ascertain the condition of the weeping orifice during the hot firing when the data began to fade out.

The ballistics performance of the two solid propellant gas generators is shown in Figure 73. The data indicate that the 2000°F SPGG operated at an average pressure of 2210 psia, which is lower than the 2600 psia expected. This pressure loss was partly due to a leak at the pilot stage vent orifice.

The test data recorded the modulation of hot gas flow by the main stage system for 57 cycles over an eight-second period until the flow measurement system ceased to function. The test movies indicate that the complete system was still functioning and modulating hot gas flow at 12 seconds. After this time, smoke obscured the view of the test operation. The recorded test data showed that the pilot stage functioned as intended for 33 seconds, at which time the 2000°F SPGG burned out.

The test data indicated that the main stage vortex valves produced a maximum turndown of 3.46 to 1 at a control-to-supply pressure ratio of approximately 1.7. Two typical hot gas turndown curves obtained from the

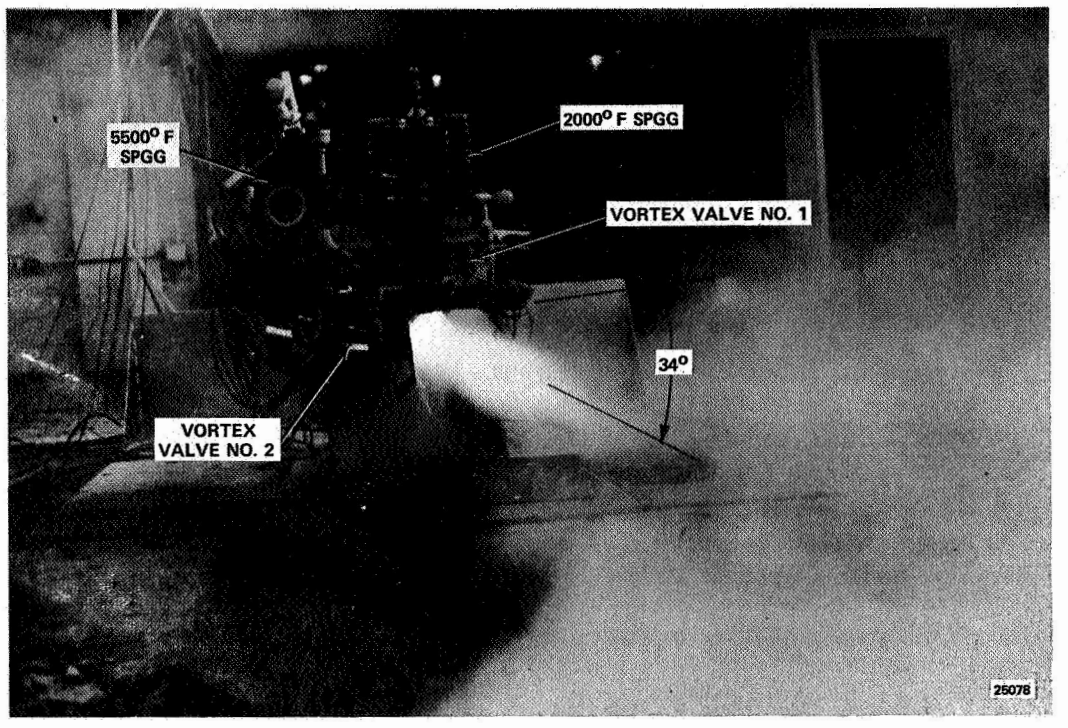

Figure 69 - Hot Gas Test No. 6 During Operation (Vortex Valve No. 2 Predominant)

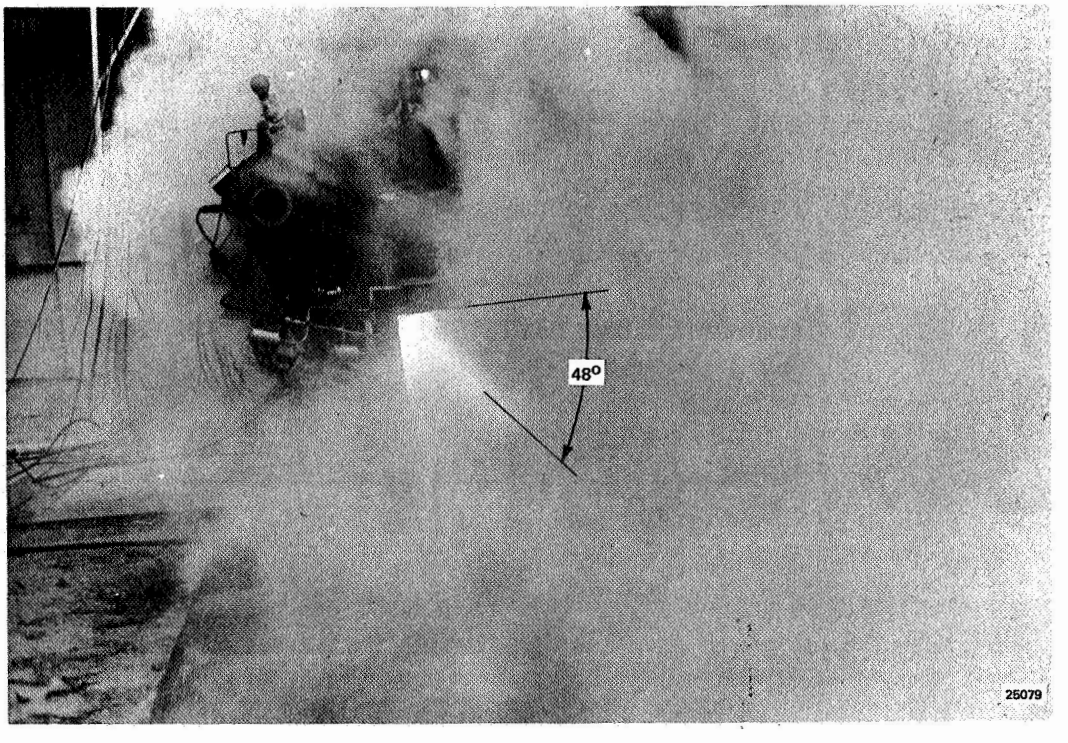

Figure 70 - Hot Gas Test No. 6 (During Operation (Vortex Valve No. 1 Predominant)

test for each vortex valve are shown in Figures 74 and 75. The differences between the turndown curves for each valve were due to the response differences between the techniques used for flow measurement. These two sets of performance curves indicate that the valves were not fully turned down and would have required a control-to-supply pressure ratio of approximately 1.75 for full turndown.

The validity of the hot gas flow measurements was determined from a main stage system flow balance that utilized the following recorded data for test time 3.15 seconds:

P_{10} = 505 psia (5500°F SPGG pressure)

P_6 = 530 psia (Vortex Valve No. 1 control pressure)

P_8 = 825 psia (Vortex Valve No. 2 control pressure)

P_{12} = 188 psia (Vortex Valve No. 1 weeping orifice pressure)

P_{13} = 155 psia (Vortex Valve No. 1 outlet pressure)

P_{14} = 132 psia (Vortex Valve No. 2 weeping orifice pressure)

P_{15} = 110 psia (Vortex Valve No. 2 outlet pressure)

The flow balance was made by comparing the total weight flow of gas into the two main stage vortex valves with the total weight flow of gas out of the valves as determined from the flow measurement techniques.

The total weight flow into the two main stage vortex valves was

$$\dot{W}_{in(total)} = \dot{W}_{(5500\ SPGG)} + \dot{W}_{(control\ flow\ No.\ 1\ valve)} + \dot{W}_{(control\ flow\ No.\ 2\ valve)}$$

$$\dot{W}_{in(total)} = A\rho c_1 P_{10}^{\,n} + \frac{C_d\ C_2\ A_7\ P_6}{\sqrt{T_6}}\ f_1\left(\frac{P_{10}}{P_6}\right) + \frac{C_d\ C_2\ A_{13}\ P_8}{\sqrt{T_6}}\ f_1\left(\frac{P_{10}}{P_8}\right)$$

$$= 48(0.0637)0.0428(505)^{0.3} + \frac{0.828(0.412)0.04(530)}{\sqrt{2360}}\ f_1\left(\frac{505}{530}\right) + \frac{0.776(0.412)0.04(825)}{\sqrt{2360}}\ f_1\left(\frac{505}{825}\right)$$

$$W_{in(total)} = 1.1207\ lb/sec$$

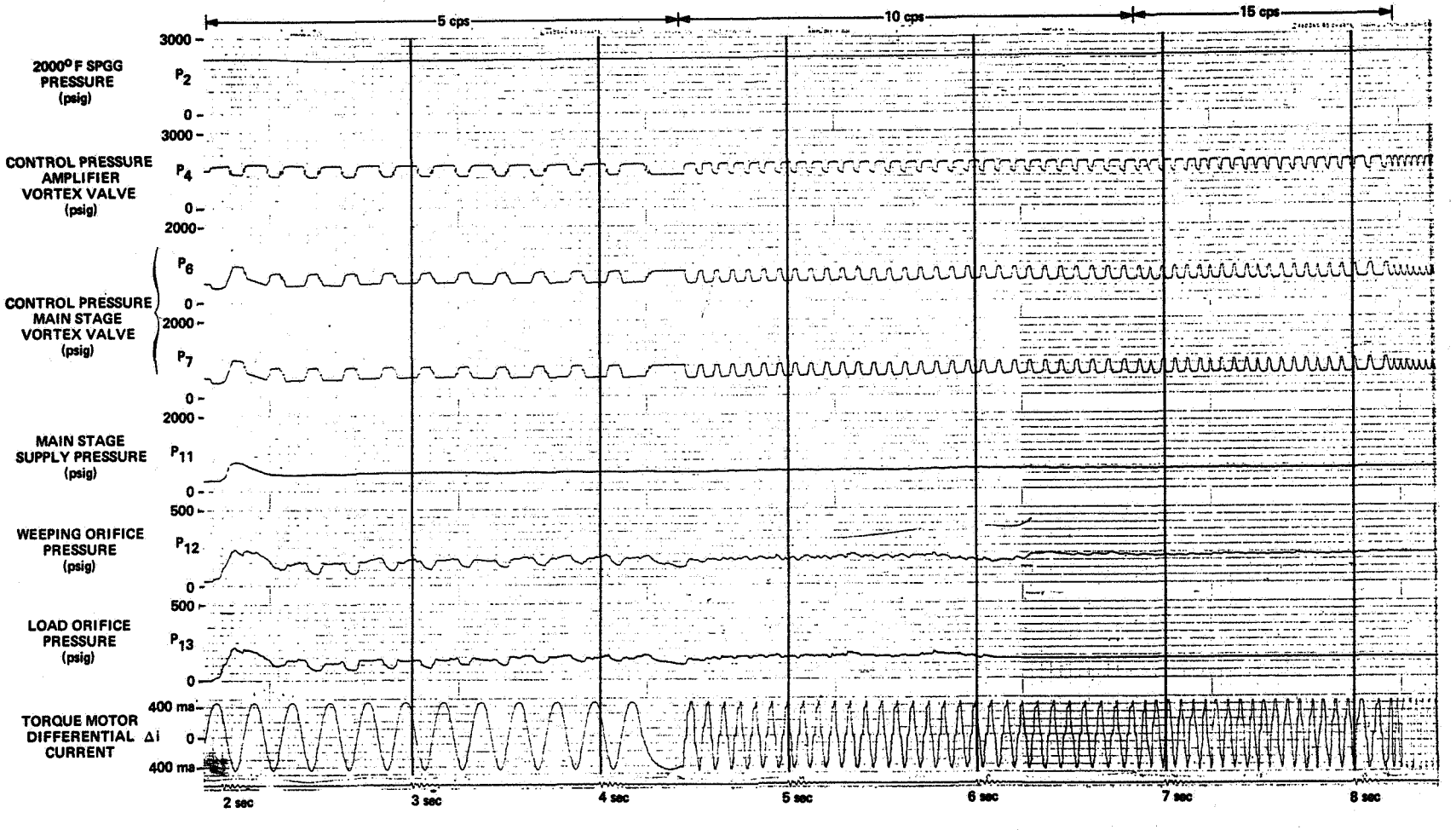

Figure 71 - Test Data From Hot Gas Test No. 6 (Sheet 1)

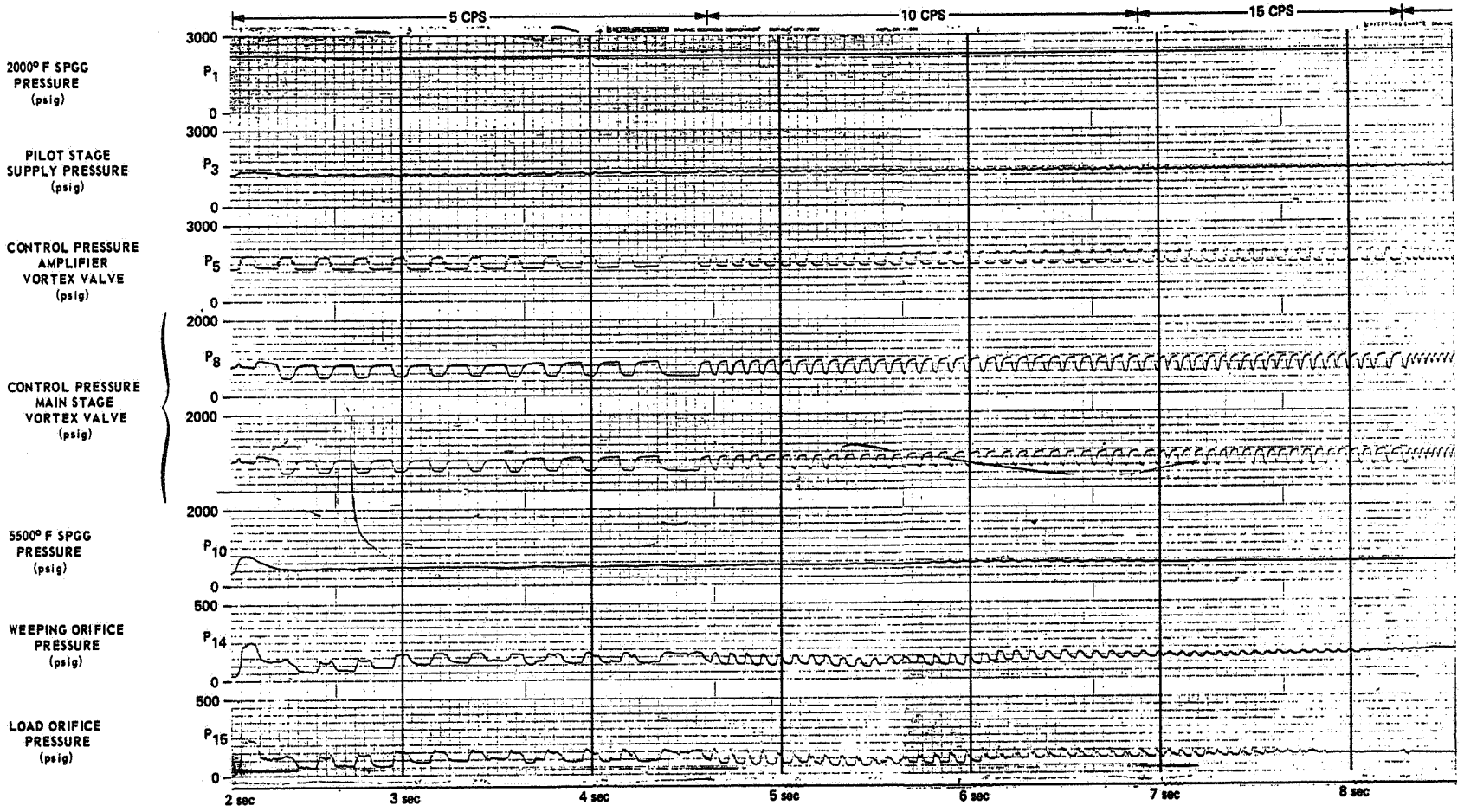

Figure 72 - Test Data From Hot Gas Test No. 6 (Sheet 2)

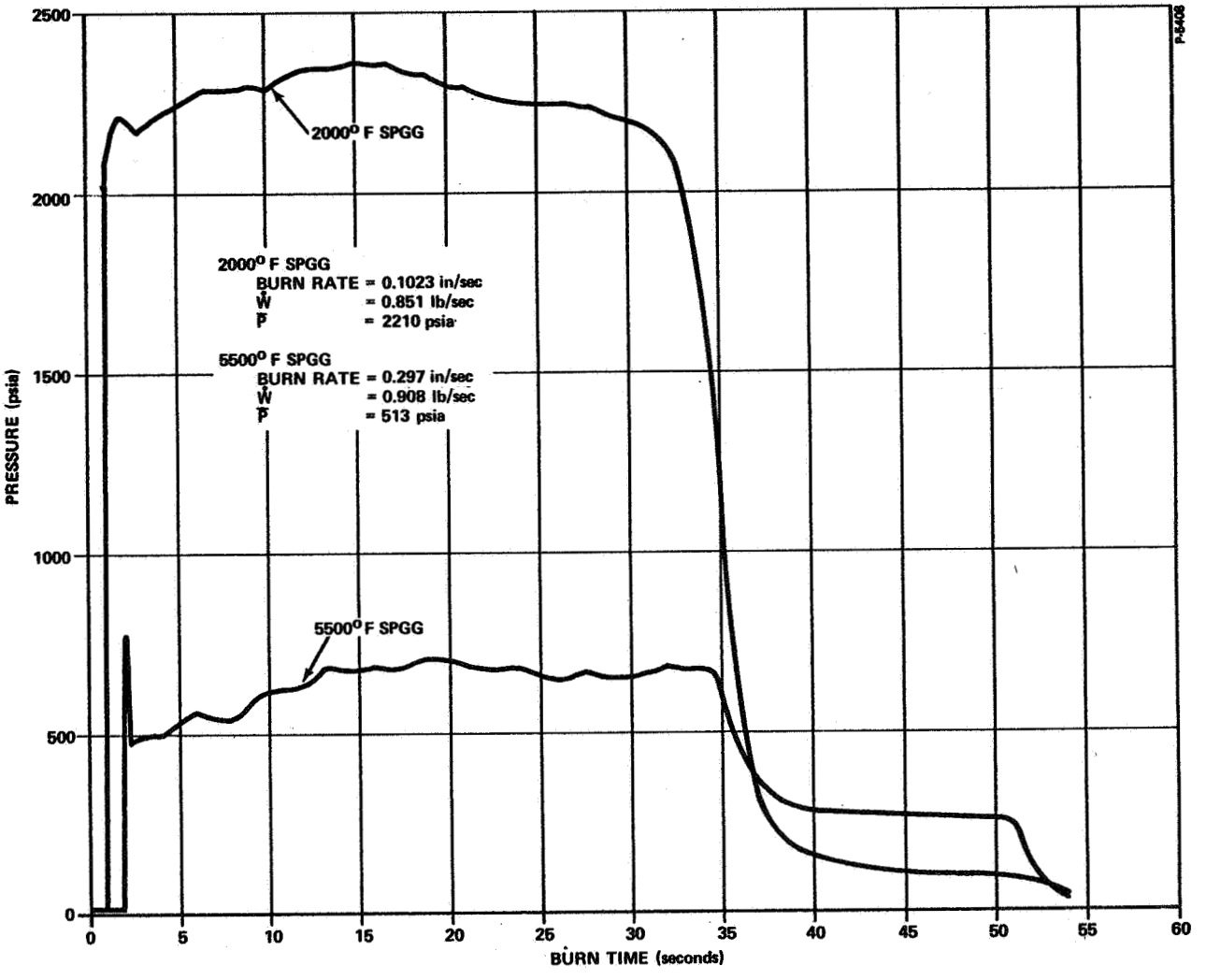

Figure 73 - 5500°F SPGG and 2000°F SPGG Ballistics Performance (Hot Gas Test No. 6)

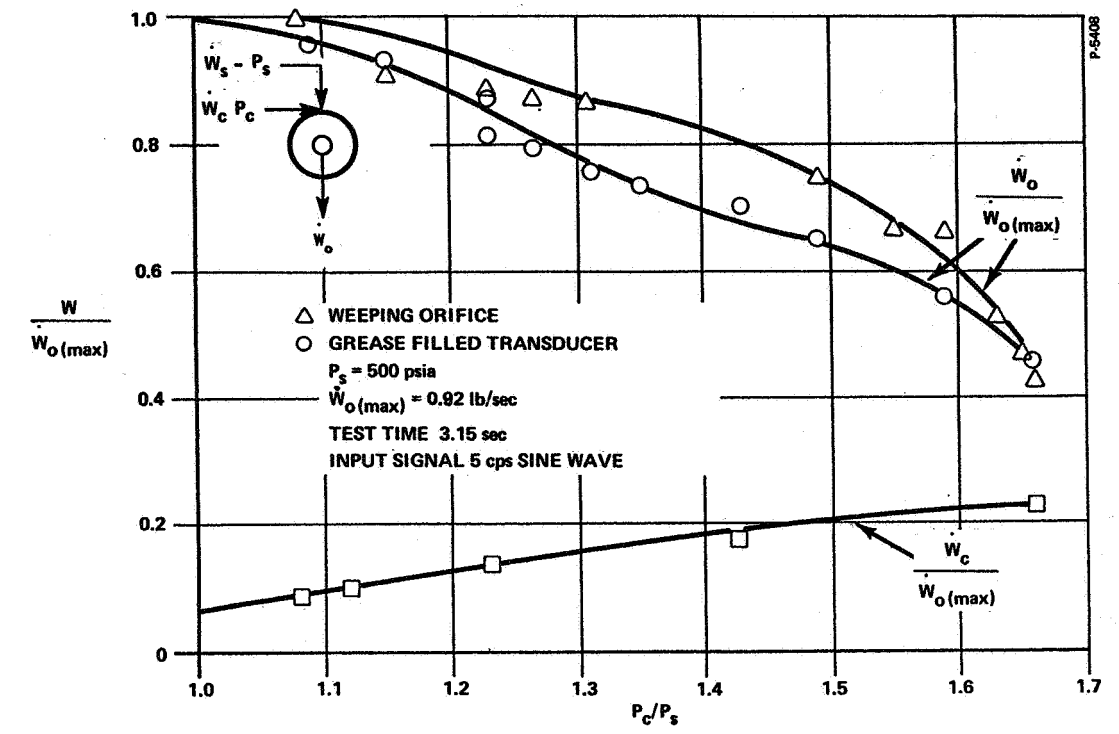

Figure 74 - Main Stage Vortex Valve No. 1 Hot Gas Performance

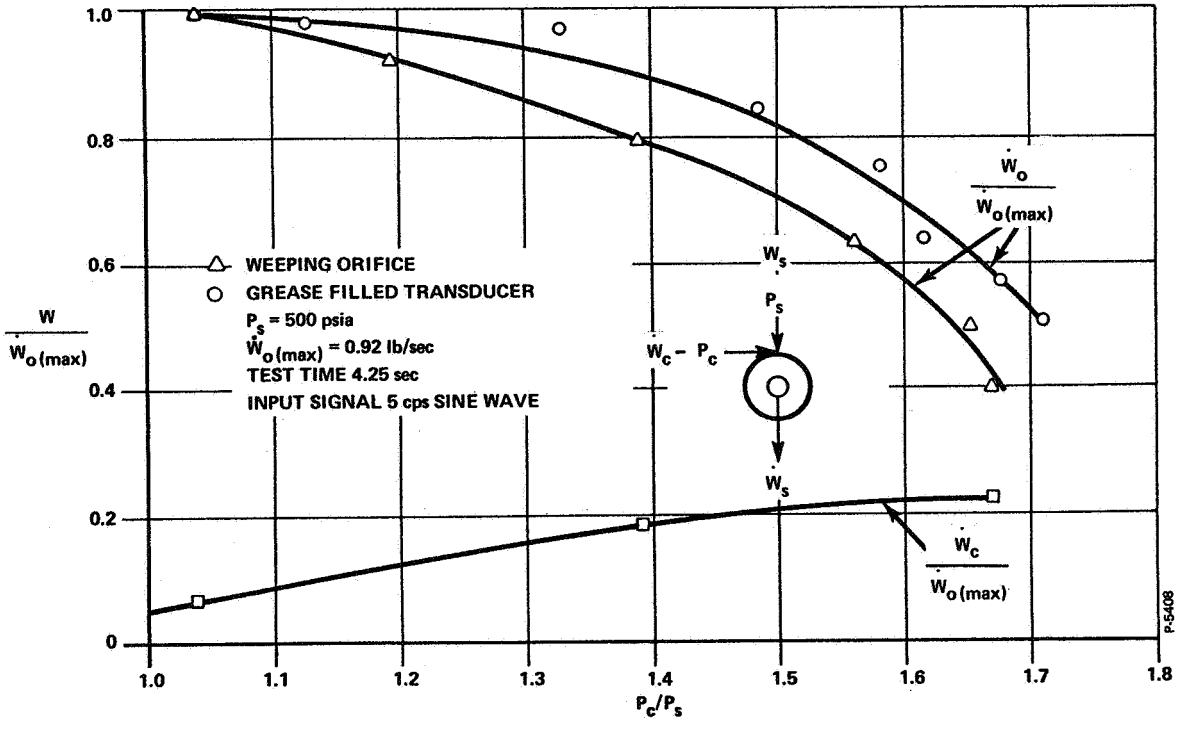

Figure 75 - Main Stage Vortex Valve No. 2 Hot Gas Performance

The total weight flow out of the two vortex valves based on weeping orifice flow data as taken from Figure 65 was:

$$\dot{W}_{out}\ (w.o.) = \dot{W}_{out}\ (No.\ 1) + \dot{W}_{out}\ (No.\ 2)$$

$$= 0.84\ (at\ P_{12} = 188\ psia) + 0.32\ (at\ P_{14} = 132\ psia)$$

$$\dot{W}_{out}\ (w.o.) = 1.16\ lb/sec$$

The total weight flow out of the two vortex valves based on the conventional flow measurement orifice flow data as taken from Figure 65 was:

$$\dot{W}_{out}\ (c.o.) = \dot{W}_{out}\ (No.\ 1) + \dot{W}_{out}\ (No.\ 2)$$

$$= 0.64\ (at\ P_{13} = 155\ psia) + 0.465\ (at\ P_{15} = 110\ psia)$$

$$\dot{W}_{out}\ (c.o.) = 1.105\ lb/sec$$

The results indicate that the flow measurement accuracy is within 5%.

The Hot Gas Test No. 6 installation is shown after the test in Figure 76. All of the test components, with the exception of the flow measurement system and a vent orifice gasket, performed their intended functions over the 50-second test duration without any structural failures. Components of a main stage vortex valve after test are shown in Figure 77.

Test Conclusions

The following conclusions have been drawn from Hot Gas Test No. 6:

(1) The main stage vortex valves modulated the flow of 5500°F gas for 57 cycles over a time span of 18 seconds at rates of 5, 10 and 15 cps.

(2) Test movies indicated that the system was still modulating flow after 12 seconds of operation.

(3) The main stage vortex valves were capable of a maximum of 3.46-to-1 flow modulation of 5500°F hot gas.

(4) The main stage system handled the flow of highly aluminized 5500°F solid propellant gas for 51 seconds with no component degradation.

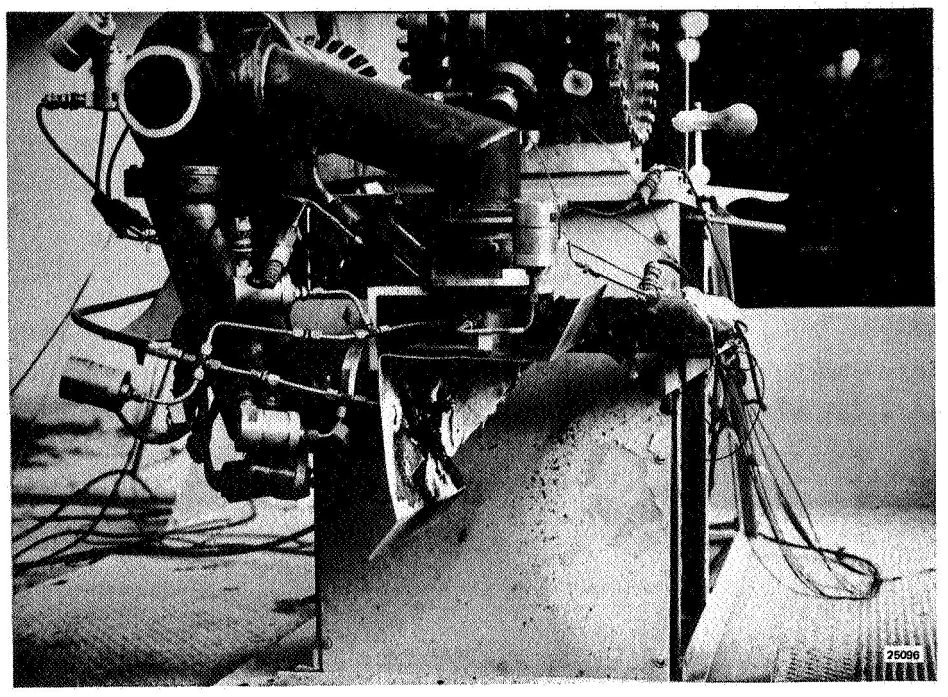

Figure 76 - 5500°F SITVC System Hot Gas Test No. 6 Installation (Post Test)

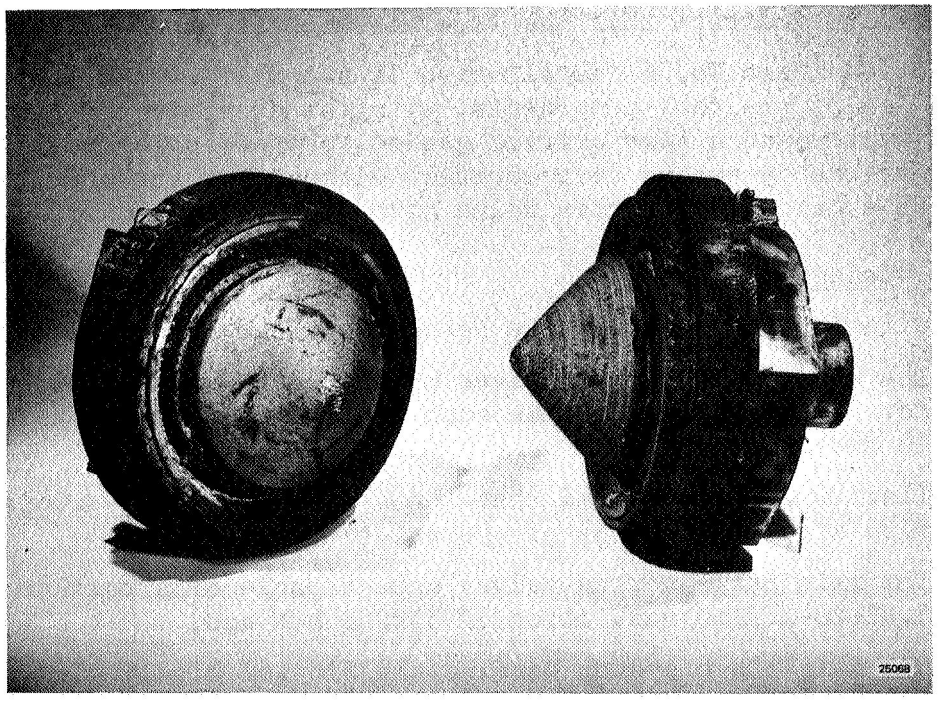

Figure 77 - Interior Components of Main Stage Vortex Valves (Post Test)

(5) The pilot stage functioned as intended for 33 seconds until the 2000°F SPGG burned out.

(6) The flow measurement techniques were accurate within 5%; however, the flow data measurements were not realized for the complete test.

CONCLUSIONS AND RECOMMENDATIONS

Conclusions

This program has demonstrated that the vortex valve, a no-moving-part fluidic device, has repeatedly and successfully modulated the flow of a highly aluminized and erosive hot gas as required by a secondary injection thrust vector control system. As a result of the development effort described in this report, the following conclusions are drawn:

(1) The vortex valve has demonstrated the capability of throttling the flow of highly aluminized (16%) 5500°F solid propellant gas over a modulation range from approximately 1 lb/sec to complete shutoff of the hot gas supplied to the valve.

(2) The vortex valve design developed in this program was capable of controlling the flow of erosive hot gas for more than 50 seconds.

(3) The 2000°F pilot stage gas used to control the vortex valve was at too low a temperature to demonstrate the 5-to-1 turndown ratio capability of the vortex valve. The theoretical turndown ratio with 2000°F control gas is 3.56 to 1, and a 3.46-to-1 turndown ratio was demonstrated.

(4) The vortex valve is a suitable valving element for throttling the flow of a typical high-performance rocket engine gas for applications requiring direct chamber bleed gas control.

Recommendations

As the result of successfully demonstrating the hot gas throttling capability of the vortex valve, and based on experience gained during the accomplishment of Phase I of the program, the following recommendations are made.

(1) A vortex valve controlled SITVC system should be demonstrated on a rocket motor using direct chamber bleed gas from the rocket engine as the injectant. The recent design trend of buried nozzle rocket motors provides a practical configuration for such a demonstration. The high-pressure differential available between the thrust chamber and the divergent nozzle section requires that a vortex valve be located in the thrust chamber with the outlet hole becoming the injection port. Four such valves can provide complete pitch and yaw thrust vector control on a small rocket motor. Larger rocket motors can use multiple valves in quadrant.

(2) It is recommended that a new pilot stage be designed to allow for the individual control of the main stage vortex valves rather than the push-pull type of operation of a pair of valves. A simple orifice and flapper-nozzle valve type of pilot stage would be more compatible with SITVC system installation and performance requirements for small rocket motors.

(3) The flow modulation performance of the main stage vortex valves can be improved if the pilot stage is supplied from a 4000°F gas generator. With the main stage valves receiving 4000°F control gas, rather than 2000°F control gas, the turndown performance should improve from 3.56:1 to approximately 4.50:1.

(4) The system tested to date has been a heavyweight workhorse type. Enough experience with materials has been acquired in this development program to permit the design of flightweight hardware. Concurrent with such design should be a weight tradeoff study to establish the competitive position of the vortex valve controlled secondary injection control system in comparison with other types of thrust vector control. It is recommended that all future efforts be accomplished with flightworthy hardware.

(5) It is recommended that additional effort be made toward the development of a technique for measuring the flow of aluminized 5500°F solid propellant gases. Since materials have been used in this program which survive for reasonable periods of time in this environment, it appears that the design and development of a reliable hot gas flow measurement device is possible.

APPENDIX A
SYSTEM PERFORMANCE ANALYSIS

APPENDIX A

SYSTEM PERFORMANCE ANALYSIS

A description and analysis of each of the three basic systems tested is provided in the following sections. The first system was used for a hot gas materials evaluation. The second system tested the performance of a single hot gas vortex valve. Two hot gas tests were performed with this type of system. The third system simulated a single-axis SITVC system incorporating two hot gas vortex valves in a push-pull arrangement controlled by two pilot stage vortex amplifier valves. Three hot gas tests were performed with this type of system.

The analyses made for the materials evaluation system and the single vortex valve system were based on preliminary 5500°F SITVC system calculations, the results of which are shown in Figure 78. These calculations were made utilizing a theoretical main stage vortex valve performance (Figure 79) and the gas properties supplied by the manufacturer of the 5500°F solid propellant gas generator. After Hot Gas Test No. 3, another analysis of the 5500°F SITVC system was accomplished for the following reasons: (1) the decision was made to eliminate the 5500°F SPGG load orifice and utilize a plenum chamber type of supply to the main stage vortex valves; (2) the first three hot gas tests indicated that some of the 5500°F solid propellant gas properties differed from those assumed in the original analysis; (3) a more representative theoretical vortex valve performance definition was obtained from a recently developed Bendix digital computer simulation of vortex valves.

The vortex valve computer simulation was based on an analytical curve, verified by experiment, that describes the nonlinear flow characteristics of a vortex valve over a wide range of operating conditions.[1]

The results of the computer study which utilized previous nitrogen cold gas test data as a model are shown in Figure 80. The computer study revealed that vortex valve flow modulation performance is influenced by the thermodynamic properties of the valve control and supply gases. The resulting theoretical hot gas performance of the main stage vortex valve utilizing 2000°F control gas was a flow modulation of 3.56 to 1 at a control pressure-to-supply ratio of 1.4 to 1.

The computer study also indicated that the vortex valve performance would improve to a flow modulation of 4.55 to 1 with 4000°F control gas and to 5.00 to 1 with 6000°F control gas.

The sizing of the main stage vortex valves in the following system analyses were conducted utilizing the theoretical vortex valve performance and various Bendix-developed parameters that interrelate the internal proportions of a vortex valve.

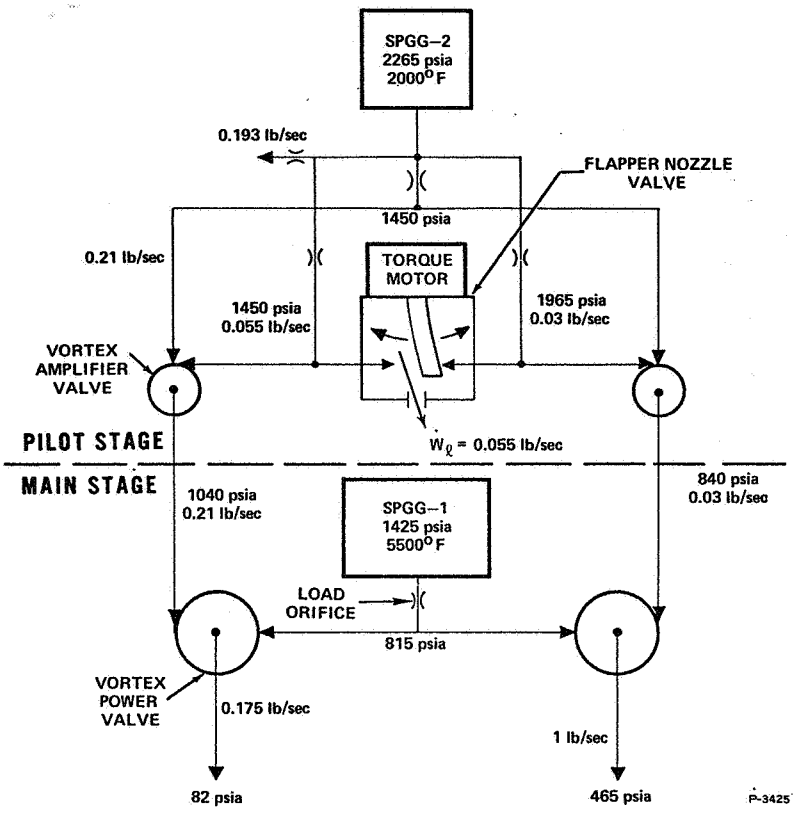

Figure 78 - 5500°F SITVC System (Preliminary)

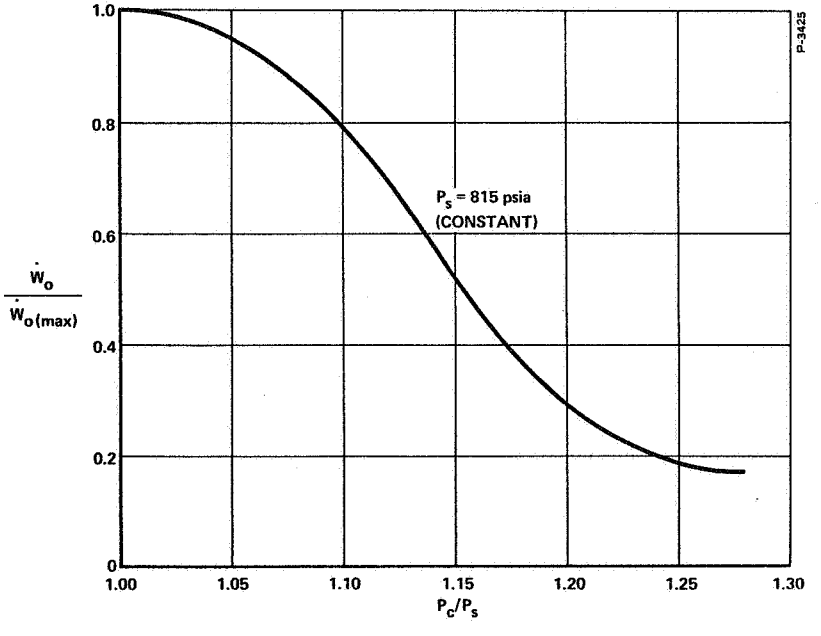

Figure 79 - Main Stage Vortex Valve Performance Characteristics (Theoretical)

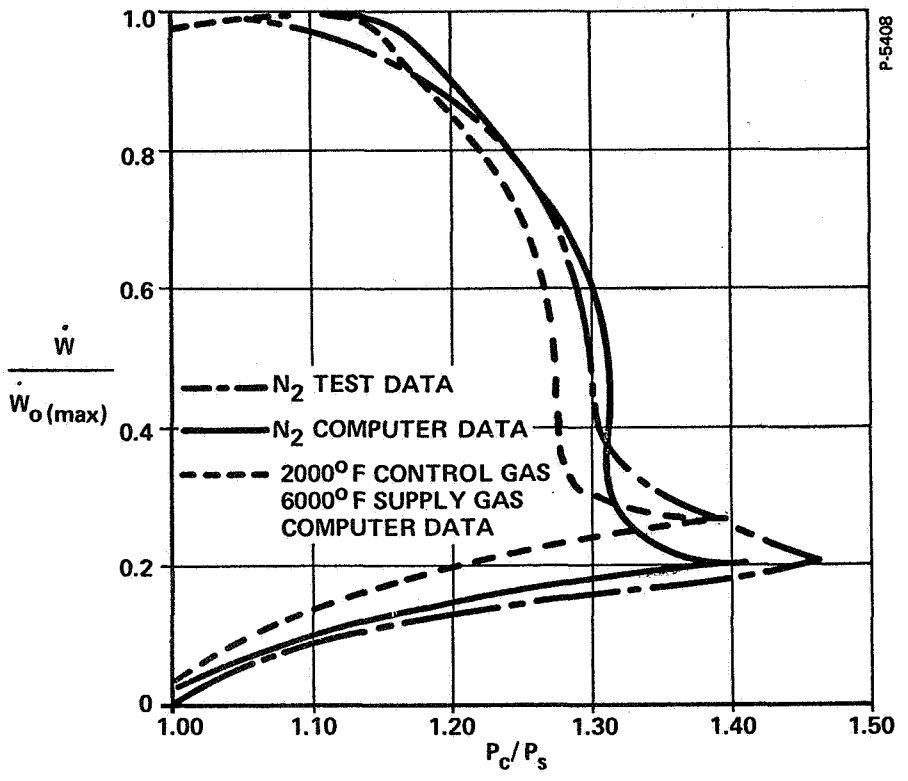

Figure 80 - Computer Study of Vortex Valve Performance Showing Effect of Gas Temperature

Performance Analysis for Materials Evaluation Test

The Hot Gas Test No. 1 was conducted to evaluate the materials selection and structural design of the main stage vortex valve and associated manifolding. The system is shown schematically in Figure 81.

In this test no effort was made to modulate the flow of hot gas with the main stage vortex valve, and the vortex valve contained no control gas injection ports. The vortex valve was essentially an orifice in the system. The vent orifice was necessary to provide the correct impedance for the SPGG.

Preliminary calculations of the system indicated that the main stage vortex valve outlet hole (A_2) should be 0.197 in^2 and that the 5500°F SPGG would operate at a pressure (P_g) of 1450 psia. At this pressure the flow rate produced by the 5500°F SPGG was determined to be

$$\dot{W}_g = A_g \rho P_g^n$$

$$\dot{W}_g = 48(0.0637)\ 0.0428(1450)^{0.30}$$

$$\dot{W}_g = 1.10 \text{ lb/sec}$$

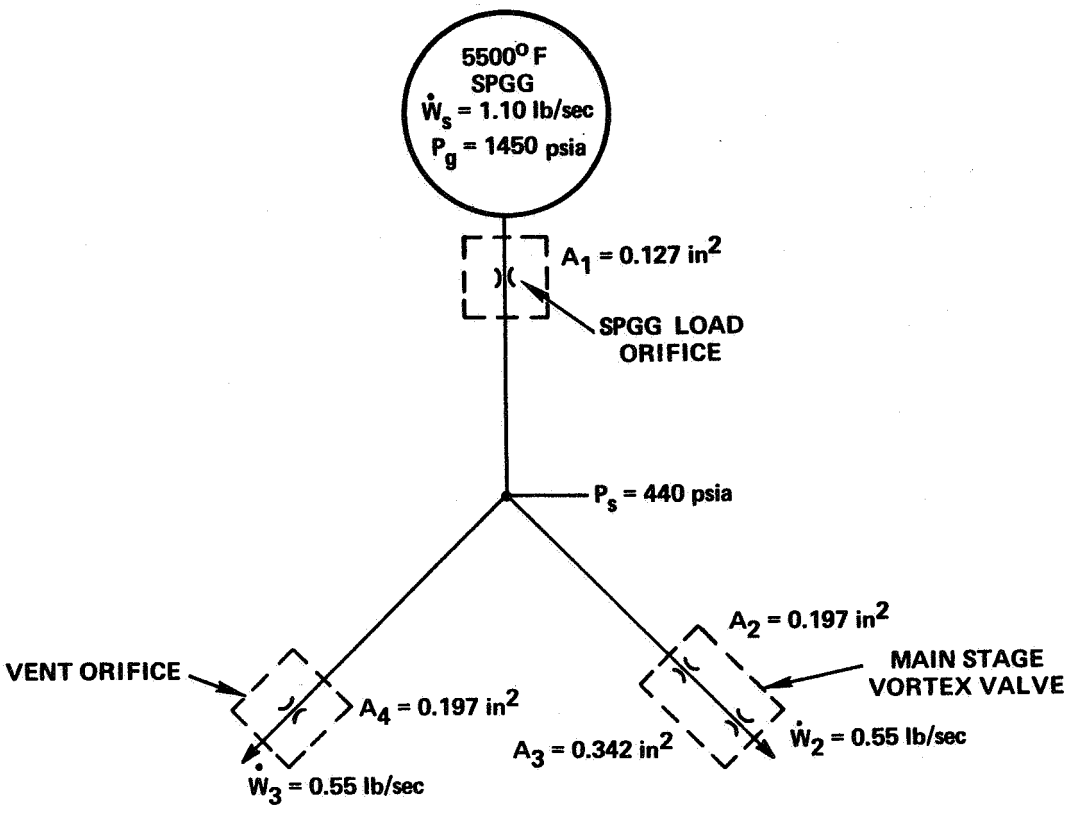

Figure 81 - Materials Evaluation System Schematic
(Hot Gas Test No. 1)

The size of the 5500°F SPGG load orifice and the supply pressure (P_s) to the main stage vortex valve and system vent orifice were calculated by assuming that orifices A_1, A_2, and A_4 were sonic.

Performance Analysis for Single Vortex Valve Test

The single vortex valve system that was used for Hot Gas Test No. 2 and No. 3 is shown schematically in Figure 82. These two hot gas tests were conducted to obtain hot gas vortex valve performance and to evaluate the system structural integrity before testing a full system including two main stage vortex valves.

The control gas to the main stage vortex valve is supplied by a 2000°F SPGG. The flow of control gas to the main stage vortex valve was modulated by a vented manual control valve.

The single vortex valve system performance and component sizes were determined by utilizing a 2000°F SPGG operating pressure (P_4) of 2265 psia, the theoretical vortex valve performance from Figure 79, and the main stage vortex valve outlet and control hole sizes of 0.197 in^2 and 0.0362 in^2 as obtained from preliminary 5500°F SITVC calculations based on flows and pressures in Figure 78.

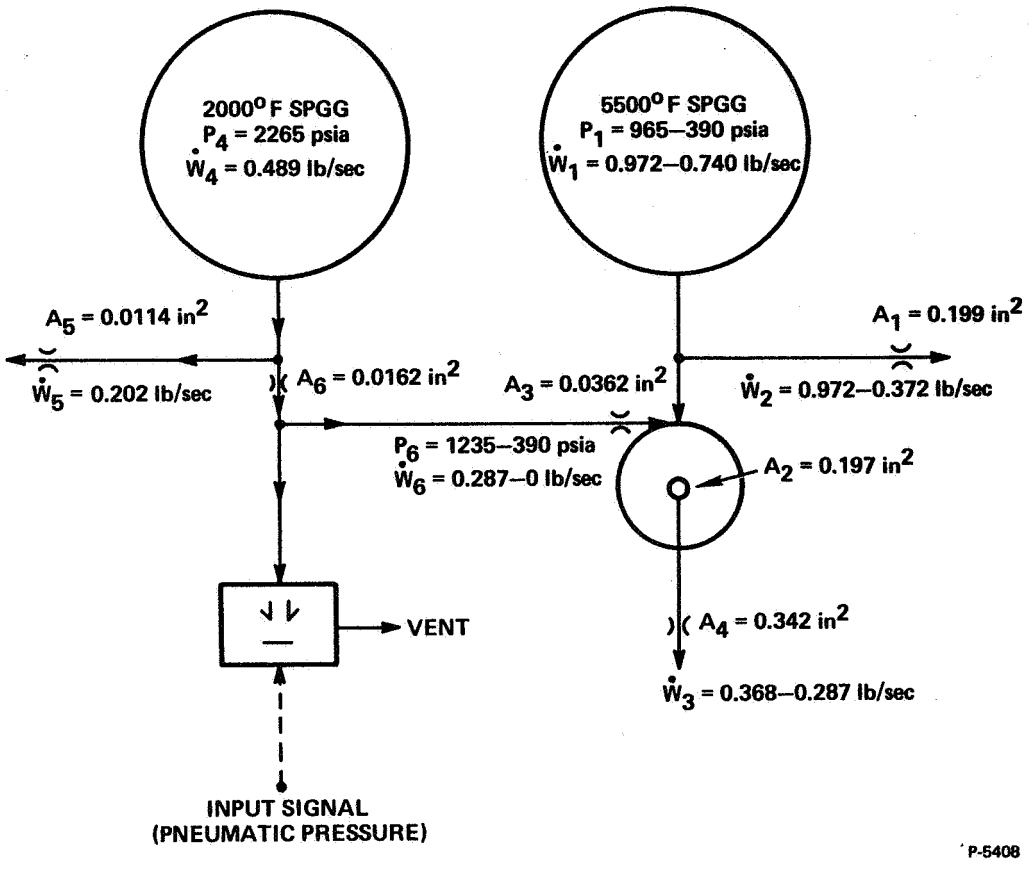

Figure 82 - Single Vortex Valve System Schematic
(Hot Gas Tests No. 2 and 3)

The maximum main stage vortex valve control pressure (P_6), with orifice A_6 (Figure 82) sonic at all times, was found to be

$$P_{6(max)} = P_4 \left(\frac{P_d}{P_u} \right) \text{ crit-2000°F}$$

$$= 2265 \ (0.547)$$

$$P_{6(max)} = 1235 \text{ psia}$$

By utilizing a control-to-supply pressure ratio ($P_c/P_s = P_6/P_1$) of 1.28 to obtain full main stage vortex valve turndown (Figure 79), the maximum operating pressure ($P_{1(max)}$) and flow rate ($W_{1(max)}$) of the 5500°F SPGG was found to be

$$P_{1(max)} = \frac{P_{6(max)}}{1.28}$$

$$= \frac{1235}{1.28}$$

$$P_{1(max)} = 965 \text{ psia}$$

and

$$\dot{W}_{1(max)} = A_g \rho c p^n$$

$$= 48(0.0637)\ 0.0428(965)^{0.3}$$

$$\dot{W}_{1(max)} = 0.972 \text{ lb/sec}$$

The maximum flow through the 5500°F SPGG vent orifice ($\dot{W}_{2(max)}$) and the size of the vent orifice were determined for system conditions when the main stage vortex valve is fully turned down. In this condition, $\dot{W}_{2(max)} = 0.972$ lb/sec, P_1 is maximum, and A_1 is calculated to be 0.199 in^2.

The minimum flow through the main stage vortex valve ($\dot{W}_{3(min)}$) is equal to the maximum control flow into the valve ($W_{6(max)}$) during full turndown, which was calculated to be 0.287 lb/sec.

With the main stage vortex valve operating in the full open mode, the control pressure ($P_{6(min)}$) was assumed to equal the supply pressure $P_{1(min)}$. This condition results in zero control flow into the main stage valve. The 5500°F SPGG, the SPGG vent orifice, and the main stage vortex valve flow of hot gas were determined as follows.

The 5500°F hot gas flow balance is

$$\dot{W}_1 = \dot{W}_2 + \dot{W}_3$$

writing the simultaneous equations and solving for the SPGG pressure, $P_{1(min)}$ is found to be

$$P_{1(min)} = 390 \text{ psia} = P_{6(min)}$$

Therefore,

$$\dot{W}_{1(min)} = A_g \rho c P_{1(min)}^{n}$$

$$= 48(0.0637)\ 0.0428(390)^{0.3}$$

$$\dot{W}_{1(min)} = 0.740 \text{ lb/sec}$$

Using $P_{1(min)}$ with sonic flow through the vortex valve outlet,

$$\dot{W}_{3(max)} = 0.368 \text{ lb/sec}$$

By subtraction,

$$\dot{W}_{2(min)} = 0.372 \text{ lb/sec}$$

The flow modulation of the main stage vortex valve in this system was found to be

$$\frac{\dot{W}_{3(max)}}{\dot{W}_{3(min)}} = \frac{0.368}{0.287} = 1.267 \text{ to } 1$$

This value of main stage vortex valve flow modulation is low because SPGG operating pressure (P_1) varies with the valve modulation. A better measure of valve performance is to compare maximum and minimum vortex valve flows for the same supply pressure.

The valve turndown at constant pressure would be

$$\frac{\dot{W}_{3(proj.max)}}{\dot{W}_{3(min)}} = \frac{0.91}{0.287} = 3.17$$

Performance Analysis for SITVC System Tests No. 4 through No. 6

The 5500°F SITVC system used in Hot Gas Tests No. 4 and No. 5 is shown schematically in Figure 83. An analysis of the system was made to determine component sizes and to predict system performance. The results of the analysis are depicted in the pressure and flow maps (Figures 83 and 84) for pilot stage flapper positions of full stroke and null.

The analysis was based on theoretical performances of the pilot stage and the main stage vortex valves. The pilot stage vortex valve theoretical performance (Figure 85) was obtained by projecting the known performance of a similar Bendix vortex amplifier valve to fit the operating conditions of this system. The theoretical performance of the main stage vortex valve (Figure 86) was obtained from a Bendix digital computer simulation of a vortex valve which utilized previous main stage cold gas data as a model.

The selected operating range of the main stage valve was from a P_c/P_s ratio of 1.05 to 1.5. The lower limit ($P_c/P_s = 1.05$) was made greater than unity to prevent the backflow of the aluminized 5500°F supply gas into the main stage vortex valve control injectors. The wide operating range of P_c/P_s from 1.05 to 1.5 was utilized to encompass possible test performance variations from the theoretical valve performance.

To minimize the possibility of a wide variation in the 2000°F SPGG operating pressures, a relief valve was assumed to be in the pilot stage as shown in Figures 83 and 84.

With the pilot stage flapper at full stroke to the right, the main stage valve on the right side of the circuit will be operating in a full-open mode; i.e., $P_{10}/P_{22} = 1.05$. The main stage valve on the opposite side of the circuit will be in full turndown mode with $P_{19}/P_{22} = 1.5$. The two main stage vortex valve supply flows, $\dot{W}_{20}$ and $\dot{W}_{11}$, can be expressed as follows:

$$\dot{W}_{20} = 0$$

$$\dot{W}_{11} = \dot{W}_{22} = A_g \rho c P_{22}^{n} = 48(0.0637)0.0428(P_{22})^{0.3}$$

$$\dot{W}_{11} = 0.131(P_{22})^{0.3} \qquad \text{(A-1)}$$

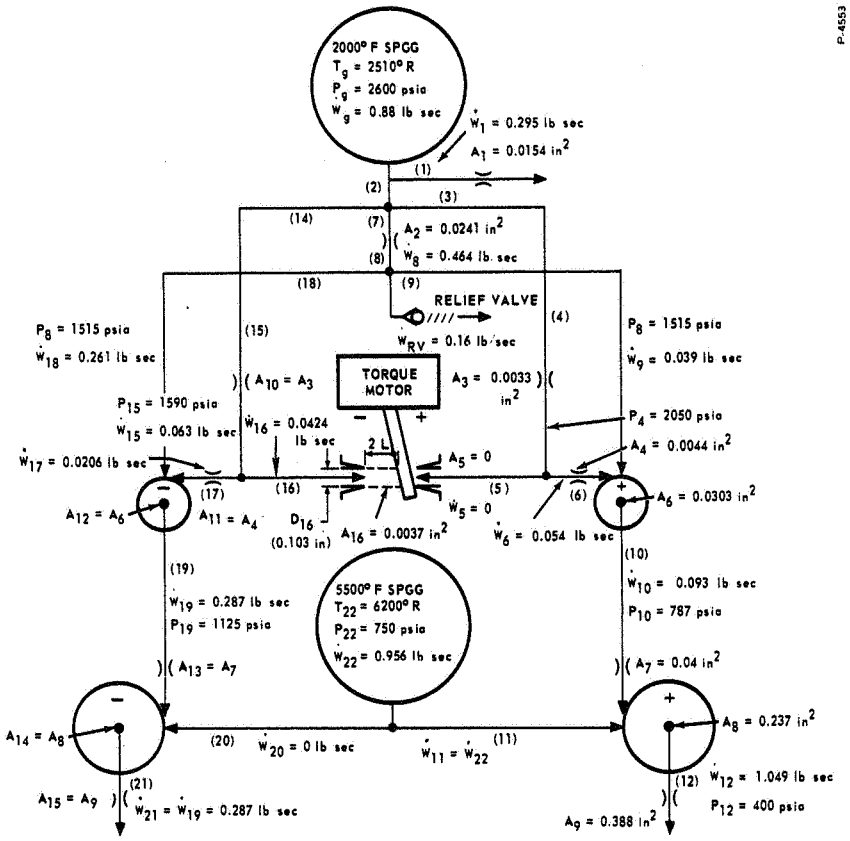

Figure 83 - 5500°F SITVC System Pressure-Flow Map With the Pilot Stage Flapper at Full Stroke

P-4553

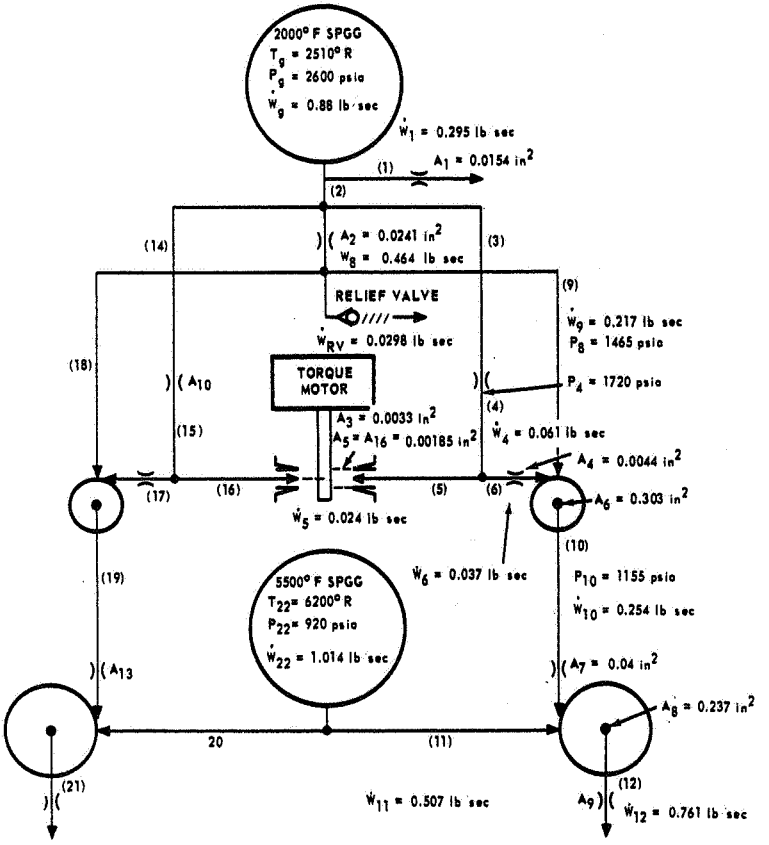

Figure 84 - 5500°F SITVC System Pressure-Flow Map With the Pilot Stage Flapper at Null

Since $P_{10}/P_{22} = 1.05$ the main stage vortex valve control flow, $\dot{W}_{10}$ is,

$$\dot{W}_{10} = \frac{C_{d7}\ C_2(\text{Omax})\ A_7\ P_{10}}{\sqrt{T_g}}\ f_1\left(\frac{P_{22}}{P_{10}}\right) = \frac{0.8(0.412)A_7(1.05P_{22})}{\sqrt{2510}}\ f_1\left(\frac{1}{1.05}\right)$$

$$\dot{W}_{10} = 0.00311\ A_7\ P_{22} \qquad \text{(A-2)}$$

For the left-hand main stage vortex valve with $P_{19}/P_{22} = 1.50$, the control flow, $\dot{W}_{19}$, is

$$\dot{W}_{19} = \frac{C_{d7}\ C_2(\text{Omax})\ A_{13}\ P_{19}}{\sqrt{T_g}}\ f_1\left(\frac{P_{22}}{P_{19}}\right) = \frac{0.8(0.412)A_7(1.5P_{22})}{\sqrt{2510}}\ f_1\left(\frac{1}{1.5}\right)$$

$$\dot{W}_{19} = 0.00951\ A_7\ P_{22} \qquad \text{(A-3)}$$

From Figure 86, the relationship between $\dot{W}_{19}$ and the maximum supply flow of the valve ($\dot{W}_{s(max)} = \dot{W}_{11}$) is

$$\dot{W}_{19} = (0.3)\dot{W}_{s(max)} = (0.3)\dot{W}_{11} \qquad \text{(A-4)}$$

Assuming sonic flow through the right-hand main stage vortex valve outlet hole, A_8, the total outlet flow, $\dot{W}_{12}$, is

$$\dot{W}_{12} = \frac{C_{d8}\ C_2(PJS_c)\ A_8\ P_{22}}{\sqrt{T_{22}}} = \frac{0.84(0.556)A_8\ P_{22}}{\sqrt{6200}}$$

$$\dot{W}_{12} = 0.00594\ A_8\ P_{22} \qquad \text{(A-5)}$$

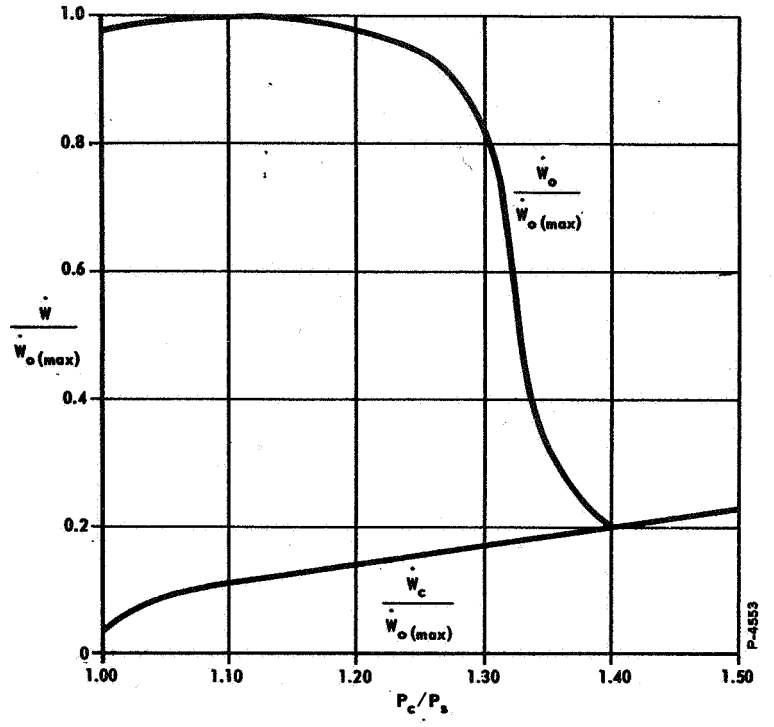

Figure 85 - Theoretical Performance of Pilot Stage Vortex Amplifier Valve

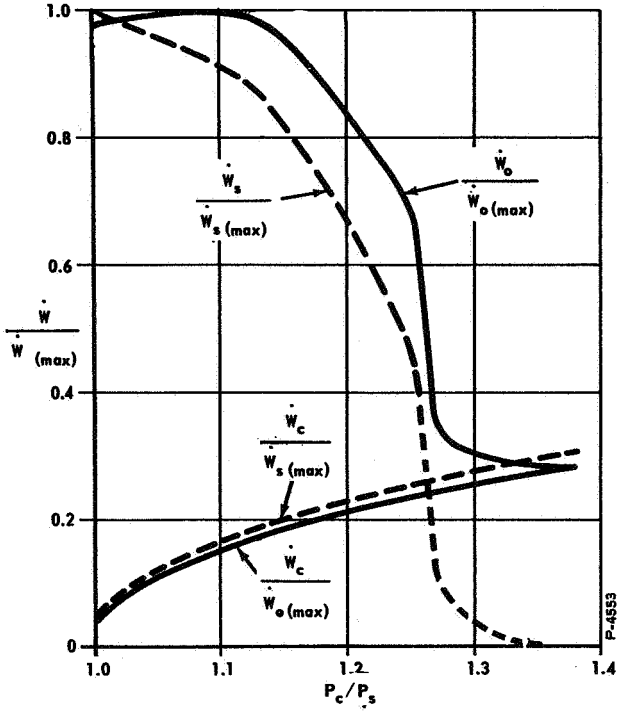

Figure 86 - Computer Simulation of 5500°F SITVC System Main Stage Vortex Valve Performance

But $\dot{W}_{12}$ can also be expressed as

$$\dot{W}_{12} = \dot{W}_{11} + \dot{W}_{10} \qquad \text{(A-6)}$$

Combining equations (A-1) through (A-6), P_{22} was determined to be

$$P_{22} = \frac{96}{(A_8)^{1.43}} \qquad \text{(A-7)}$$

Preliminary computations revealed that the 5500°F SPGG should be operated at 750 psia, in order to limit the 2000°F SPGG to 2600 psia operating pressure while maintaining the desired pressure distribution through the system. Utilizing P_{22} = 750 psia and equations (A-1) through (A-7), the main stage vortex valve component sizes, operating pressures and flow rates were determined to be:

$$A_8 = \left(\frac{96}{P_{22}}\right)^{\frac{1}{1.43}} = \left(\frac{96}{750}\right)^{\frac{1}{1.43}} = 0.237 \text{ in}^2 \qquad \text{(A-7)}$$

$$\dot{W}_{11} = 0.131(P_{22})^{0.3} = 0.131(750)^{0.3} = 0.956 \text{ lb/sec} \qquad \text{(A-1)}$$

$$\dot{W}_{19} = 0.3(\dot{W}_{11}) = 0.3(0.956) = 0.2868 \text{ lb/sec} \qquad \text{(A-4)}$$

$$A_7 = \frac{\dot{W}_{19}}{0.00951(P_{22})} = \frac{0.2868}{0.00951(750)} = 0.04 \text{ in}^2 \qquad \text{(A-3)}$$

$$\dot{W}_{10} = 0.00311\ P_{22}\ A_7 = 0.00311(750)0.04 = 0.0933 \text{ lb/sec} \qquad \text{(A-2)}$$

$$P_{19} = 1.5(P_{22}) = 1.5(750) = 1125 \text{ psia}$$

$$P_{10} = 1.05(P_{22}) = 1.05(750) = 787 \text{ psia}$$

$$\dot{W}_{12} = \dot{W}_{11} + \dot{W}_{10} = 0.956 + 0.093 = 1.049 \text{ lb/sec} \qquad \text{(A-6)}$$

The computations for the pilot stage portion of the 5500°F SITVC system were made by utilizing main stage vortex valve control flow and pressure requirements determined above, a minimum P_c/P_s ratio of 1.05, and a maximum P_c/P_s ratio of 1.4 as obtained from Figure 85, and by assuming $P_8 = 1.35\ P_{19}$ and $P_g = 2600$ psia.

The pilot stage vortex valve outlet hole size is found from

$$A_{12} = \frac{\dot{W}_{19}\sqrt{T_g}}{C_{d16}\ C_2(0\text{max})\ 1.35P_{19}\ f_1\left(\frac{1}{1.35}\right)} = \frac{0.287\sqrt{2510}}{0.84(0.412)1.35(1125)0.904}$$

$$A_{12} = A_6 = 0.0303 \text{ in}^2$$

From Figure 85 at $P_c/P_s = 1.05$, $\dot{W}_c/\dot{W}_{o(max)} = 0.09$; therefore

$$\dot{W}_{18} = 0.91(\dot{W}_{19}) = 0.91(0.287) = 0.261 \text{ lb/sec}$$

Also, from Figure 85 at $P_c/P_s = 1.4$, $\dot{W}_c = 0.2\ \dot{W}_{o(max)}$

Therefore

$$\dot{W}_{6(max)} = 0.2(\dot{W}_{19}) = 0.2(0.287) = 0.0574 \text{ lb/sec}$$

The relationship for maximum vortex valve control flow, $\dot{W}_{6(max)}$, can also be written as

$$\dot{W}_{6(max)} = \frac{C_{d4}\ C_2(Omax)\ A_4\ P_{4(max)}}{\sqrt{T_g}}\ f_1\left(\frac{P_8}{P_{4(max)}}\right)$$

From this expression the pilot stage vortex valve injector area, A_4, was determined, using $P_8 = 1515$ psia and $P_{4(max)} = 1.4\ P_8$:

$$A_4 = \frac{\dot{W}_{6(max)}\sqrt{T_g}}{C_{d4}\ C_2(Omax)\ P_{4(max)}\ f_1\left(\frac{P_8}{P_{4(max)}}\right)} = \frac{0.0574\ \sqrt{2510}}{0.8(0.412)1.4(1515)(0.93)}$$

$$A_4 = A_{11} = 0.0044\ in^2$$

The minimum pilot stage vortex valve control flow was found to be

$$\dot{W}_{17} = \frac{C_{d11}\ C_2(Omax)\ P_{15}\ A_{11}}{\sqrt{T_g}}\ f_1\left(\frac{P_8}{P_{15}}\right) = \frac{0.8(0.412)1590(0.0044)}{\sqrt{2510}}\ f_1\left(\frac{1}{1.05}\right)$$

$$\dot{W}_{17} = 0.0206\ lb/sec$$

The maximum operating level of control pressure and flow for the pilot stage vortex valve was determined as follows.

Since

$$\dot{W}_{10(max)} = \dot{W}_{19}$$

then

$$\frac{\dot{W}_{10}}{\dot{W}_{10(max)}} = \frac{0.0933}{0.287} = 0.325$$

From Figure 85 at $\dot{W}_o/\dot{W}_{o(max)} = 0.325$, the ratio of P_c to P_s is equal to 1.35.

Therefore

$$P_4 = 1.35\ P_8 = 1.35(1515) = 2050 \text{ psia}$$

and

$$\dot{W}_6 = \frac{C_{d4}\ C_2(\dot{O}max)\ P_4\ A_4}{\sqrt{T_g}}\ f_1\left(\frac{P_8}{P_4}\right) = \frac{0.8(0.412)2050(0.0044)}{\sqrt{2510}}(0.904)$$

$$\dot{W}_6 = 0.0539 \text{ lb/sec}$$

Also

$$\dot{W}_9 = \dot{W}_{10} - \dot{W}_6 = 0.0933 - 0.0539$$

$$\dot{W}_9 = 0.0394 \text{ lb/sec}$$

From Figure 83, nozzle area A_5 is zero; the resulting nozzle flow is also zero, and the flow $\dot{W}_4$ is equal to $\dot{W}_6$. From this consideration, the size of orifices A_3 and A_{10} were found, as follows:

$$\dot{W}_4 = \dot{W}_6 = \frac{C_{d3}\ C_2(\dot{O}max)\ P_g\ A_3}{\sqrt{T_g}}\ f_1\left(\frac{P_4}{P_g}\right)$$

or

$$A_3 = \frac{\dot{W}_6\ \sqrt{T_g}}{C_{d3}\ C_2(\dot{O}max)\ P_g\ f_1\left(\frac{P_4}{P_g}\right)} = \frac{0.0539\sqrt{2510}}{0.9(0.412)2600\ f_1\left(\frac{2050}{2600}\right)}$$

$$A_3 = A_{10} = 0.0033 \text{ in}^2$$

Utilizing the area for A_{10}, the flow rate $\dot{W}_{15}$ was found to be

$$\dot{W}_{15} = \frac{C_{d10}\, C_2(\text{Omax})\, P_g\, A_{10}}{\sqrt{T_g}}\, f_1\left(\frac{P_{15}}{P_g}\right) = \frac{0.9(0.412)2600(0.0033)}{\sqrt{2510}}(0.99)$$

$$\dot{W}_{15} = 0.063 \text{ lb/sec}$$

where

$P_{15} = 1.05(1515) = 1590$ psia

From the above results, the flow through flow area A_{16}, the size of the nozzle, D_{16}, and flapper stroke, L, were determined as follows:

$$\dot{W}_{16} = \dot{W}_{15} - \dot{W}_{17} = 0.063 - 0.0206 = 0.0424 \text{ lb/sec}$$

$$A_{16} = \frac{\dot{W}_{16}\sqrt{T_g}}{C_{d16}\, C_7(\text{Omax})\, P_{15}} = \frac{0.0424\sqrt{2510}}{0.9(0.412)1590} = 0.0037 \text{ in}^2$$

The nozzle flow area, A_{16}, is the cylindrical orifice area between the flapper and the nozzle at full stroke. Thus,

$$A_{16} = 2\pi D_{16} L$$

or

$$L = \frac{A_{16}}{2\pi D_{16}}$$

where

L = flapper stroke from null to full stroke

Because the nozzles were existing hardware, a D_{16} of 0.103 inch was selected.

Then

$$L = \frac{0.0037}{2\pi(0.103)} = 0.0057 \text{ in.}$$

The remaining component sizes and flow rates were calculated with the pilot stage flapper in null position. The component sizes and the system performance for null position of the pilot stage flapper were determined by utilizing the schematic shown in Figure 84 and the following assumptions.

The first assumption was that the 2000°F SPGG would remain operating at 2600 psia. Secondly, it was assumed that the relief valve would compensate for any increased supply flow requirement of the two pilot stage vortex valves, while allowing P_8 to drop 50 psi from 1515 psia at flapper full-stroke position to 1465 psia at flapper null position.

With the pilot stage flapper at null position, the areas A_5 and A_{16} were found to be:

$$A_5 = A_{16} = \pi D_5 L = \pi(0.103)0.0057 = 0.00185 \text{ in}^2$$

Therefore

$$\dot{W}_5 = \dot{W}_{16} = \frac{C_{d5}\ C_2(\text{Omax})\ \ A_5\ P_4}{\sqrt{T_g}} = \frac{0.9(0.412)0.00185}{\sqrt{2510}} P_4$$

$$\dot{W}_5 = 0.138 \times 10^{-4}\ P_4 \qquad \text{(A-8)}$$

The flow through the control injectors is

$$\dot{W}_6 = \frac{C_{d4}\ C_2(\text{Omax})\ \ A_4\ P_4}{\sqrt{T_g}} f_1\left(\frac{P_8}{P_4}\right) = \frac{0.8(0.412)0.0044\ P_4}{\sqrt{2510}} f_1\left(\frac{1465}{P_4}\right)$$

$$\dot{W}_6 = 0.29 \times 10^{-4}\ P_4\ f_1\left(\frac{1465}{P_4}\right) \qquad \text{(A-9)}$$

The flow through orifice A_3 is

$$\dot{W}_4 = \frac{C_{d3}\ C_2(\text{Omax})\ \ A_3\ P_g}{\sqrt{T_g}}\ f_1\left(\frac{P_4}{P_g}\right) = \frac{0.9(0.412)0.0033(2600)}{\sqrt{2510}}\ f_1\left(\frac{P_4}{2600}\right)$$

$$\dot{W}_4 = 0.0622\ f_1\left(\frac{P_4}{2600}\right) \qquad \text{(A-10)}$$

But

$$\dot{W}_4 = \dot{W}_5 + \dot{W}_6 \qquad \text{(A-11)}$$

By solving equations (A-8), (A-9), (A-10), and (A-11) simultaneously, P_4 was found to be 1720 psia.

$$\frac{P_4}{P_8} = \frac{1720}{1465} = 1.175$$

Therefore, from Figure 85 at $P_c/P_s = 1.175$,

$$\frac{\dot{W}_{10}}{\dot{W}_{10(\text{max})}} = 0.98 \qquad \text{(A-12)}$$

Also

$$\dot{W}_{10(\text{max})} = \frac{C_{d6}\ C_2(\text{Omax})\ A_6\ P_8}{\sqrt{T_g}}\ f_1\left(\frac{P_{10}}{P_8}\right) = \frac{0.8(0.412)0.0303(1465)}{\sqrt{2510}}\ f_1\left(\frac{P_{10}}{1465}\right)$$

$$\dot{W}_{10(\text{max})} = 0.306\ f_1 \qquad \text{(A-13)}$$

By combining equations (A-12) and (A-13), $\dot{W}_{10}$ was found to be

$$\dot{W}_{10} = (0.98)0.306\ f_1\left(\frac{P_{10}}{1465}\right)$$

$$\dot{W}_{10} = 0.30\ f_1\left(\frac{P_{10}}{1465}\right) \qquad \text{(A-14)}$$

Also, the flow $\dot{W}_{10}$ was expressed as flow through the main stage valve control injector:

$$\dot{W}_{10} = \frac{C_{d7}\ C_2(\text{Omax})\ A_7\ P_{10}}{\sqrt{T_g}}\ f_1\left(\frac{P_{22}}{P_{10}}\right) = \frac{0.8(0.412)0.04\ P_{10}}{\sqrt{2510}}\ f_1\left(\frac{P_{22}}{P_{10}}\right)$$

$$\dot{W}_{10} = 2.63 \times 10^{-4}\ P_{10}\ f_1\left(\frac{P_{22}}{P_{10}}\right) \qquad \text{(A-15)}$$

Combining equations (A-14) and (A-15),

$$f_1\left(\frac{P_{10}}{1465}\right) = 9.76 \times 10^{-4}\ P_{10}\ f_1\left(\frac{P_{22}}{P_{10}}\right) \qquad \text{(A-16)}$$

Each main stage valve will be receiving one half of the 5500°F SPGG's output. Thus,

$$\dot{W}_{11} = 1/2\ \dot{W}_{22}$$

From equation (A-1),

$$\dot{W}_{11} = 0.0655\ (P_{22})^{0.3} \qquad \text{(A-17)}$$

The total flow through the main stage vortex valve at partial turndown is expressed as

$$\dot{W}_{12} = \frac{C_{d8}\, C_2 (PJS_c)\, A_8\, P_{22}}{\sqrt{T_{22}}}\, C_v = \frac{(0.84)(0.556)0.237\, P_{22}}{\sqrt{6200}}\, C_v$$

$$\dot{W}_{12} = 14.8 \times 10^{-4}\, P_{22}\, C_v \qquad \text{(A-18)}$$

where

$C_v = \dot{W}_o / \dot{W}_{o(max)}$ from Figure 86 at various values of $P_c/P_s = P_{10}/P_{22}$.

Combining equations (A-15), (A-17), and (A-18) to express $\dot{W}_{12}$ as the sum of $\dot{W}_{10}$ and $\dot{W}_{11}$, the following relationship is obtained.

$$P_{22} C_v = 0.178\, P_{10}\, f_1\left(\frac{P_{22}}{P_{10}}\right) + 44.3\, (P_{22})^{0.3} \qquad \text{(A-19)}$$

By iteration

$$P_{10} = 1155 \text{ psia}$$

and

$$P_{22} = 920 \text{ psia}$$

Various flow rates are found to be

$$\dot{W}_{11} = 0.0655 (P_{22})^{0.3} = 0.0655 (920)^{0.3} = 0.507 \text{ lb/sec} \qquad \text{(A-17)}$$

$$\dot{W}_{10} = 0.3\ f_1\left(\frac{P_{10}}{1465}\right) = 0.3\ f_1\left(\frac{1155}{1465}\right) = 0.254 \text{ lb/sec} \qquad \text{(A-14)}$$

$$\dot{W}_{12} = \dot{W}_{11} + \dot{W}_{10} = 0.507 + 0.254 = 0.761 \text{ lb/sec} \qquad \text{(A-6)}$$

$$\dot{W}_5 = 0.138 \times 10^{-4}\ P_4 = 0.138 \times 10^{-4}(1720) = 0.0238 \text{ lb/sec} \qquad \text{(A-8)}$$

$$\dot{W}_6 = 0.29 \times 10^{-4}\ P_4\ f_1\left(\frac{1465}{P_4}\right) = 0.29 \times 10^{-4}\ (1720)\ f_1\left(\frac{1465}{1720}\right) \qquad \text{(A-9)}$$

$$\dot{W}_6 = 0.037 \text{ lb/sec}$$

$$\dot{W}_4 = \dot{W}_6 + \dot{W}_5 = 0.037 + 0.0238 = 0.0608 \text{ lb/sec} \qquad \text{(A-11)}$$

$$\dot{W}_9 = \dot{W}_{10} - \dot{W}_6 = 0.254 - 0.037 = 0.217 \text{ lb/sec}$$

The variation in relief valve flow was found as follows:

$$(\dot{W}_9 + \dot{W}_{18}) \text{ at null} = 0.217 + 0.217 = 0.434 \text{ lb/sec}$$

$$(\dot{W}_9 + \dot{W}_{18}) \text{ at full stroke} = 0.0398 + 0.264 = 0.3038 \text{ lb/sec}$$

$$\Delta\dot{W}_{R.V.} = 0.434 - 0.3038 = 0.1302 \text{ lb/sec}$$

The relief valve characteristics indicated that its maximum flow should be 0.16 lb/sec at P_8 = 1515 psia for full-stroke position of the pilot stage flapper. The relief valve flow rate at null was determined to be

$$\dot{W}_{R.V.(null)} = 0.16 - \Delta\dot{W}_{R.V.} = 0.16 - 0.1302 = 0.0298 \text{ lb/sec}$$

The flow rate through orifice A_2 was found to be

$$\dot{W}_8 = \dot{W}_{R.V.(null)} + \dot{W}_9 + \dot{W}_{18} = 0.0298 + 0.217 + 0.217$$

$$\dot{W}_8 = 0.4638 \text{ lb/sec}$$

and

$$A_2 = \frac{\dot{W}_8 \sqrt{T_g}}{C_{d8}\ C_2(\mathbb{O}\max)\ P_g\ f_1\left(\frac{P_8}{P_g}\right)} = \frac{0.4638\sqrt{2510}}{0.9(0.412)2600(0.997)}$$

$$A_2 = 0.0241 \text{ in}^2$$

The output of the 2200°F SPGG for an operating pressure of 2600 psia was found to be

$$\dot{W}_g = A_g\ \rho\ c\ P_g^{\ n} = 157(0.053)0.0203(2600)^{0.21}$$

$$\dot{W}_g = 0.88 \text{ lb/sec}$$

The flow through the dumping orifice, A_1, is the 2200°F SPGG output flow less the relief valve flow and the pilot stage vortex valve supply and control flows.

$$\dot{W}_1 = \dot{W}_g - (\dot{W}_8 + \dot{W}_4 + \dot{W}_{15}) = 0.880 - (0.4638 + 0.0608 + 0.0608)$$

$$\dot{W}_1 = 0.295 \text{ lb/sec}$$

Therefore

$$A_1 = \frac{\dot{W}_1 \sqrt{T_g}}{C_{d1}\, C_2(\Theta max)\, P_g} = \frac{0.295 \quad \sqrt{2510}}{0.9(0.412)2600}$$

$$A_1 = 0.0154 \text{ in}^2$$

The foregoing calculations were utilized in the fourth and fifth hot gas tests. The results from these tests showed that the actual pilot stage performance presented a reasonably constant impedance to the 2000°F SPGG. Based on this information, a decision was made to eliminate the relief valve for Hot Gas Test No. 6. The only change made to the system to facilitate the relief valve removal was the enlargement of orifice A_1.

APPENDIX B
THERMAL ANALYSIS

APPENDIX B

THERMAL ANALYSIS

A transient heat transfer and thermal stress analysis[2] was conducted as a supporting effort to the development of the hot gas vortex valve. The analysis was undertaken to aid in the selection of materials and design configuration for the vortex valve and for a 5500°F SITVC system.

Since the vortex valve and all of the manifolds are cylindrical shapes, the model used in the analyses was a composite cylinder. The composite cylinder's constituent materials were tungsten, graphite, reinforced plastic, and stainless steel as shown in Figure 87.

Tungsten was selected as the inner liner material because of its high melting temperature and high strength. Graphite was selected as an intermediate layer because of its increasing strength and Young's modulus at high temperatures, high strength/weight ratio and high thermal shock resistance. A reinforced plastic was utilized as the outer-intermediate layer to act as a heat shield to insulate the outer housing by a sacrificial thermal degradation process, which is known as the pyrolysis reaction. This phenomenon is characterized by a pyrolysis zone (Figure 88) in which the virgin plastic decomposes to form pyrolysis gases and carbonaceous residue. The fourth layer was a stainless steel housing which contained and supported the inner laminae.

The numerical exactness of the thermal analysis is limited by the lack of available high-temperature material properties. The unobtainable material properties were approximated by interpolation from existing data.

Transient Heat Transfer Analysis

The transient heat transfer analysis of a thick composite cylinder containing a layer of char-forming reinforced plastic was based on the following assumptions.

(1) Temperature variations will be in the radial direction only.

(2) The pyrolysis gas velocity is proportional to the pressure gradient, and the gases obey the equation of state for a perfect gas.

(3) The pyrolysis gases do not react chemically with the char or with themselves.

(4) The local gas and char material have the same temperature.

(5) The inner boundary of the composite tube is exposed to 5500°F aluminized solid propellant gas and the heat flux into the wall is by convection and radiation from the hot gas.

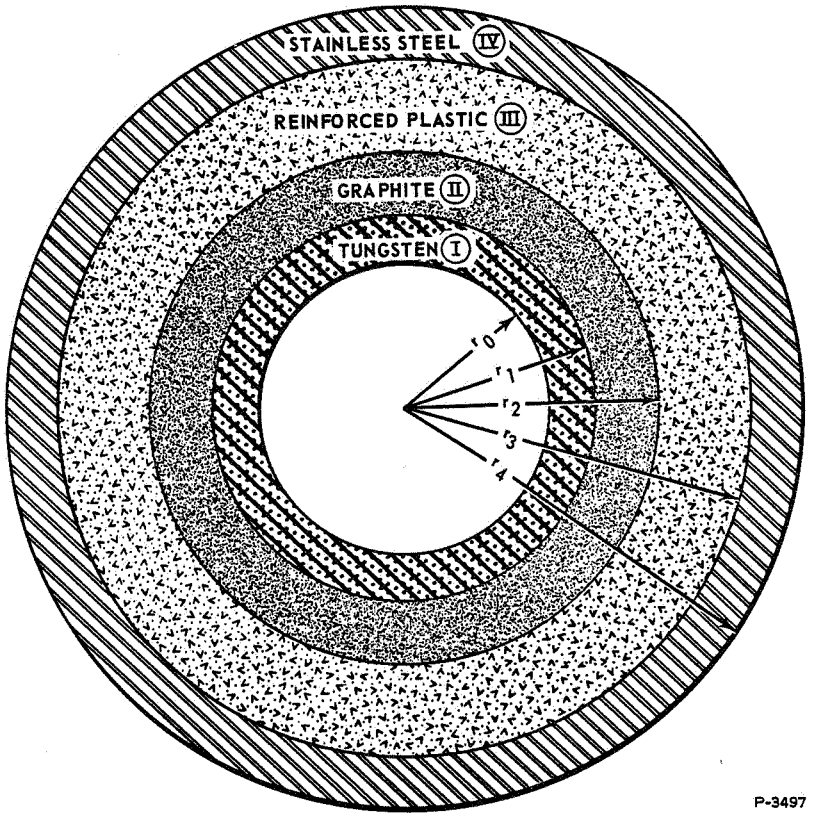

Figure 87 - Geometry of the Composite Cylinder

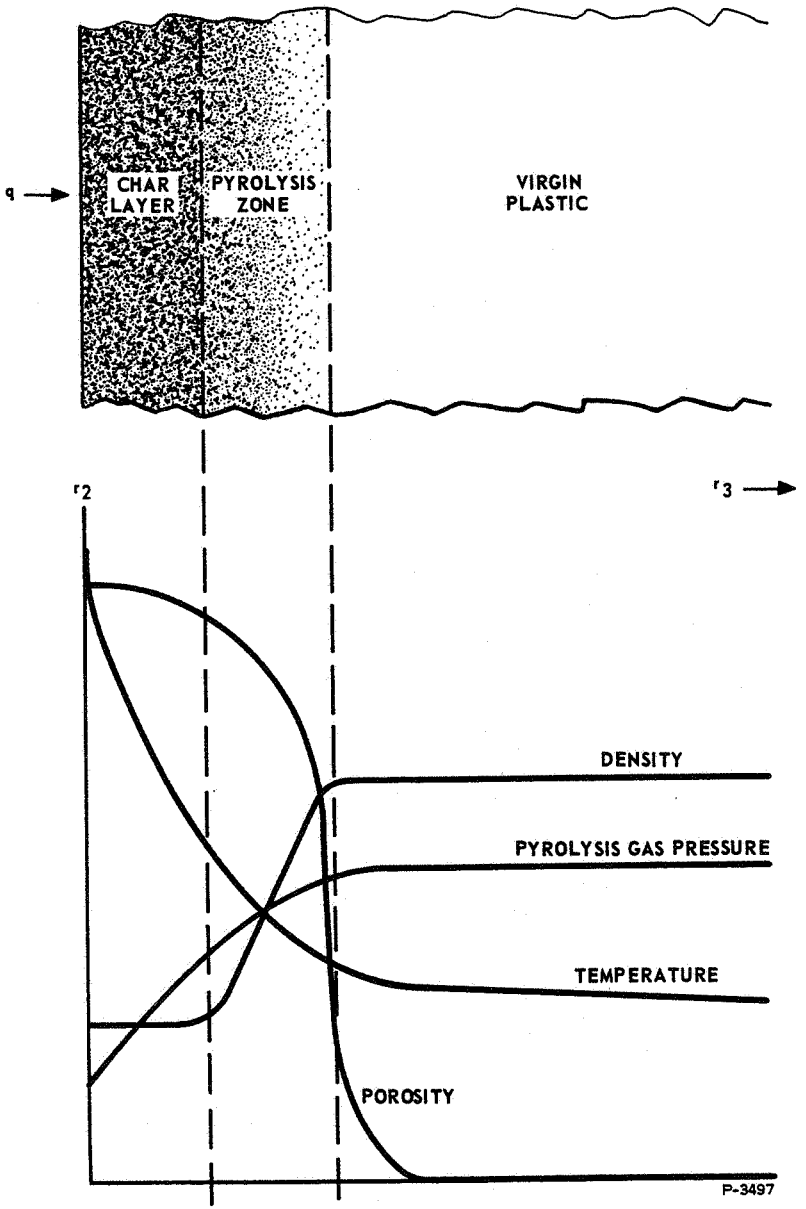

Figure 88 - Representation of a Charring Reinforced Plastic Layer

(6) The laminate interfaces are in contact and the temperature and heat flows are constant.

(7) The exterior of the composite tube is exposed to ambient air.

The transient heat transfer relationships developed based on the above assumption were numerically evaluated for the six sets of composite tube dimensions shown in Table 4. The first four configurations contained all four of the laminate materials, and in the fifth and sixth configurations the graphite layer was eliminated. The numerical solution was made with the hot gas film temperature rising from ambient to 5960°F in 0.2 second.

The results of the numerical analysis in the form of temperature responses at the composite cylinder boundaries and interfaces are shown in Figures 89 through 94. The effectiveness of the insulation and the heat-sink effect of each layer are represented by the vertical distance between two neighboring temperature curves.

The general trends deduced from the transient heat transfer analysis are:

(1) With other conditions being held constant, to increase the thickness of the tungsten layer or to decrease the thickness of the graphite layer (including complete elimination of the

Table 4 - Dimensions for Parametric Numerical Evaluation

Radius and Thickness (in.)	Case Number					
	1	2	3	4	5	6
r_0	0.3375	0.5	0.5	0.5	0.5	0.5
$r_1 - r_0$ (Tungsten)	0.08	0.06	0.08	0.1	0.08	0.205
r_1	0.4175	0.56	0.58	0.6	0.58	0.705
$r_2 - r_1$ (Graphite)	0.125	0.145	0.125	0.105	(None)	(None)
r_2	0.5425	0.705	0.705	0.705	0.58	0.705
$r_3 - r_2$ (Reinforced Plastic)	0.2075	0.295	0.295	0.295	0.420	0.295
r_3	0.75	1.0	1.0	1.0	1.0	1.0
$r_4 - r_3$ (Stainless Steel)	0.125	0.125	0.125	0.125	0.125	0.125
r_4	0.875	1.125	1.125	1.125	1.125	1.125

P-5408

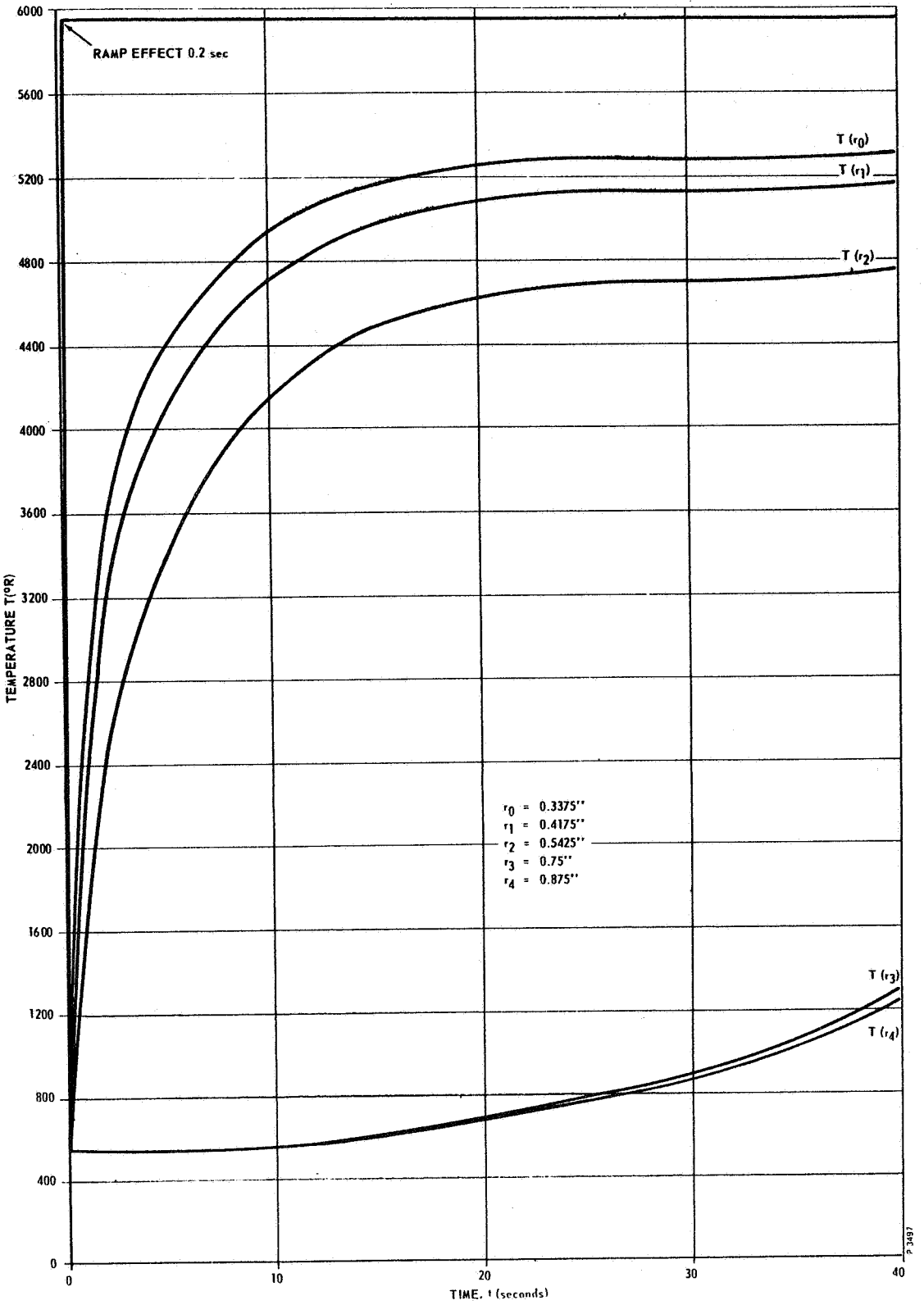

Figure 89 - Transient Temperature Response at the Boundaries and Interfaces of a Composite Cylinder (Case 1)

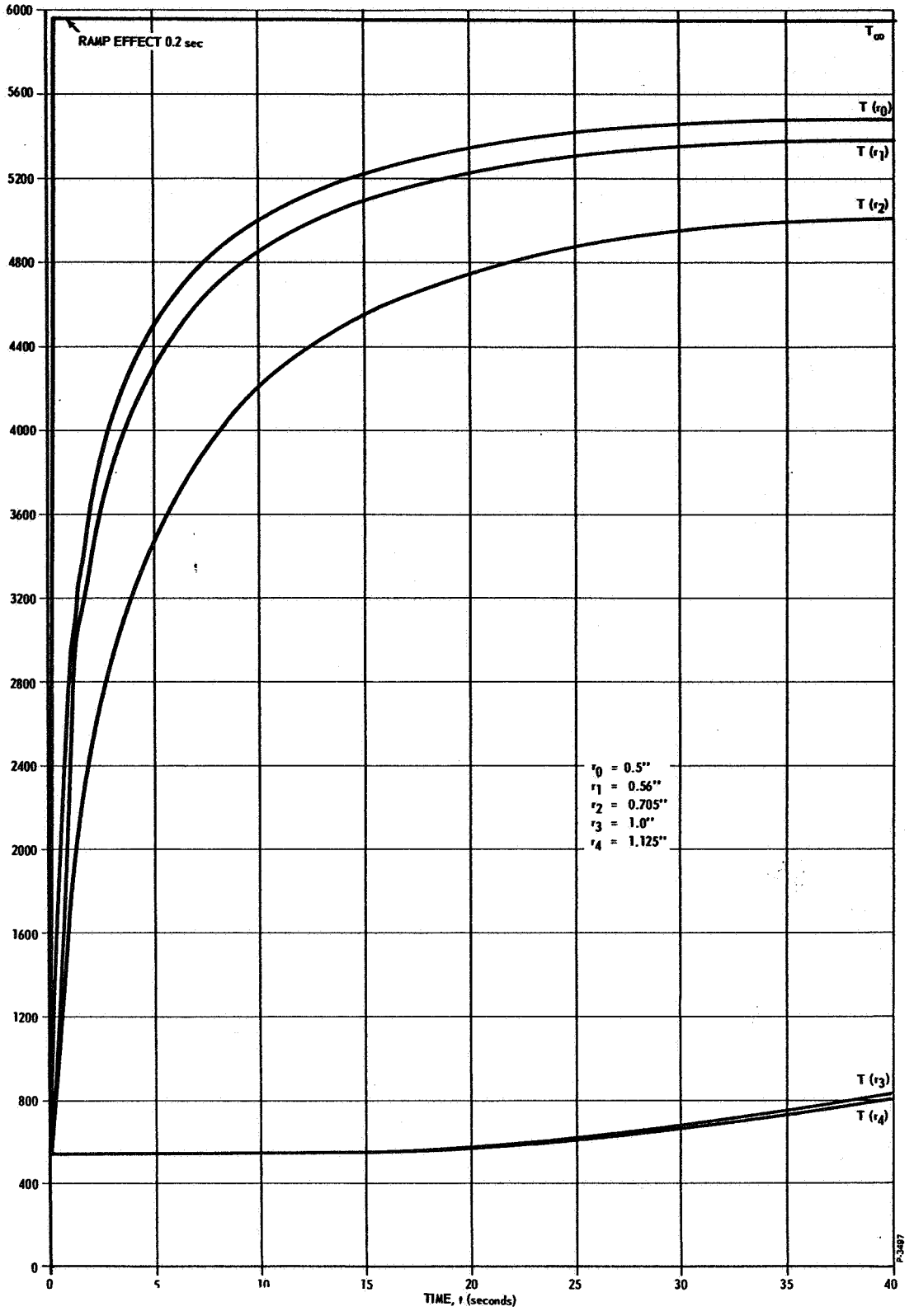

Figure 90 - Transient Temperature Response at the Boundaries and Interfaces of a Composite Cylinder (Case 2)

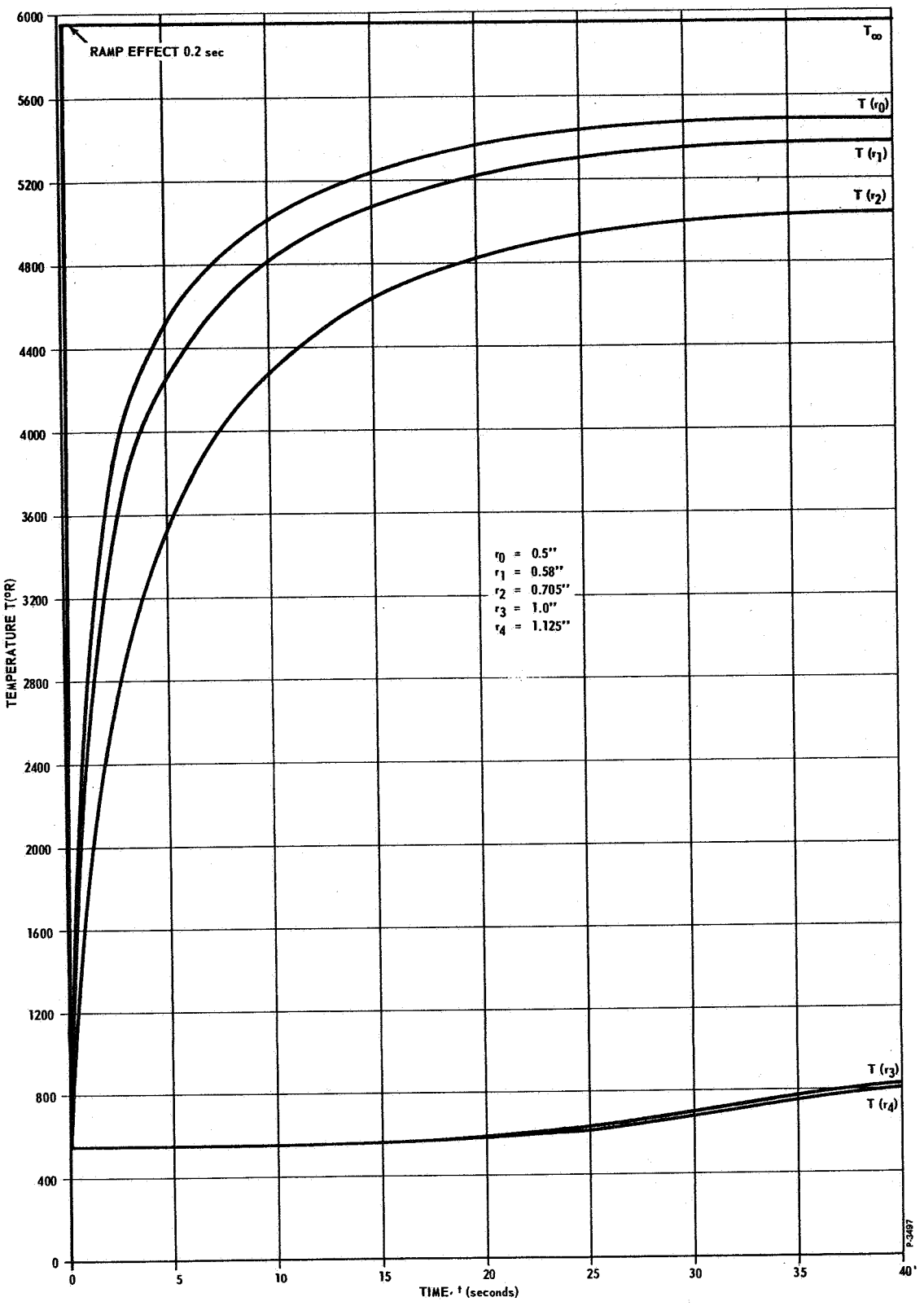

Figure 91 - Transient Temperature Response at the Boundaries and Interfaces of a Composite Cylinder (Case 3)

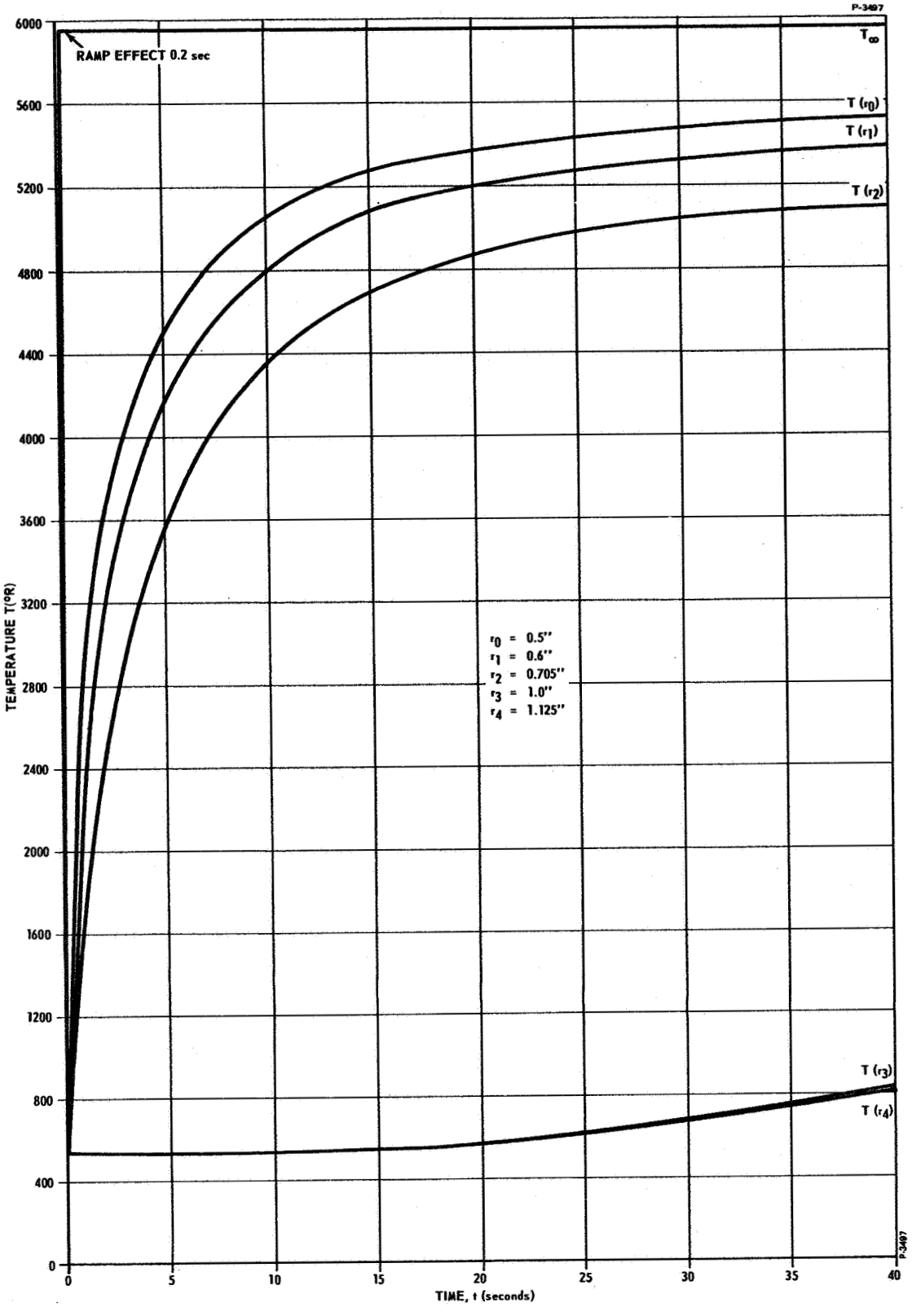

Figure 92 - Transient Temperature Response at the Boundaries and Interfaces of a Composite Cylinder (Case 4)

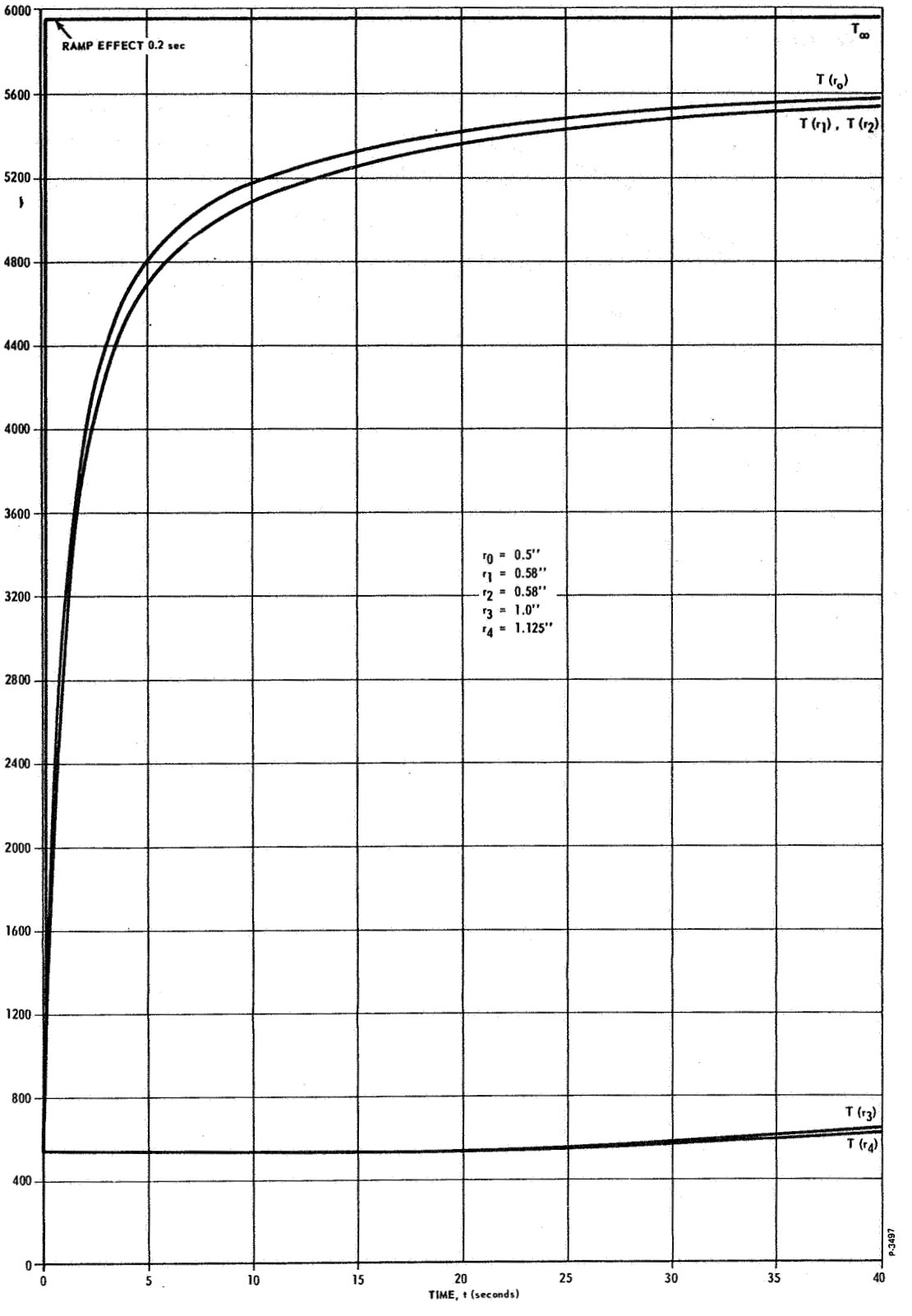

Figure 93 - Transient Temperature Response at the Boundaries and Interfaces of a Composite Cylinder (Case 5)

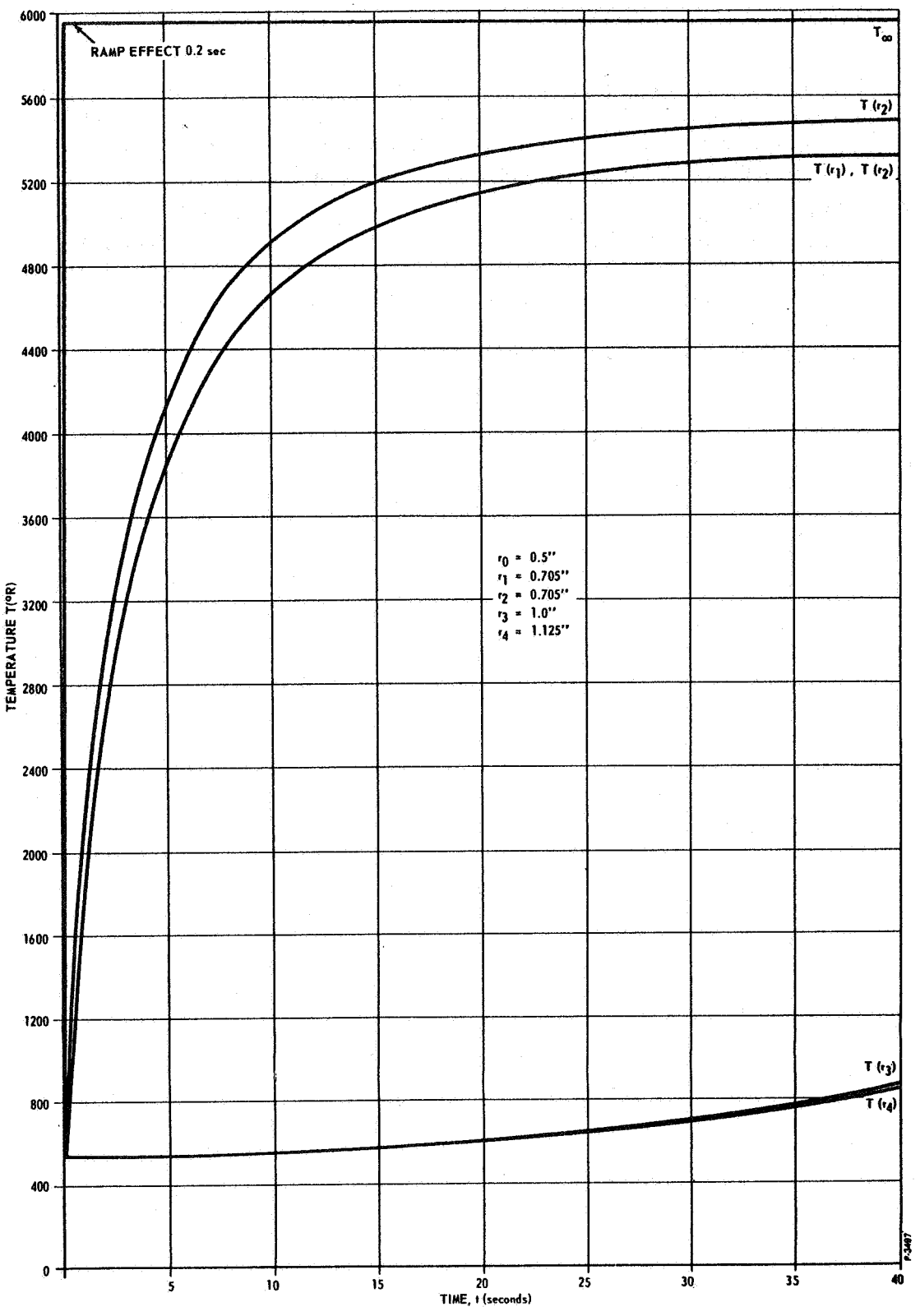

Figure 94 - Transient Temperature Response at the Boundaries and Interfaces of a Composite Cylinder (Case 6)

graphite layer) results in lowering the temperature levels in the frontal layers in the initial stage of the transient heating process, but reverses the trend and increases the temperature levels in all later stages.

(2) When the graphite layer is completely replaced by thickening the reinforced plastic layer, the temperature responses between the inner boundary and the charred zone tend to increase but the back zone temperatures are lowered. This result is attributed to conductive heat-sink properties of graphite and effective insulation properties of reinforced plastic.

Thermal Stress Analysis

The thermal stress analysis was made to determine if the stresses induced in the composite cylinder model by dissimilar thermal expansion and radial temperature gradients would cause structural failures. The thermal stress analysis was based on the framework of the linear, quasi-static, uncoupled theory of thermoelasticity. The composite cylinder materials which exhibit distinct behavioral characteristics were classified and analyzed in three categories: isotropic, anisotropic and porous media. Three sets of governing differential equations of stress for the material categories were made assuming that Poisson's ratio and Young's Modulus of Elasticity are constant. Numerical solutions for the thermal stress relationships were determined for the six composite cylinder configurations that were used in the heat transfer analysis. The predetermined temperature distribution, pyrolysis gas pressure, and the reinforced plastic porosity were also used in the numerical solution. Typical solutions are shown in Figures 95 through 97, which are plots of stress versus radius for case 4 at times 1, 2 and 10 seconds. The stress components σ_r, σ_z and σ_θ are normal components of stress in cylindrical coordinates with r the radial direction, and z the axial direction. The results of the numerical solution indicated that case 4 is the most favorable dimensional combination.

The transient heat transfer and thermal stress analysis provided qualitative thermal characteristics of a composite cylindrical structure to aid the selection of materials and the design of structures that are to contain the flow of 5500°F highly aluminized hot gas. The lack of moderate and high-temperature mechanical behavior, thermophysical and chemico-kinetic material properties makes the absolute numerical results uncertain, but the trends between various combinations are believed to be representative.

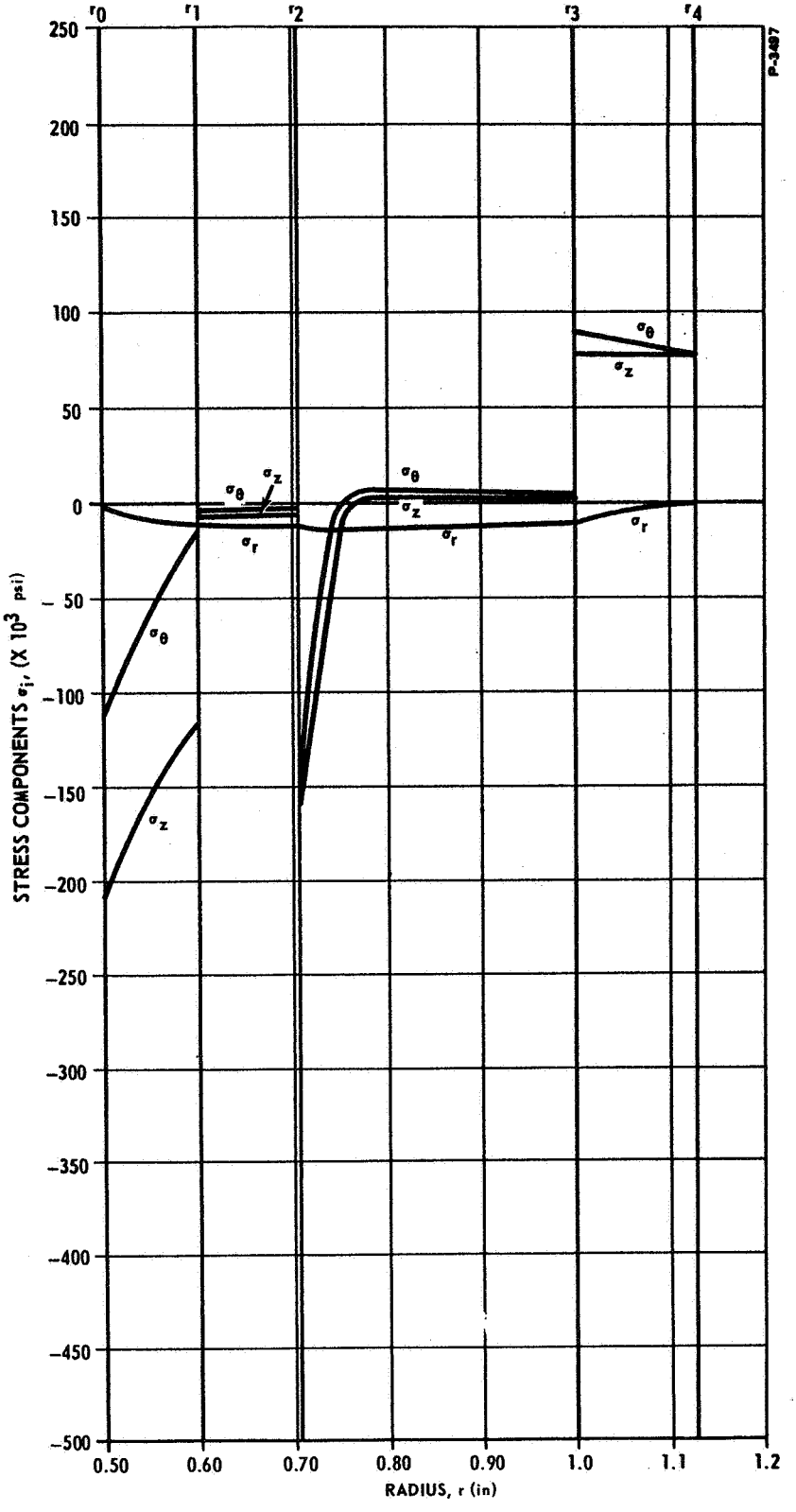

Figure 95 - Thermal Stresses in the Composite Cylinder (Case 4), t = 1.0 sec

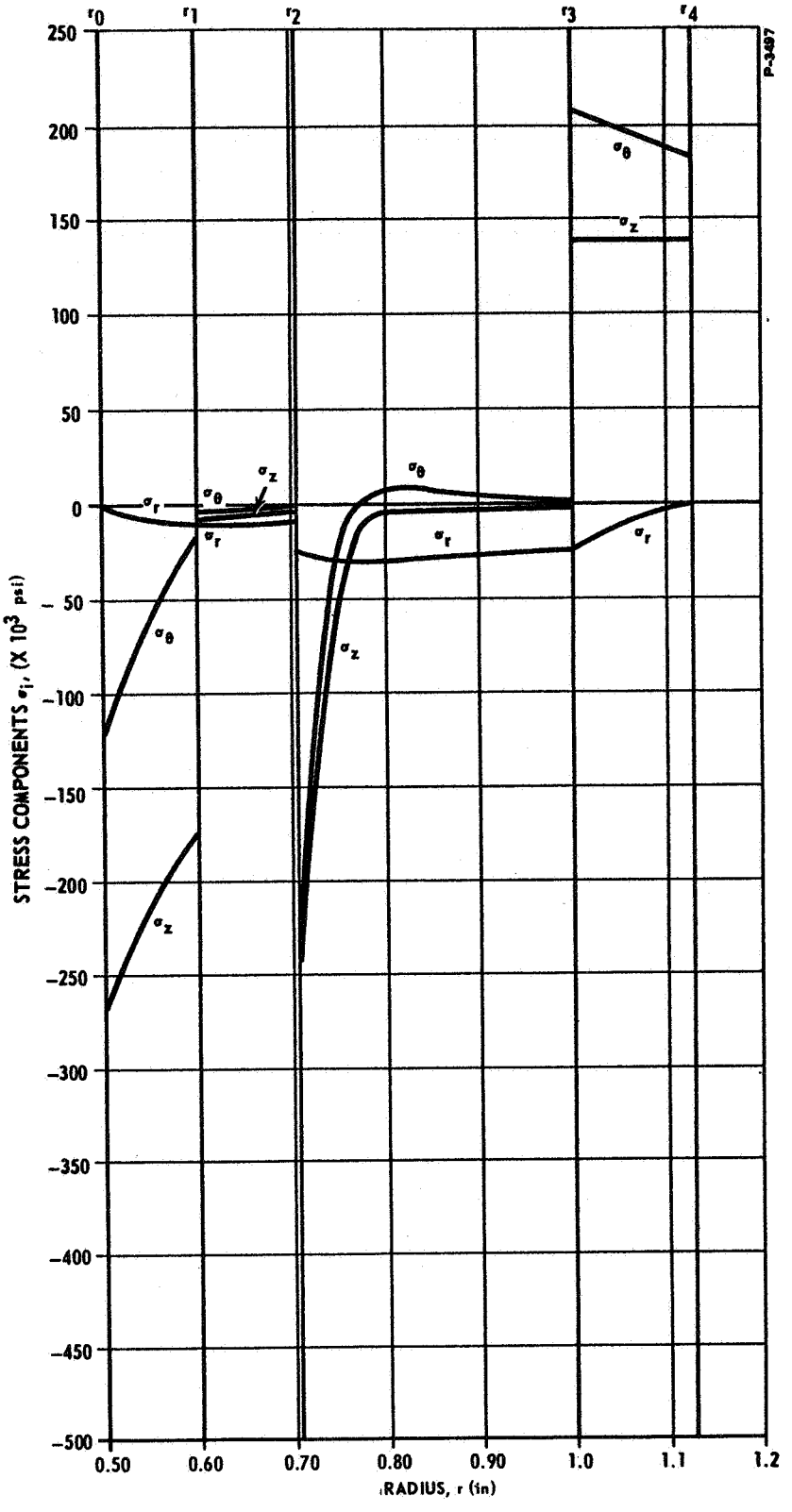

Figure 96 - Thermal Stresses in the Composite Cylinder (Case 4), t = 2.0 sec

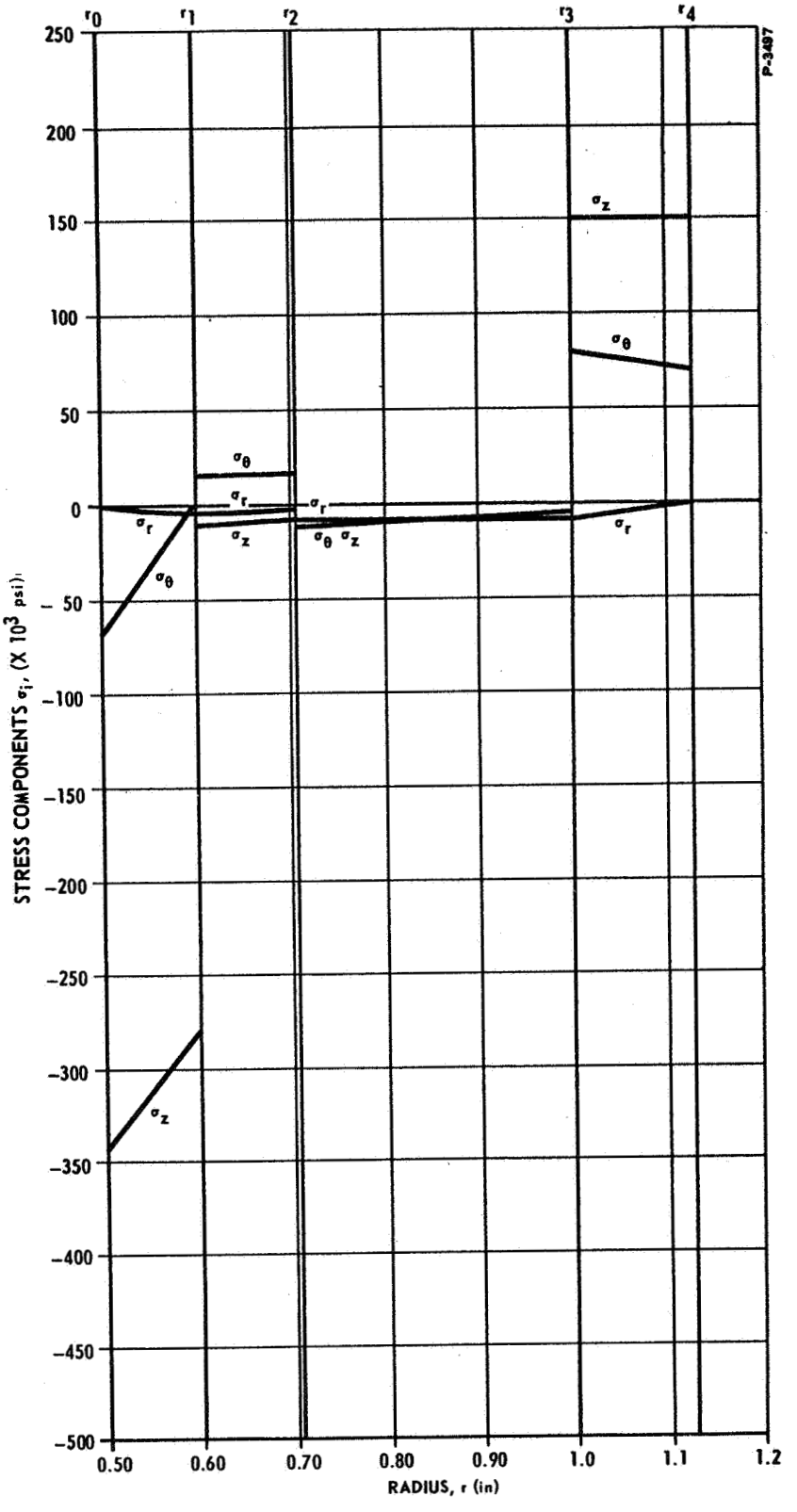

Figure 97 - Thermal Stresses in the Composite Cylinder (Case 4), t = 10.0 sec

APPENDIX C
GLOSSARY OF SYMBOLS

GLOSSARY OF SYMBOLS

A = orifice area, in^2

A_g = solid propellant grain cross-sectional area, in^2

c = solid propellant burn characteristic constant

C_d = orifice flow discharge coefficient

cps = cycles per second

C_v = ratio of vortex valve total flow to maximum total flow

C_2 = thermodynamic gas constant, $^\circ R^{1/2}/sec$

D = nozzle diameter, in.

f_1 = orifice flow function

k = specific heat ratio

L = flapper stroke, in.

n = solid propellant burn characteristic pressure exponent

N_2 = nitrogen gas

P = pressure, psia

$\bar{P}$ = average pressure, psia

P_c = vortex valve control pressure, psia

P_g = gas generator pressure, psia

P_s = vortex valve supply pressure, psia

$(P_d/P_u)_{crit.}$ = pneumatic critical pressure ratio

r = solid propellant burn rate, in/sec

$r_{(0,1,2,etc.)}$ = radius, in.

SITVC = secondary injection thrust vector control

SPGG = solid propellant gas generator

T = temperature, °F or °R

$\dot{W}$ = gas weight flow, lb/sec

Δi = torque motor differential current, ma

ρ = solid propellant grain density, lb/in^3

σ = stress, psi

REFERENCES

1. E. A. Mayer, "Large-Signal Vortex Valve Analysis," Advances in Fluidics, Proceedings of the 1967 Fourth Fluidics Symposium, ASME/HDL, May 1967.
2. H. P. Lee, "Transient Response of Temperature Distributions and Analysis of Thermoelastic Stresses in a Composite Cylinder Containing a Layer of Char-Forming Reinforced Plastic," Bendix Research Laboratories Report No. 3221, presented to NASA-Langley Research Center, December 1965.

BIBLIOGRAPHY

1. Holt, W. D., and Rivard, J. G., "Research Study of the Vortex Valve for Medium Temperature Solid Propellants," NASA CR-424, prepared under NASA Contract NAS 1-4158 for Langley Research Center by Bendix Research Laboratories, April 1966.
2. Vickers Incorporated, "Study of Proportional Solid Propellant SITVC Under Simulated Altitude Conditions," prepared under NASA Contract NAS 1-4102 for Langley Research Center, June 1966.
3. Sutton, G. P., Rocket Propulsion Elements, John Wiley & Sons, Incorporated.
4. Rivard, J. G., "Secondary Injection Thrust Vector Control Using Fluidic Vortex Valves," presented at Western Electronic Show and Convention, San Francisco, California, August 1967.

NATIONAL AERONAUTICS AND SPACE ADMINISTRATION
WASHINGTON, D.C. 20546

OFFICIAL BUSINESS

FIRST CLASS MAIL

POSTAGE AND FEES PAID
NATIONAL AERONAUTICS AND
SPACE ADMINISTRATION

POSTMASTER: If Undeliverable (Section 158
Postal Manual) Do Not Return

"The aeronautical and space activities of the United States shall be conducted so as to contribute . . . to the expansion of human knowledge of phenomena in the atmosphere and space. The Administration shall provide for the widest practicable and appropriate dissemination of information concerning its activities and the results thereof."

— NATIONAL AERONAUTICS AND SPACE ACT OF 1958

NASA SCIENTIFIC AND TECHNICAL PUBLICATIONS

TECHNICAL REPORTS: Scientific and technical information considered important, complete, and a lasting contribution to existing knowledge.

TECHNICAL NOTES: Information less broad in scope but nevertheless of importance as a contribution to existing knowledge.

TECHNICAL MEMORANDUMS: Information receiving limited distribution because of preliminary data, security classification, or other reasons.

CONTRACTOR REPORTS: Scientific and technical information generated under a NASA contract or grant and considered an important contribution to existing knowledge.

TECHNICAL TRANSLATIONS: Information published in a foreign language considered to merit NASA distribution in English.

SPECIAL PUBLICATIONS: Information derived from or of value to NASA activities. Publications include conference proceedings, monographs, data compilations, handbooks, sourcebooks, and special bibliographies.

TECHNOLOGY UTILIZATION PUBLICATIONS: Information on technology used by NASA that may be of particular interest in commercial and other non-aerospace applications. Publications include Tech Briefs, Technology Utilization Reports and Notes, and Technology Surveys.

Details on the availability of these publications may be obtained from:

SCIENTIFIC AND TECHNICAL INFORMATION DIVISION

NATIONAL AERONAUTICS AND SPACE ADMINISTRATION

Washington, D.C. 20546